Report BRL 6048

DEVELOPMENT OF A HIGH-RELIABILITY ROTARY ACTUATOR FOR SPACEFLIGHT USE

Volume I - Technical Report

R. G. Read
N. L. Sikora
R. W. Presley

Bendix Research Laboratories
Bendix Center
Southfield, Michigan 48076

Approved June 1972

Final Report for Period February 1970 to April 1972

Prepared for
GODDARD SPACE FLIGHT CENTER
Greenbelt, Maryland 20771

1. Report No.	2. Government Accession No.	3. Recipient's Catalog No.
BRL 6048		

4. Title and Subtitle	5. Report Date
Development of a Space Qualified High Reliability Rotary Actuator (Volume I - Technical Report)	May 1972
	6. Performing Organization Code
7. Author(s)	8. Performing Organization Report No.
R. W. Presley, R. G. Read, N. L. Sikora	6048
9. Performing Organization Name and Address	10. Work Unit No.
Bendix Research Laboratories Bendix Center Southfield, Michigan 48076	11. Contract or Grant No. NAS 5-21142
	13. Type of Report and Period Covered
12. Sponsoring Agency Name and Address	Final Report
Goddard Space Flight Center Greenbelt, Maryland 20771 Technical Monitor: E. J. Devine	14. Sponsoring Agency Code

15. Supplementary Notes

16. Abstract

The program objective was to develop a space-qualified, high reliability, 150 ft-lb rated torque rotary actuator based on the Bendix Dynavector® drive concept. This drive is an integrated variable reluctance orbit motor-epicyclic transmission actuator. The performance goals were based on future Control Moment Gyro torquer applications and represent a significant advancement in the torque-to-weight ratio, backlash, inertia and response characteristics of electric rotary drives.

The program accomplishments have been in two areas (1) the development of two high ratio (818:1) actuator configurations (breadboard and flightweight) and (2) the invention of a reliable proximity switch sensor system for self-commutation without use of optical or electrical brush techniques.

Other significant accomplishments used in the actuator and controller hardware include: (1) Design of a 818:1 single pass orbital epicyclic transmission using a difference of 6 teeth between working meshes; (2) Procedures for fabricating precision gearing from nitrided maraging steel; (3) Development of a low inertia, responsive actuator which requires only two bearings and two moving parts; (4) Energy transfer techniques for optimum coil energization; (5) Controller logic analyses by which a 8-pole motor is commutated by 4 proximity sensors; (6) Test results indicating zero backlash and stiffness of 3.9 to 4.2 arc-min/100 lb-ft; and (7) Frequency response tests and analyses to predict performance with gimbal inertias up to 500 slug-ft^2.

17. Key Words	18. Distribution Statement
Electric Drives Epicyclic Transmissions Variable Reluctance Motor Commutation Techniques	

19. Security Classif. (of this report)	20. Security Classif. (of this page)	21. No. of Pages	22. Price
Unclassified	Unclassified	151	

TABLE OF CONTENTS

LIST OF ILLUSTRATIONS

LIST OF TABLES

SECTION 1

INTRODUCTION AND OBJECTIVES

This report was prepared by The Bendix Corporation Research Laboratories, Southfield, Michigan, on NASA Contract NAS 5-21142, "Development of a Space Qualified, High Reliability Rotary Actuator." The work was administered under the direction of NASA Goddard Space Flight Center by Mr. E. J. Devine of the Electro-Mechanical Branch of the Mechanical Division.

The work on this contract was performed between February 1970 and April 1972 by the Machine Systems Department of the Mechanical Sciences and Controls Laboratory of the Bendix Research Laboratories. Mr. R. G. Read, Senior Project Engineer was responsible as project supervisor and was assisted by Mr. N. L. Sikora, Project Engineer (responsible engineer for mechanical design) and Mr. R. W. Presley, Project Engineer (responsible engineer for electrical design).

The objective of the program was to develop a high-reliability, 150 lb-ft rated-torque rotary actuator based on the Dynavector® actuator drive concept. The actuator performance goals, which were based on future Control Moment Gyro torquer applications, represent a significant advancement in the torque-to-weight ratio, backlash, inertia and response characteristics of electric rotary drives.

SECTION 2

SUMMARY

2.1 BACKGROUND

The application of geared electric torquers for Control Moment Gyro space platform stabilization could be limited, to a certain extent, by the lack of high torque electric actuators with the required reliability, backlash, stiffness and response characteristics and high torque-to-weight and volume ratios. Future space platform applications will require CMG torquers that provide improved characteristics in all of the above areas. This program has been directed toward establishing the feasibility of applying an integrated variable-reluctance orbit motor-epicyclic transmission actuator technique to meet a set of performance goals summarized as follows in Table 2-1.

Table 2-1 - Design Performance Goals

Rated Torque (lb-ft)	150
Rated Speed (rpm)	1
Peak Torque (lb-ft)	200
Rated Power (watts)	100
Voltage (dc)	28
Weight (lb)	20
Diameter (in.)	8
Length (in.)	4
Inertia; output ($lb\text{-}ft\text{-}sec^2$)	2
Backlash (arc-sec)	5
Windup (arc-min/100 lb-ft)	3
Life; 10%/rated torque (hrs)	10,000
Vacuum (mm Hg)	10^{-6}
Temperature Range (°C)	-10 to +70

2.2 PROGRAM ACCOMPLISHMENTS

The accomplishments of this program have been in two areas: (1) the design, fabrication and test of two high ratio (818:1) actuator

configurations (breadboard and flightweight) and (2) the invention of a highly reliable proximity-switch sensor system for self-commutation without use of optical techniques or sliding electrical contacts.

The breadboard actuator, Model EH-818-U1, is shown in Figures 2-1 and 2-2.

Two flightweight actuators Models EH-818-U2 (S/N 1 and S/N 2) were built and tested. The output shaft end of the actuator is shown in Figure 2-3 and a view of the housing is shown in Figure 2-4.

The schematic for the use of non-contact type proximity sensors to provide feedback signals for switching the motor coils is shown in Figure 2-5. The ring gear member moves with both orbital and rotational motion and the sensor detects a varying radial air gap. Four sensors are used to provide signals for controlling the 8-phase motor. The sensors are located 45 degrees apart.

The hardware implementation of this sensor technique is shown in Figure 2-6.

Other significant analytical and design accomplishments that have been used in the actuator and controller hardware built on this program include:

(1) Design of a 818:1 single-pass orbital epicyclic transmission using 64 diametral pitch gearing with 6 teeth difference between working meshes.

(2) Processing procedures established for fabricating precision gearing from 18 Ni 350 grade maraging steel with nitrided surface treatment.

(3) Development of an actuator concept which requires only two bearings and two moving parts (orbital ring gear and output shaft) which results in a low inertia (2.7 lb-ft-sec^2) but high stiffness.

(4) Development of an 8-pole laminated (M-19 sheet steel) stator and coil (22 gage wire, 450 turns) assembly.

(5) Controller design analysis of energy transfer techniques for optimum coil energization.

(6) Controller logic analyses by which the 8-pole motor is commutated by 4 proximity sensors in both CW and CCW directions.

(7) Stiffness, hysteresis and backlash analysis and test results indicating zero backlash and stiffness of 3.9 to 4.2 arc-min/100 lb-ft.

(8) Frequency response analyses of the actuator functioning as a dc torquer by which the 90 degree phase lag occurs at frequency of at least 2.5 Hertz when driving a gimbal inertia of 500 slug-ft^2.

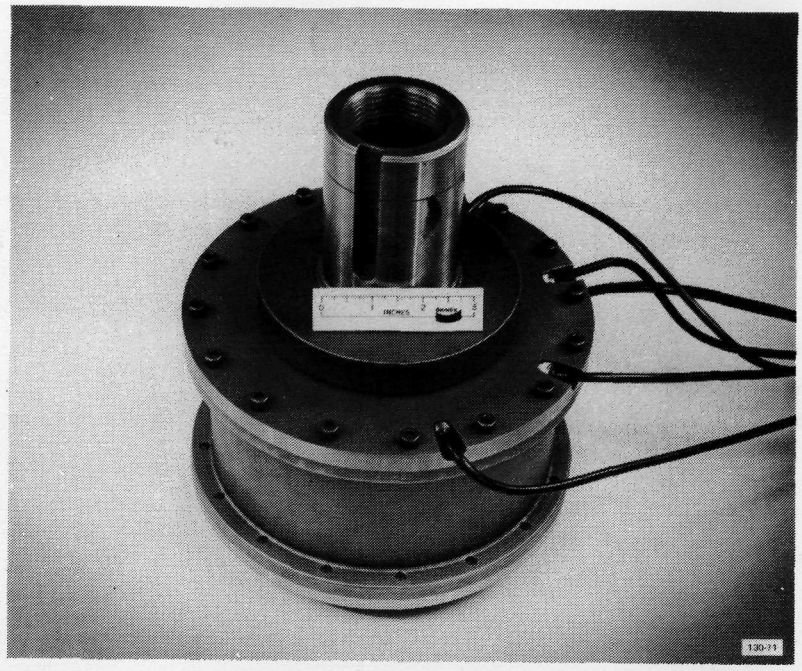

Figure 2-1 - Breadboard Actuator Model EH-818-U1 Assembled

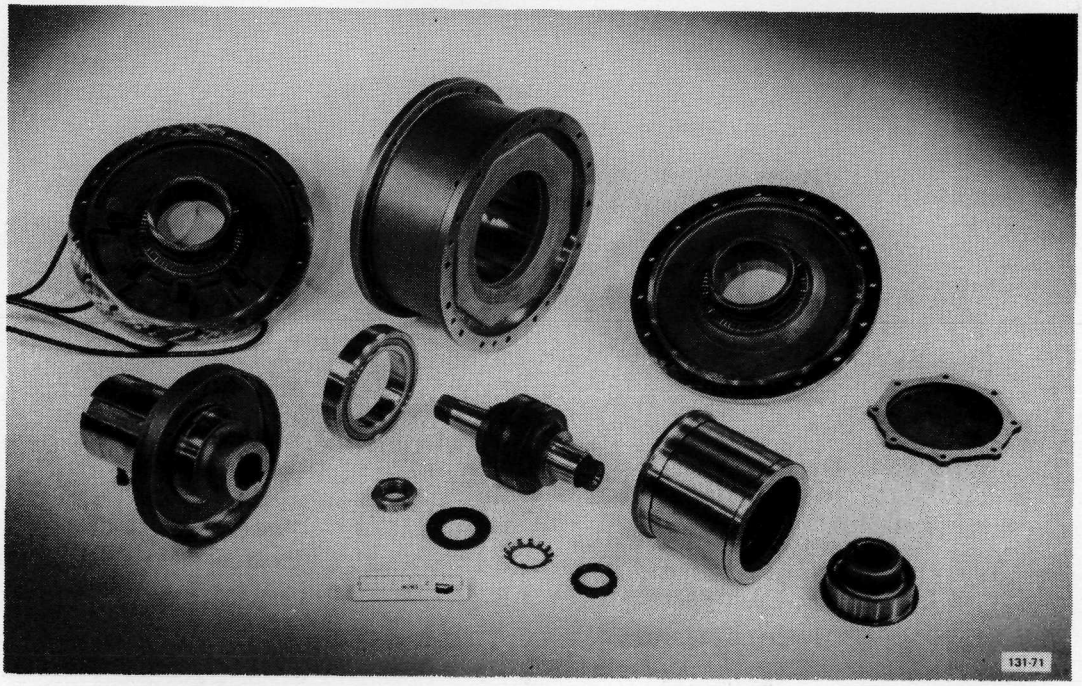

Figure 2-2 - Model EH-818-U1 Disassembled

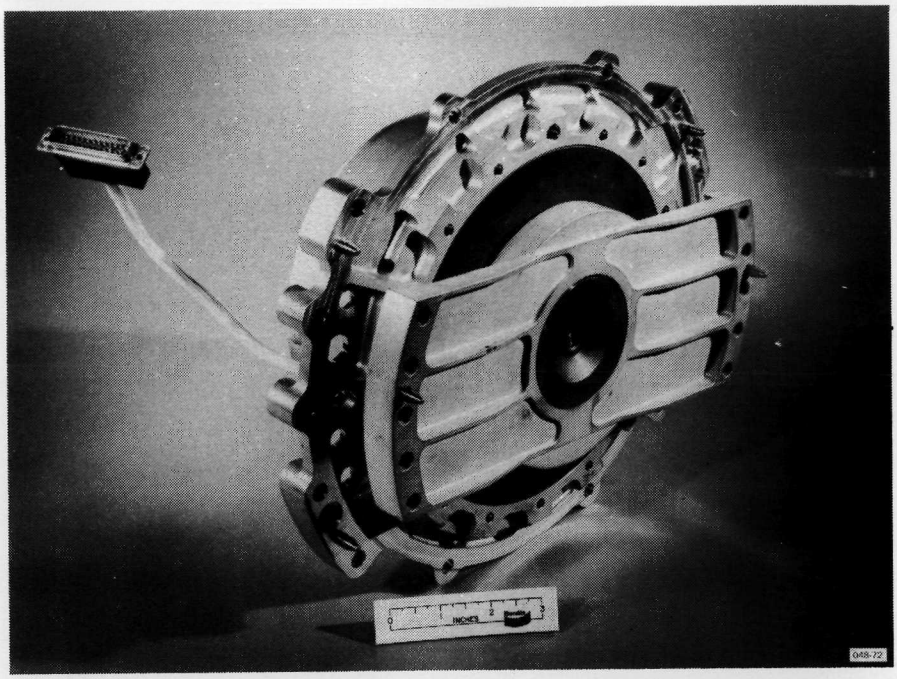

Figure 2-3 - Flightweight Actuator Model EH-818-U2 Assembly (Front View)

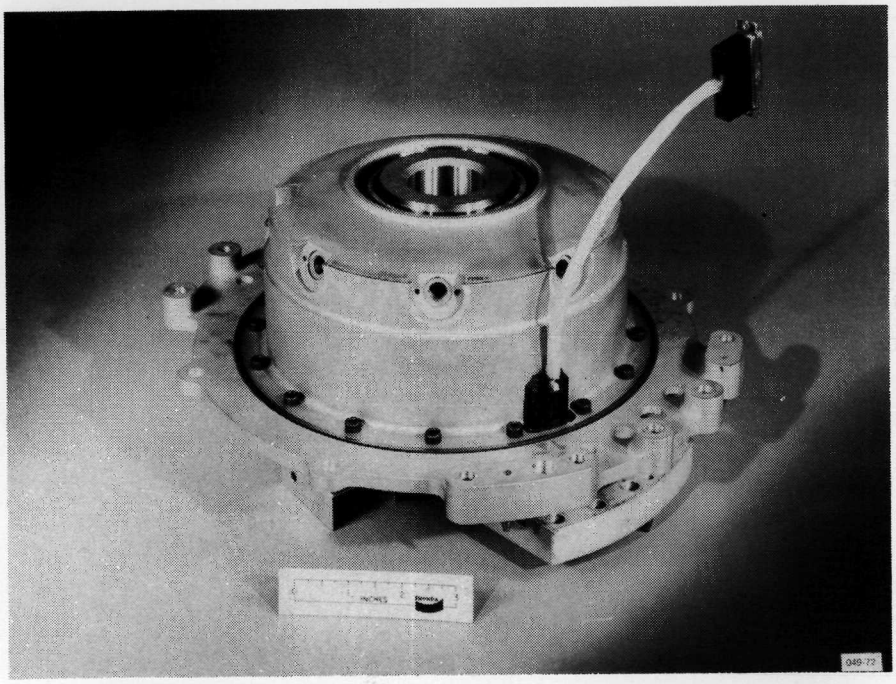

Figure 2-4 - Flightweight Actuator Assembly (Rear View)

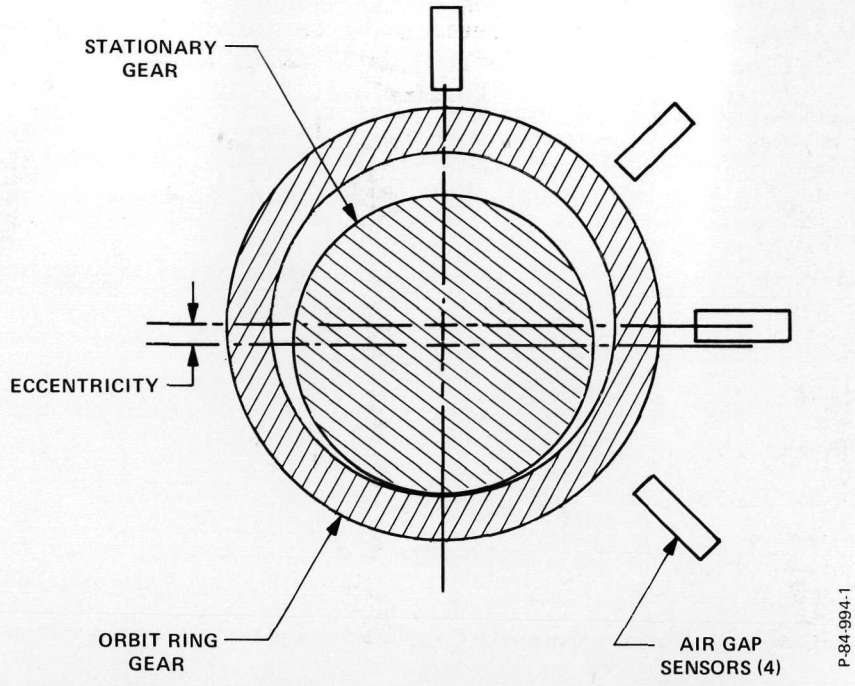

Figure 2-5 - Schematic of Commutator Configuration

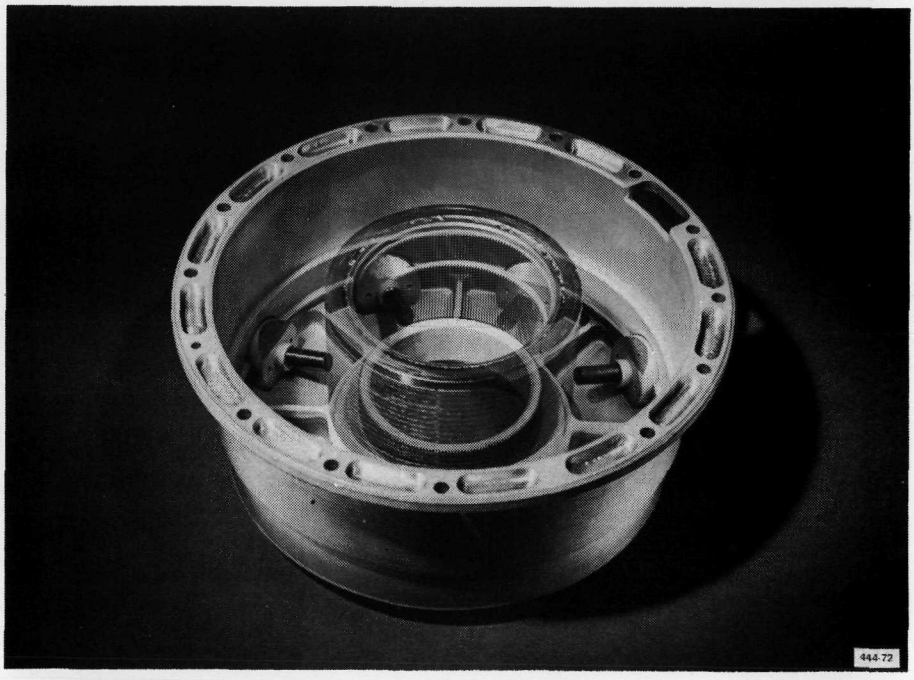

Figure 2-6 - Flightweight Actuator Self-Commutator Sensor Assembly

(9) Frequency response tests results indicating a 90 degree phase lag at 12.5 Hertz and 23 Hertz with inertia loads of 20 and 2.0 slug-ft^2 respectively.

The performance characteristics of actuator SN/2 operating in the self-commutated mode are summarized in Table 2-2.

Table 2-2 - Actuator Model EH-818-U2 SN/2 Performance

Rated Torque (lb-ft)	133
Rated Speed (rpm)	1.0
No-Load Speed (rpm)	3.0
Peak Torque (lb-ft)	183
Rated Power (watts)	150
Voltage (D.C.)	28
Weight excluding mounting pivot (lb)	33.5
Diameter (in.)	7.5
Length (in.)	4.0
Inertia; output (lb-ft-sec^2)	2.7
Backlash (arc-sec)	0
Windup (arc-min/100 lb-ft)	3.9 to 4.2

The limitations of the actuators evolved under this program were found to be:

(1) Because the orbit rotor gear is a single unbalanced member, air induced vibration level proportional to orbit speed occurs. (Vibration force is 3.2 pounds at rated speed.)

(2) Because of the high ratio gearing configuration the unit will hold a load without power on but conversely cannot be backdriven.

(3) The overall efficiency of the controller-torquer concept was lower than the performance goals (150 watts versus 100 watts).

SECTION 3

PERFORMANCE REQUIREMENTS AND TECHNICAL APPROACH

The objective of this program was to apply the established technology of the Dynavector drive concept to meeting a set of performance requirements for advanced CMG torquer applications. The actuator technology established at the beginning of this program was founded on the use of a reluctance type, direct current stepper motor with an integral orbital high ratio transmission. In this motor, work is done by magnetic attraction acting across a variable air gap, parallel to the magnetic field, rather than by interaction between a magnetic field and conductors which move transversely in the field. Only one dynamic mechanical element (rotor ring gear assembly) is used to convert this attraction force to rotary output shaft motion.

The performance capabilities of this type of actuator concept were demonstrated prior to the start of this program with an 8-pole motor, designated Model EH-195-U1. The motor envelope was 3.2-inches diameter by 1.3-inches long and weighed 1.6 pounds. The motor demonstrated a maximum torque capacity of 26 lb-in. and no-load stepping rates in excess of 1000 steps per second with a shaft step increment of 0.46 degrees.

In a survey conducted in 1969 of 125 models of various types of commercially available dc stepper and torque motors, the following comparison factors were identified:

- The torque-to-weight ratio of Model EH-195-U1 was 4 to 8 times better than equivalent sized stepper motors.
- The package volume was 2 to 4 times less.
- The torque-to-inertia ratio was calculated as 2 to 14 times higher than equivalent torque capacity motors.

In summary, the specific technical goal of this program was to advance the technology demonstrated by the 24 lb-in. capacity stepper motor (Model EH-195-U1) to a flightweight CMG torquer of 2400 lb-in. capacity with an 818:1 high stiffness - low backlash transmission capable of operating in a self-commutated mode for 10,000 hours life. These goals were accomplished under a program plan by which (1) a breadboard test unit, designated Model EH-818-U1 was designed, built, tested and optimized and (2) the design, fabrication and test of two flightweight units, designated Model EH-818-U2, Serial Numbers 1 and 2, was completed.

3.1 PERFORMANCE REQUIREMENTS

The design and performance requirement objectives of the program were as follows:

(a) Torque Capacity: Rated torque shall be 150 lb-ft. Stall torque shall be 200 lb-ft.

(b) Speed Capacity: Rated speed shall be 1.0 rpm. No-load speed undefined.

(c) Power and Voltage: Allowable power consumption at rated conditions shall not exceed 100 watts. The supply voltage shall be 28 volts dc.

(d) Envelope and Weight: Actuator diameter shall be 8.0 inches maximum, length 4.0 inches maximum and weight 20 pounds.

(e) Backlash: Output shaft backlash shall not exceed 5.0 arc-seconds.

(f) Inertia: Actuator inertia reflected to the output shaft shall not exceed 2 lb-ft-sec^2.

(g) Stiffness: Actuator output shaft windup at a load of 100 lb-ft torque shall not exceed 3 arc-minutes.

(h) Reliability: A reliability of 95 percent is required for a lifetime of 10,000 hours continuous operation at an average torque level of 10 percent rated torque.

(i) Temperature: The actuator must be capable of operating continuously at a temperature of -10° to +70°C.

(j) Vacuum: The actuator must be capable of operating continuously in a vacuum of 1×10^{-6} mm Hg.

(k) Shock: The actuator must be capable of operating during and after a 50-g shock of 2 msec duration and 5 minutes of 15-g rms random vibration in each of three mutually perpendicular planes.

(l) Interface: The mechanical interface shall be in accordance with reference drawings X1872780 (Actuator Assembly), X1872801 (Mounting Pivot), X1872802 (Actuator Housing). These are representative of the Langley Control Moment Gyroscope gimbal interface and are Bendix Navigation and Control Division drawings. The only necessity is to maintain all hole patterns and the gimbal side interface of both the Mounting Pivot and Actuator Housing. There will not be a need to maintain the exact weights of each of these items.

(m) Hardware Inspection (NPC 200-3): An inspection system conforming to the requirements of NASA Quality Publication NPC-200-3, "Inspection System Provisions for Suppliers of

Space Materials, Parts, Components, and Services," shall be maintained with the following exceptions:

(1) The inspection plan required by Paragraph 2.2 of NPC-200-3 is waived.

(2) Paragraph 1.2, "Applicability," is modified as follows: Delete last sentence and substitute the following: "The requirements of this publication are also applicable to any major subcontracts resulting from this contract to which the provisions are deemed pertinent either by the contractor or the designated representative of the Contracting Officer. Monitoring of the contractor's inspection system will be accomplished through the combined efforts of NASA/GSFC personnel and the cognizant Government inspection agency. The authority and responsibility of the Government inspection agency will be defined by the Contracting Officer.

3.2 TECHNICAL APPROACH - OPERATION OF DYNAVECTOR DRIVE

3.2.1 Dynavector Actuator Description

The Dynavector actuator is a recent development of the Bendix Research Laboratories. This actuator concept is applicable for electrical, pneumatic, or hydraulic power control applications. Those built and tested are listed in Table 3-1. It offers significant advantages over any other rotary servo design in the following areas:

- Reliability
- Simplicity
- High torque-to-inertia ratio
- High stiffness
- High dynamic performance
- High torque-to-weight ratio

The Dynavector motor is an integral high-speed motor and high-ratio transmission without high-velocity mechanical elements. The major components of the Dynavector motor assembly consist of a series of electromagnet poles and a unique integral epicyclic transmission. The transmission and motor use elements common to both, resulting in a much simpler and more reliable design.

The power generating elements are an electromagnet stator and a very low inertia armature. The armature moves with combined orbiting motion and low-speed rotation in the 818:1 high-ratio configuration. The output of the power generating section is a radial force vector which rotates at high speed and in either direction of rotation. The absence of high-velocity members in the motor significantly reduces the inertia, resulting in high acceleration capability.

Table 3-1 - Dynavector Units Built and Tested by Bendix Research Laboratories

*The model number designates:

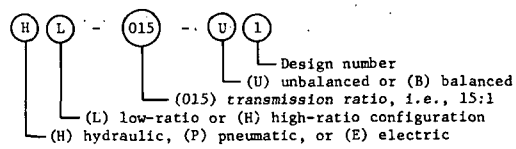

Model*	No. of Units Built	Maximum Torque Capacity (lb-in)	Gear Design Configuration	Maximum Speed (rpm)	Rated Speed (rpm)	Rated Horsepower	Weight (lb)	Size - Length x O.D. (inches)	Comments
HL-015-U1	1	1000	c	450	275	2.75	6.5	2.1 x 4.0	First low-ratio unit
HL-015-U2	15	1000	c	450	275	2.75	6.5	2.1 x 4.0	Basic low-ratio design
HL-015-U3	5	1000	c	100	60	0.50	7.0		Low cost sintered metal model
HH-258-U1	1		a	75					High-ratio feasibility model
HH-267-U3	1	100000	a	5.8	4	4.5	230	9.5 x 11.5	Evaluation test model
PL-015-U1	1	60	c						Plastic feasibility model
PL-015-U2	1	1200	c	100	50	0.55	23		Life tested 1000 hours
PL-015-U3	1	60	c						Plastic feasibility model
PL-015-U5	1	350	c	1000	500	1.6	6.5	2.1 x 4.0	Same as HL-015-U2. Life test 1 x 10^6 load cycles
PL-015-B1	1	2700	c	210	105	2.4			Gimbal actuator drive
PL-018-U1	9	10	c	400	175	0.015	0.7	1 x 3	Hot gas missile fin control
PH-098-U1	1	2000	d		25	0.4	4		Missile fin control feasibility model
PH-391-U1	1	10000	d	10		0.4		6.6 x 7.0	Developmental pneumatic secondary flight control
EH-015-U1	1	2	c						Plastic feasibility model
EH-195-U1	1	26	d	90	35	0.015	1.6		Stepper motor feasibility model
EH-207-U2	2	10	d	125	50	0.01	1.6	1.34 x 3.12	Prototype industrial motor
EH-050-U1	2	25	d				4.9	2.87 x 3.25	1.8 degree stepper
EH-818-U1	1	2400	d	2.0	1.0		45	6.2 x 8.5	CMG aerospace torquer (breadboard)
PL-010-U1	1	180	c				5.2	5.6 x 2.7	Air tool nutrunner
EH-207-U3	1	10	d				1.7	1.1 x 3.12	Vacuum environment 4 and 8 pole stepper
HL-010-U1	1	2000	c		80	1.0	15	5.75 x 4.12	Decouples from load, redundant drive
HL-001-U1	1							5.89 x 5.0	High speed industrial motor
HL-005.6-U1	1		c		540			5.89 x 5.0	Industrial continuous duty motor
PH-391-U2	1	10000	d	10				6.6 x 7.0	Standby actuator for flight control
EH-195-U1	1	26	a	75			1.6	1.3 x 3.2	Prototype automotive throttle control
EH-207-U2	2	10	d	50				1.5 x 3.2	Proto low cost industrial
EH-441-U1	1	400	d	10			17.5	3.6 x 5.5	Reactor control drum drive
EH-818-U1	1	2400	d	6	1		56.5	6.5 x 8.5	Breadboard CMG drive
EH-818-U2	2	2400	d	6	1		35	4.0 x 7.5	Flightweight CMG drive

P-83-222-1

The integration of the power section and epicyclic transmission into an integral actuator design results in an ideal servo actuator with a high torque-to-inertia ratio. The epicyclic transmission design may be either a low-ratio configuration (10 to 100:1), or a high-ratio design (300 to 1000:1).

The operation of the Dynavector motor is illustrated by Figure 3-1 basic electromagnetic operation, and Figure 3-2 basic mechanical operation. When current is flowing in coils 1 through 4, the magnetic flux lines crossing the air gap between the stator and armature result in a radial force vector F in the direction shown in Figure 3-1 The first electrical step input turns off coils 1 and 2 and turns on coils 5 and 6. The force vector then rotates 90 degrees clockwise. The next input step turns off coils 3 and 4 and turns on coils 7 and 8, resulting in another 90 degrees force vector rotation. This sequence continues with one complete vector rotation occurring for every four input steps. The reaction of the rotating force vector on the armature produces an orbiting motion of the armature. The direction of rotation is reversed by reversing the sequence of input steps.

The basic mechanical operation shown in Figure 3-2 is for a low-ratio configuration transmission. The basic components are the ring gear, the ground gear and housing, and the center output gear. The armature is rigidly fastened to the ring gear. The ground gear mesh provides displacement without rotation because both gears have exactly the same number of teeth. It may be considered as a loose spline, but is a true involute gear mesh. The internal portion of the ring gear forms the transmission between the motor and the output shaft and represents the epicyclic transmission. The ring gear does not rotate, but orbits about a small radius and drives the output gear.

If the force vector on the ring gear is located at approximately 90 degrees from the ring and output gear contact point, the ring gear will move, causing the output gear to turn and causing the contact point to move to the force vector position. As the force vector rotates, the output shaft turns continuously, but at a much slower speed than the force vector.

Several limiting factors present in conventional rotary motors plus transmission systems are significantly improved by the Dynavector actuator design and operation. The relative velocities between dynamic and static members are very small, because of the small amplitude orbital motion. In a Dynavector actuator, the relative velocity between the gears and housing is only a function of the eccentricity, which is less than one-tenth of an inch, times the angular velocity; in a conventional motor, there are usually components with a radius of more than 1 inch rotating at the same angular velocity. Thus, for a force vector speed of 3000 rpm, rubbing velocity would not exceed 30 in/sec, whereas, in a conventional motor rotating at 3000 rpm, rubbing velocities would be greater than 300 in/sec. The force vector

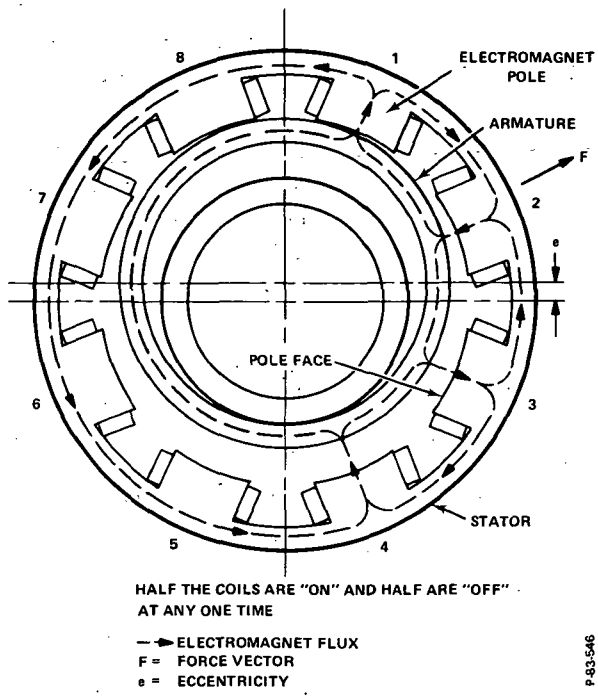

Figure 3-1 - Basic Electromagnetic Operation Electric Dynavector Motor

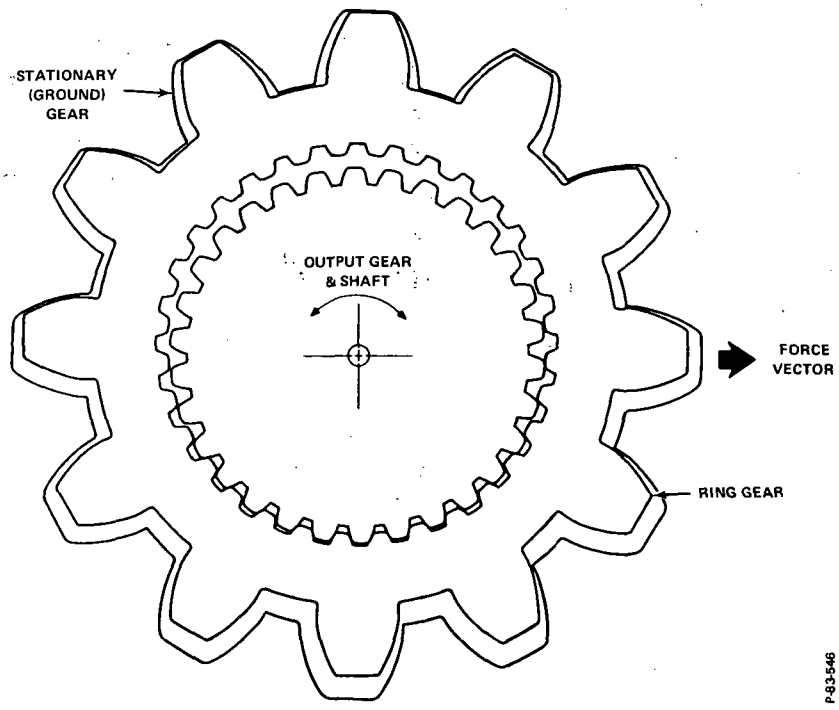

Figure 3-2 - Basic Mechanical Operation (Low-Ratio Transmission Configuration)

rated speed for the motor designs built on this program is less than 1000 rpm. The flightweight units have demonstrated no-load orbit vector speeds up to 6000 rpm.

The same holds true for the transmission, which does not have conventional input gears running at high pitch line velocities. The relative tooth velocities correspond to those found only in the last stage of a conventional transmission. The absence of high relative velocities improves the mechanical efficiency by reducing friction losses at high motor speed.

Another factor that is significantly reduced is actuator inertia. In conventional high-speed motors, the motor inertia resulting from a rotor mass rotating at high angular velocities has always limited the motor response capabilities. The extremely low inertia of the Dynavector motor results in a substantial improvement in dynamic response, when compared to a conventional rotary motor. For stepping operation, the low inertia enables the Dynavector motor to start the stop at high stepping rates with no lost pulses.

3.2.2 Transmission Design

The integral epicyclic transmission consists of the ring gear, the ground gear, and the output gear and shaft. The only input to the transmission is the rotating force vector of the Dynavector motor, which can be considered as a virtual planet member producing the required epicyclic motion of the ring gear.

In high-ratio versions of the Dynavector actuator, the ring gear rotates as it orbits. The ring gear has two different pitch diameters, with N_2 and N_3 teeth as shown in Figure 3-3. One pitch diameter engages with the ground or fixed gear and the second pitch diameter engages with the output gear on the output shaft. If the two meshes had equal pitch diameters, there would be no rotation of the output shaft with respect to ground; yet the ring gear could rotate freely. The ratio would then be infinite. By making the pitch diameters nearly equal, instead of equal, a very high ratio can be obtained with ease. The overall ratio is given by the formula

$$R = \frac{N_2 N_4}{N_2 N_4 - N_1 N_3} \qquad (3\text{-}1)$$

where

N_2 and N_3 = number of teeth in the two diameters of the ring gear

N_1 = number of teeth in the ground gear

N_4 = number of teeth in the output gear

N_1 meshes with N_2 and N_4 meshes with N_3. The ratio between ground and the ring gear (i.e., between the ring gear's orbiting and rotating speeds) is given by

$$R_R = \frac{N_2}{N_1 - N_2} \qquad (3\text{-}2)$$

The ratio between the ring gear and ground may easily be varied through a wide range, with little change in the basic ratio. Therefore, in designing the transmission, the eccentricity may be chosen first, setting R_R and N_1 and N_2. Then N_3 and N_4 may be chosen to provide the desired ratio. The procedure permits the use of a standard motor, having a given eccentricity, with any ratio transmission.

The transmission arrangement shown in Figure 3-3 is only one of four arrangements possible. The gears may be inverted from external meshes to internal, and vice versa, such that the output may be either a center output shaft or an outer housing hinge design, and either low-ratio or high-ratio configuration. The four transmission arrangements are shown in Figure 3-4.

These are differential transmissions, which have formerly been considered inefficient devices. However, the inefficiencies in conventional differential gearing result from the high pitch-line velocities of the input member and planet gears, which also are heavily loaded. These factors are not present in the Dynavector actuator. A rotating force vector is used in place of an input gear, and the pitch diameters of the ring gear are nearly equal to the pitch diameters of the reaction gears; therefore, no high velocities exist in the transmission.

An advantage of having the ring gear pitch diameter nearly equal to the mating gear pitch diameter is the high load capacity. Under load, many teeth come into contact as separation distances are very small and normal deflections quickly allow many teeth to share the load. This same feature provides high resistance to shock overloads and minimizes dynamic loading forces. The transmission has high torque transmitting capability because the dynamic loads are negligible and the static strength equals the dynamic strength. The tooth shape used is a standard 20-degree involute tooth profile, with tooth tips modified for smooth conjugate motion.

3.2.3 Electrical Design

Simple electromagnetic circuits are used in this section to describe the principles upon which operation of the Electric Dynavector Actuator is based. The MKS system of units is used in this section to simplify the equations.

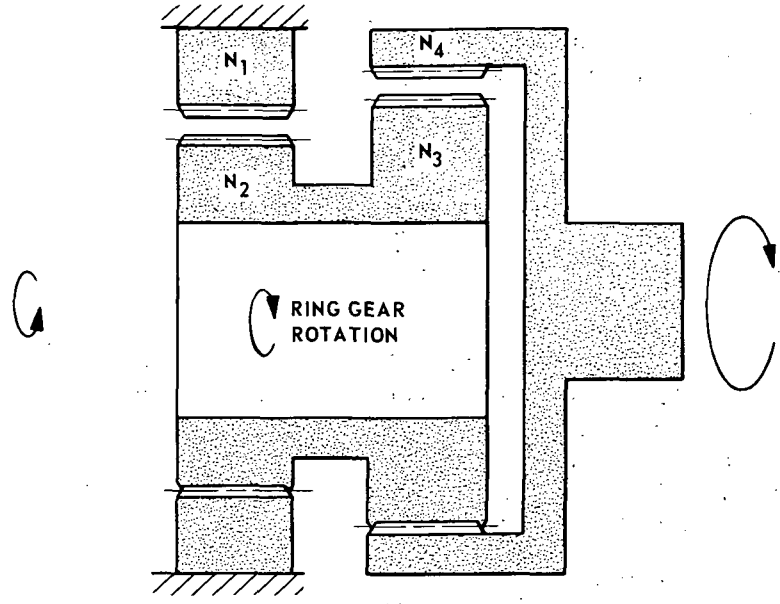

Figure 3-3 - Epicyclic Transmission Arrangement

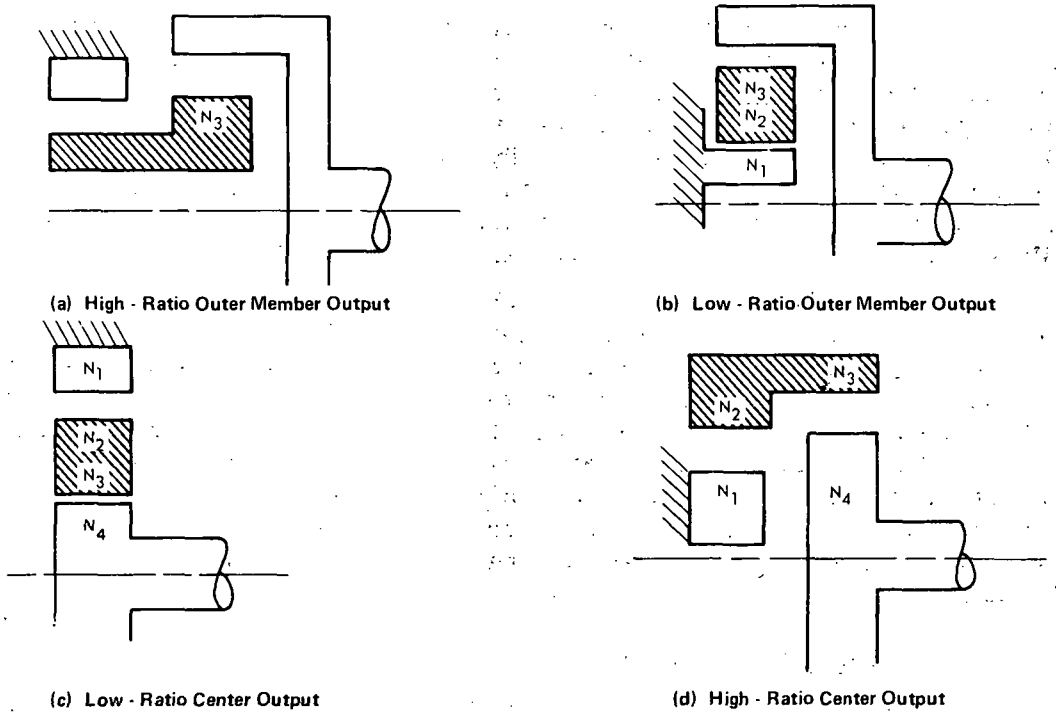

Figure 3-4 - Dynavector Actuator Epicyclic Transmission Arrangements

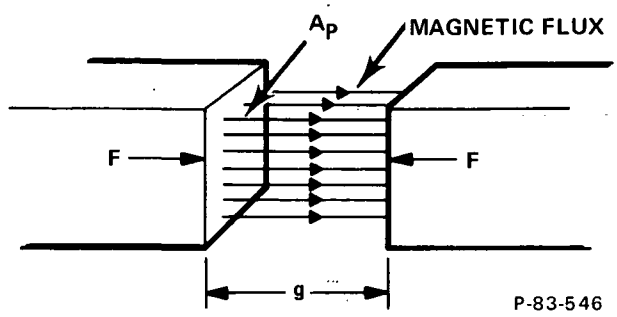

Figure 3-5 - Magnetic Poles Attractive Force Schematic

- Attractive Force Between Magnet Poles

The principle used to convert electrical energy into torque in the Electric Dynavector Actuator is illustrated in Figure 3-5. As shown in Figure 3-5. when magnetic flux crosses an air gap between two magnetic flux conductors, a force acts to pull the two magnetic conductors together. This force is proportional to the cross-sectional area of the conductor at the air gap, neglecting fringing, and to the square of the flux density. Changing the direction of magnetic flux flow does not change the force direction.

The reluctance, or resistance to magnetic flux flow, of the air gap between the magnetic conductors is given by

$$\mathcal{R} = \frac{g}{\mu_o A_p}, \quad \text{ampere turns/weber} \qquad (3\text{-}3)$$

where

A_p = pole face area, square meters

g = air gap length, meters

μ_o = permeability of space ($4\pi \times 10^{-7}$)

The force of attraction is proportional to the change in reluctance of the air gap per unit length, as shown by equation (3-4).

$$F = \frac{1}{2} \phi_a^2 \frac{d\mathcal{R}}{dg}, \quad \text{newtons} \qquad (3\text{-}4)$$

where

ϕ_a = magnetic flux crossing the air gap, webers

From equation (3-3)

$$\frac{d\,\mathcal{R}}{d\,g} = \frac{1}{\mu_o\, A_p}$$

The equation for force then becomes

$$F = \frac{1}{2\,\mu_o\, A_p}\,\phi_a^{\,2} \qquad (3\text{-}5)$$

- Torque

The torque of a rotating electromagnetic device is proportional to the change in reluctance of the air gap per unit of rotation. Thus

$$T = \frac{1}{2}\,\phi_a^{\,2}\,\frac{d\,\mathcal{R}}{d\,\theta}\text{ , newton meters} \qquad (3\text{-}6)$$

Motors that use this method of developing torque are often referred to as variable reluctance motors.

- Ampere Turns

Figure 3-6 shows a magnetic circuit and the equivalent electrical circuit. An iron ring with an air gap is shown. A coil is wound on the iron ring. The flux circulating in the iron ring is proportional to the number of ampere turns of current circulating around the ring. Changing the direction of the current changes the direction of the magnetic flux. The reluctance of the air gap is usually much greater than the iron reluctance. Therefore, the iron reluctance is usually omitted in the equations. When the iron becomes magnetically saturated, reluctance of the iron must be included in the equations.

Comparing with electrical circuits, reluctance is analogous to resistance, magnetic flux is analogous to current, and ampere turns are analogous to voltage. Thus, ohms law for magnetic circuits is

$$F = \mathcal{R}\,\phi_a = N\,i \qquad (3\text{-}7)$$

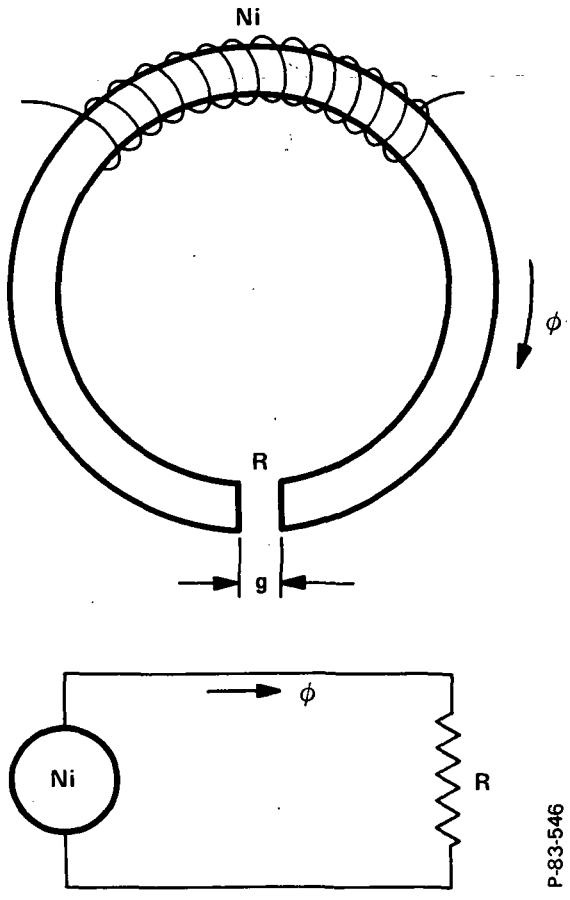

Figure 3-6 - Magnetic Circuit and Equivalent Electrical Circuit Schematic

where

F = number of ampere turns (magnetomotive force)

i = current, amperes

N = number of turns in coil

Magnetic flux equals magnetic flux density times pole face area. Thus

$$\phi_a = A_p B_a \qquad (3\text{-}8)$$

where

B_a = flux density in air gap, webers/square meter

Substituting equations (3-3) and (3-8) into (3-7) gives

$$N\,i = \frac{g}{\mu_o} B_a \tag{3-9}$$

Equation (3-9) gives the required number of ampere turns to produce flux density B_a across air gap g.

The greater the air gap length, the greater the number of ampere turns that are required to develop a given flux density.

- Back EMF and Inductance

When the flux is changing, a voltage is generated in the coil which is proportional to the rate of change of flux. The direction of this induced voltage is usually in the opposite direction to the applied voltage. In MKS units it is given by

$$E = N \frac{d\phi}{dt} \tag{3-10}$$

Substituting for ϕ from equation (3-7) gives

$$E = N \frac{d}{dt}\left(\frac{N\,i}{\mathcal{R}}\right) \tag{3-11}$$

$$E = K_e \frac{d\theta}{dt} + L \frac{di}{dt} \tag{3-12}$$

where

$K_e = -\left(\frac{N}{\mathcal{R}}\right)^2 i \frac{d\,\mathcal{R}}{d\,\theta}$, volt sec/meter

$L = \frac{N^2}{\mathcal{R}}$, henry (inductance)

The first term of equation (3-12) is called the back emf.

The coil supply voltage equals the sum of the voltage drop in the coil resistance and inductance, the back emf, and the voltage loss due to hysteresis and eddy currents. Thus

$$V = R\ i + K_e \frac{d\theta}{dt} + L \frac{di}{dt} + E_{eh} \qquad (3\text{-}13)$$

where

E_{eh} = voltage loss due to eddy currents and hysteresis

The magnetic circuit of the electric Dynavector motor is shown in Figure 3-1. The motor has eight stator poles and an iron ring armature. At any instant, when the motor is operating, one-half of the coils are on, and one-half are off. The magnetic flux paths are shown in Figure 3-1.

The coils are connected so that the direction of current circulation in adjacent coils is in opposite directions. Therefore, magnetic flux circulates between each adjacent pair of active poles. There is also some leakage flux that goes through the four inactive poles. However, since force is proportional to the square of the flux density, the force developed by the leakage flux is usually negligible.

The maximum possible torque is theoretically developed when the iron is saturated in all four active poles. However, the number of ampere turns required to saturate the pole with the largest air gap is excessive. Therefore, the motor is usually operated with only one or two poles saturated. Higher current is undesirable because of heating and control problems. An excessive number of turns will lower the motor speed, due to the high back emf and inductance, and will increase the motor size. The optimum number of turns is usually the maximum number of turns that will permit the motor to operate at the desired speed. The wire size must be large enough to prevent overheating.

The magnetic flux in a stator pole must decay rapidly to a low value when the coil is turned off, or negative torque will be developed. The material selected for the stator should have a low coercive force and high resistivity. The low coercive force will enable the air gap to lower the residual flux in the pole to a low value when the coil is turned off. A high resistivity, and laminated construction, will minimize the time for flux decay.

The material selected for the stator laminations was M-19 (transformer C). The coercivity of M-19 is 0.5 oersted, and the resistivity, 47 microhm centimeters. This material should be annealed after forming to develop the best magnetic properties.

The minimum air gap between the stator and armature should be as small as possible for maximum torque and efficiency. In the flight-weight units this airgap was 0.0017 inch for SN/1 and 0.0027 inch for SN/2.

The cross-sectional area of the iron in all parts of the magnetic circuit must be sufficiently great to permit the magnetic flux to pass without saturating. If the iron in any part of the magnetic circuit saturates, the flux crossing the air gaps will be limited, and therefore the torque will also be limited. Since the flux leaving a pole divides into two directions of travel, the cross-sectional area of the the armature,perpendicular to the direction of flux travel, should be about one-half of the cross-sectional area of the iron at the center of a coil. The minimum cross-sectional area at the stator outside diameter, perpendicular to the direction of flux travel, should be about the same as for the armature.

SECTION 4

ACTUATOR DESIGN

This section describes both the breadboard and flightweight actuator designs in regards to (1) actuator description, (2) mechanical design, and (3) electrical design.

4.1 ACTUATOR MODEL EH-818-U1 (BREADBOARD) DESCRIPTION

The assembly layout of the breadboard design as shown in Figure 4-1 indicates the assembly arrangement of the actuator that was sized to meet the performance requirements as defined in Section 3. Figures 4-2 and 4-3 are photos of the breadboard actuator hardware. The actuator was designed as a test article by which the performance characteristics of the actuator concept could be demonstrated. The actuator overall length from the mounting face of the mounting plate (Item 11, as shown in Figure 4-1) to the back cover of the actuator was 6.5 inches. The outside diameter at the stator section was 7.5 inches and at the mounting plate was 8.47 inches. The actuator weighed 56 pounds.

4.2 ACTUATOR MODEL EH-818-U2 (FLIGHTWEIGHT) DESCRIPTION

The assembly drawing for Model EH-818-U2 is shown in Figure 4-4. The unit weighs 35 pounds, has an overall length of 5.7 inches and a 7.5 inch outside diameter at the stator housing section. The interface design of the mounting flange corresponds to the specification requirements of paragraph L of Section 3.1 for the actuator housing (reference specification drawing X1872802). The design of the mounting pivot corresponds to the specification requirements for the mounting pivot member (reference specifications drawing X1872801).

Figure 4-5 is a photograph of the flightweight actuator stator housing with sensors installed and the orbiting ring gear assembly. Shown on the ring gear member are the rotor laminates and retaining sleeve which has been electron-beam welded to the ring gear to retain the laminates. The rotor is shown before the finish machining of the outside diameter and the end faces for the proper axial length.

Figure 4-6 shows the flightweight stator and coil assembly. The stator stack is 1.85 inches long and consists of approximately 132 laminants, each laminant being 0.014 inch thick. The coiles were machine-wound on the poles by the Bendix Electric Power Division, Eatontown, New Jersey. Each coil contains approximately 450 turns of AWG 22 wire.

Figure 4-7 is an exploded view of the output shaft mounting pivot and bearing preload assembly for the flightweight actuator.

REVISIONS				
SYM	ZONE	DESCRIPTION	DATE	APPROVAL

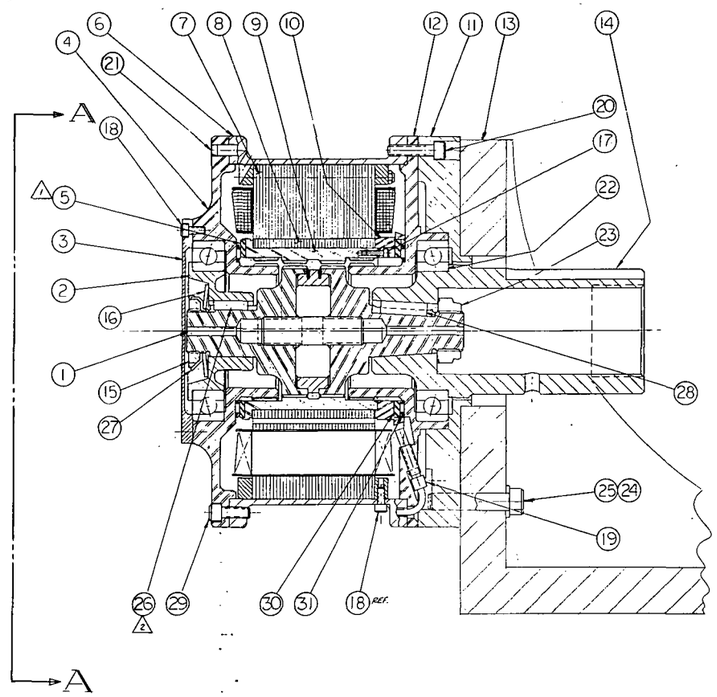

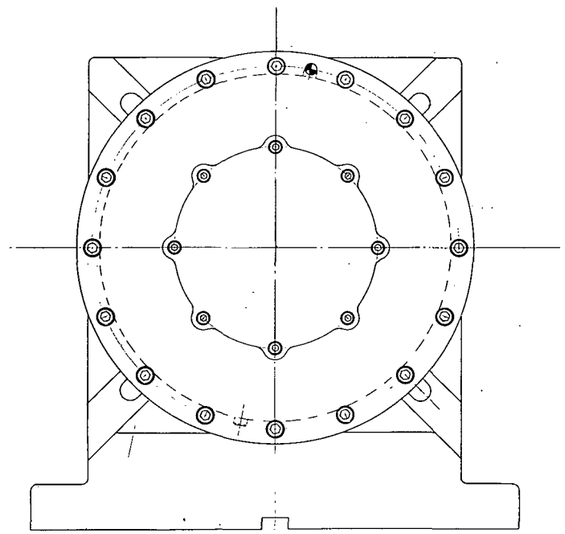

VIEW AA
REAR VIEW

QTY REQD	DWG SIZE	PART NO.	DESCRIPTION	MATERIAL DESCRIPTION & SPECIFICATION	CODE IDENT	ITEM NO.
2	-	STOCK	THRUST BRG	TORRINGTON # NTA-4860		31
1	-		RACE, THRUST BRG	TORRINGTON # TRD-4860		30
16	-		SCREW, SOC HD	.250-28 UNF-3A X .625 LG		29
1	-		KEY	.312 X .312 SQUARE X 1.00 LG		28
1	-		LOCKWASHER	WHITTET HIGGINS # WMS-172206		27
1	-		KEY	.187 X .187 SQUARE X .75 LG		26
4	-		SCREW SOC HD	.375-16UNC-3A X 1.75 LG		25
4	-		WASHER, LOCK	.375		24
1	-		NUT, SELF LOCKING	ESNA # 49NTE-184		23
1	-		BEARING BALL (DUPLEX RADIAL)	M.R.C #113KRDU		22
2	-		DOWEL	.250 DIA X .75 LG (.2501/.2503 DIA)		21
16	-		SCREW, SOC. HD.	.250-28UNF-3A X 1.00LG.		20
4	-		SENSING HEAD	ELECTRO PROD. LAB INC. MODEL # 4981		19
10	-		SCREW, SOC HD	#8-32 UNC-2A x .38 LG		18
6	-		SCREW, SOC HD	#4-40 UNC-3A x .38 LG		17
1	-	STOCK	SPRING WASHER	SCHNORR DISC SPRING #SD25.4-2 MM		16
1	B	2175543	NUT, LOCK	WHITTET HIGGINS # MS-172241		15
1	C	2175490	SHAFT, OUTPUT			14
1	E	4761309	BRACKET			13
1	D	2175502	GROUND GEAR			12
1	D	2175501	MOUNTING PLATE			11
1	C	2175491	END CAP, ROTOR LAMINATE			10
1	D	2175503	ROTOR RING GEAR			9
194	B	2175486	ROTOR LAMINATE			8
1	D	2175554	STATOR			7
1	D	2175505	HOUSING			6
1	B	2175568	THRUST WASHER			5
1	D	2175504	GROUND GEAR			4
1	C	2175434	COVER, BEARING			3
1	C	2175493	SUPPORT, BEARING			2
1	D	2175530	OUTPUT GEAR SUB ASSY			1

LIST OF MATERIAL

2175488

P-83-1911

Figure 4-1 - Assembly Drawing - Breadboard Model EH-818-U1

⚠2 ITEM 26 (KEY) TO BE PF INTO ITEM 1 (OUTPUT GEAR SUB ASSY) & SF WITH ITEM 2 (BEARING SUPPORT) REF.

⚠1 GRIND THICKNESS TO GIVE .001 TO .003 AXIAL CLEARANCE AT ASSY

UNLESS OTHERWISE SPECIFIED
- INTERPRET DRAWING IN ACCORDANCE WITH STANDARDS PRESCRIBED BY MIL-D-1000
- DIMENSIONS ARE IN INCHES
- DIMENSIONS TO BE MET AFTER PLATING
- MACHINED SURFACES TO BE SQUARE & PARALLEL TO DATUM A WITHIN .005 PER IN.
- MACHINED DIAMETERS TO BE CONCENTRIC WITH DATUM A WITHIN .005 T I R

TOLERANCES: DECIMAL X ± .040, XX ± .020, XXX ± .010; ANGLES ± 0° 30' EXCEPT SPECIFIED CHAMFER ± 10°

SURFACE FINISH MICROINCHES R H R

NEXT ASSY | FINAL ASSY | APPLICATION | CONTRACT NUMBER

DRAWN M.W.S. 7-9-76 | CHECKED | GROUP LEADER | LEC ENGR | MECH ENGR | REL & S A

APPROVED 7/11/76

APPROVED

BENDIX RESEARCH LABORATORIES
SOUTHFIELD, MICHIGAN

TITLE ASSEMBLY ELECTRIC DYNAVECTOR ROTARY ACTUATOR MODEL NO EH-818-U1

CODE IDENT NO. 11272 | SIZE E | d175488 | X-1

SCALE 1/1 | WT | SHEET

SENSIBLE ENGINEERING NOW STOPS ERRORS 2870-211-1 | DEPT NO. 830

"Page missing from available version"

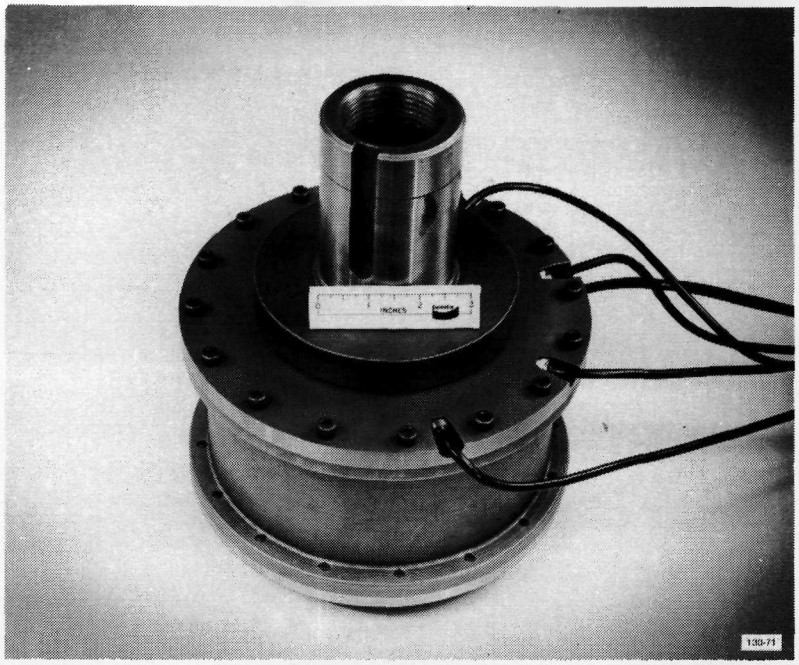

Figure 4-2 - Model EH-818-U1 Assembled

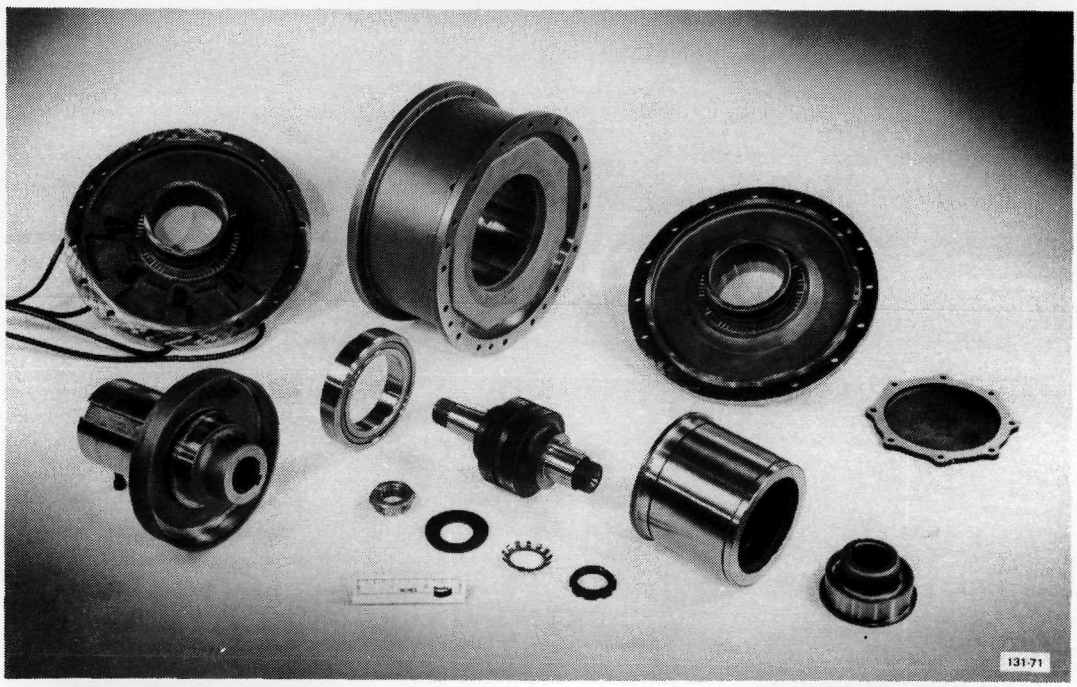

Figure 4-3 - Model EH-818-U1 Disassembled

"Page missing from available version"

REVISIONS				
SYM	ZONE	DESCRIPTION	DATE	APPROVAL
X3		ITEM 5 WAS 02176182 NOW 2176183 GEAR	7-22-71	
		ITEM 10 WAS 2 REQ'D		
X4		COILS CHANGED TO MATCH WITH DETAIL	8-25-71	
X5		ADDED ITEMS 20,21 & 22 - ADDED NOTE 2 ADDED CONNECTION DIAGRAMS	9-29-71 E.R.	
X6		TERMINAL NUMBERS REVISED ON THE SELF COMMUTATED MODE CONNECTION DIAGRAM	3-28-72	

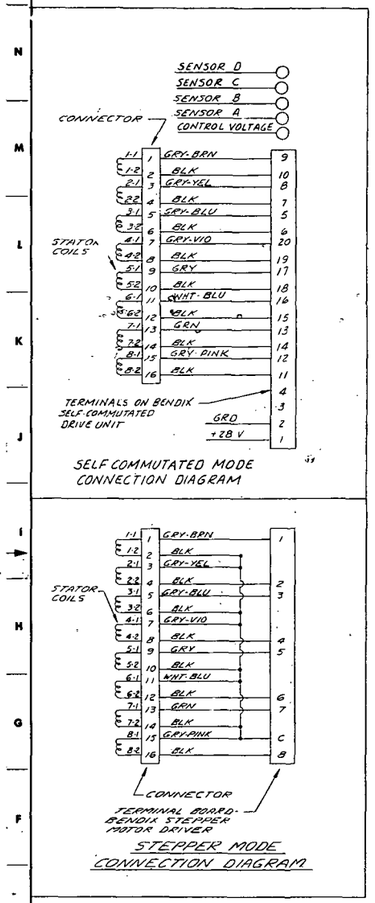

SELF COMMUTATED MODE CONNECTION DIAGRAM

STEPPER MODE CONNECTION DIAGRAM

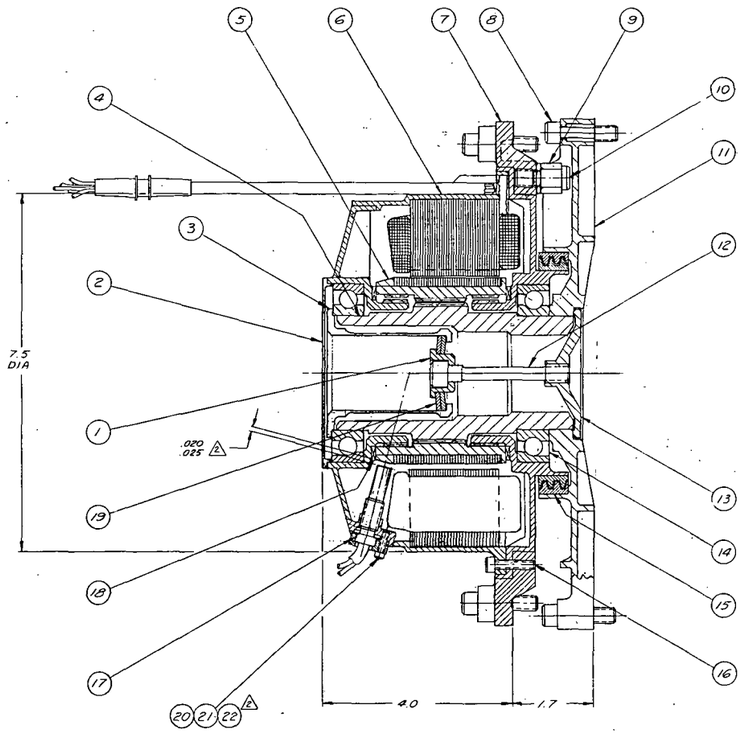

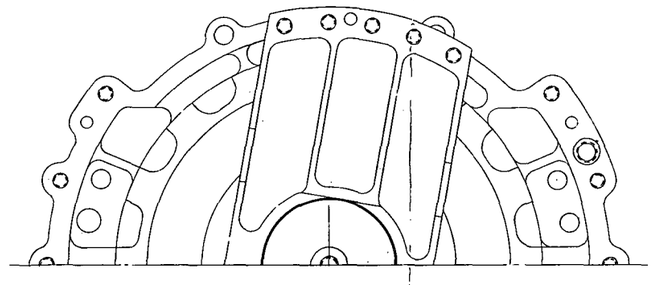

QTY REQD	DWG SIZE	PART NO.	DESCRIPTION	MATERIAL DESCRIPTION & SPECIFICATION	CODE IDENT	ITEM NO.
4	B	2176474	SPLIT WASHER			22
4	B	2176473	CLAMP SENSOR			21
8		STOCK	SCR, SOC HD	10-40 UNC-2A X .50 LG SST		20
2		STOCK	SPRING, DISC	SCHNOOR 40-204-2.0		19
2			BEARING, THRUST	TORRINGTON NTA 4860		18
4			SENSING HEAD	ELECTRO PROD. LAB INC MODEL #4943		17
14			SCREW SOC HD	#10-32 UNF-2A X .88 LG SST		16
1			CARTRIDGE TYPE LABYRINTH SEAL	SEALOL INC-1300 CLASS L110 X 130 X 15		15
2		STOCK	BEARING, ANGULAR CONTACT	FAFNIR 2MM 9112 WI-CR		14
1	B	2176218	PLATE, SPRING RETAINER			13
1	B	2176219	SCREW, SPRING RETAINER			12
1	D	2176217	PIVOT, MOUNTING			11
1	B	2176238	BUMPER POST			10
1	B	2176240	BUMPER RING			9
24	B	2176235	CAPTIVE SCREW			8
1	E	2176226	ACTUATOR MTG FLANGE			7
1	D	2176234	HOUSING & STATOR ASSY			6
1	C	2176210	ROTOR & LAMINATE ASSY			5
1	D	2176206	OUTPUT GEAR			4
1	C	2176220	HOUSING, DISC SPRING			3
1	C	2176239	COVER			2
1	B	2176222	ADAPTER, SPRING			1

LIST OF MATERIAL

2 GRIND SPLIT WASHERS (ITEM #22) TO OBTAIN DIMENSION INDICATED WHEN ROTOR IS AT IT'S CLOSEST POSITION RELATIVE TO SENSORS

1 GRIND O.D. AND ENDS OF ROTOR RING GEAR 02176189 AS DESCRIBED ON DETAIL DRAWING TO OBTAIN .001-.003 AXIAL AND RADIAL PLAY.

NOTE

UNLESS OTHERWISE SPECIFIED
- INTERPRET DRAWING IN ACCORDANCE WITH STANDARDS PRESCRIBED BY MIL-D-1000
- DIMENSIONS ARE IN INCHES
- DIMENSIONS TO BE MET AFTER PLATING
- MACHINED SURFACES TO BE SQUARE & PARALLEL TO DATUM A WITHIN .005 PER IN.
- MACHINED DIAMETERS TO BE CONCENTRIC WITH DATUM A WITHIN .005 T I R

TOLERANCES: DECIMAL X ± .040, .XX ± .020, .XXX ± .010; ANGLES ± 0°30' EXCEPT SPECIFIED CHAMFER ± 10°; SURFACE FINISH MICROINCHES R H R

DRAWN	R. Karlsen	4-1-71	BENDIX RESEARCH LABORATORIES, SOUTHFIELD, MICHIGAN
CHECKED			
GROUP LEADER			TITLE: FLIGHT WEIGHT ELECTRIC DYNAVECTOR ACTUATOR MODEL EH-818-U2
PROJ ENGR			
ENGR		4-1-71	
DESIGN ENGR			
R & A			
APPROVED		4-1-71	CODE IDENT NO. 11272 · SIZE E · 2176175 · X6
APPROVED			SCALE FULL · WT. 35 LBS · SHEET 1 of 1

NEXT ASSY | FINAL ASSY | APPLICATION | CONTRACT NUMBER

SENSIBLE ENGINEERING NOW STOPS ERRORS 2870-2114 · DEPT NO. 830

Figure 4-4 - Assembly Drawing - Flightweight Model EH-818-U2

"Page missing from available version"

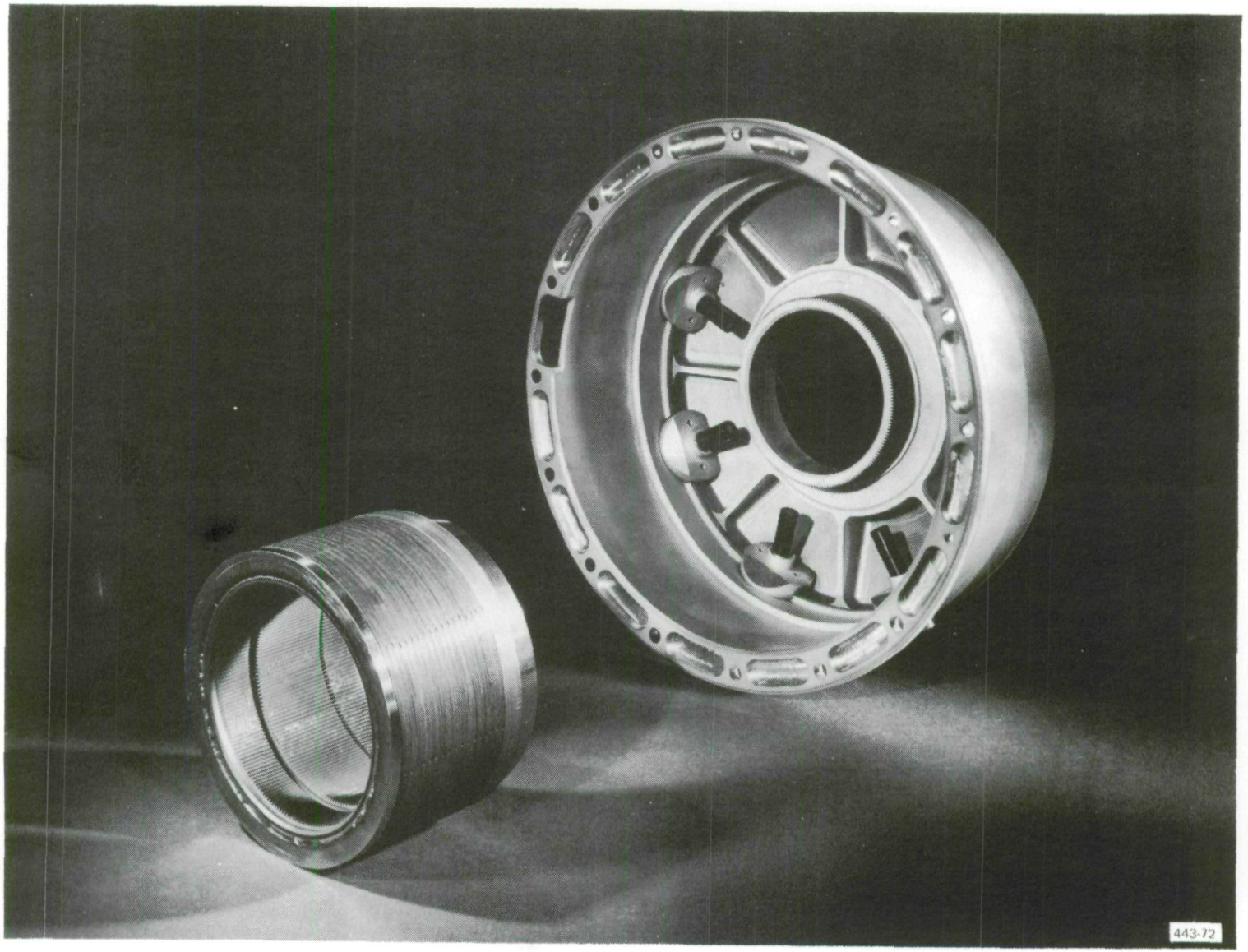

Figure 4-5 - Orbit Gear and Stator Housing (Flightweight)

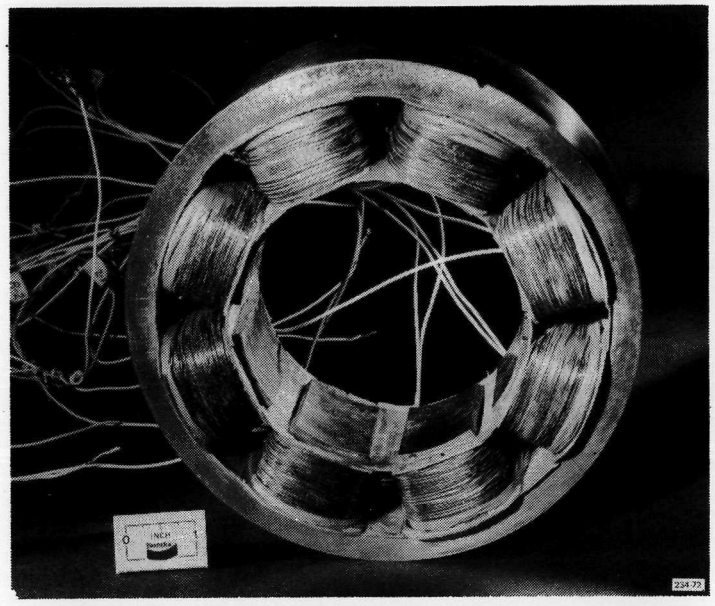

Figure 4-6 - Stator and Coil Assembly (Flightweight)

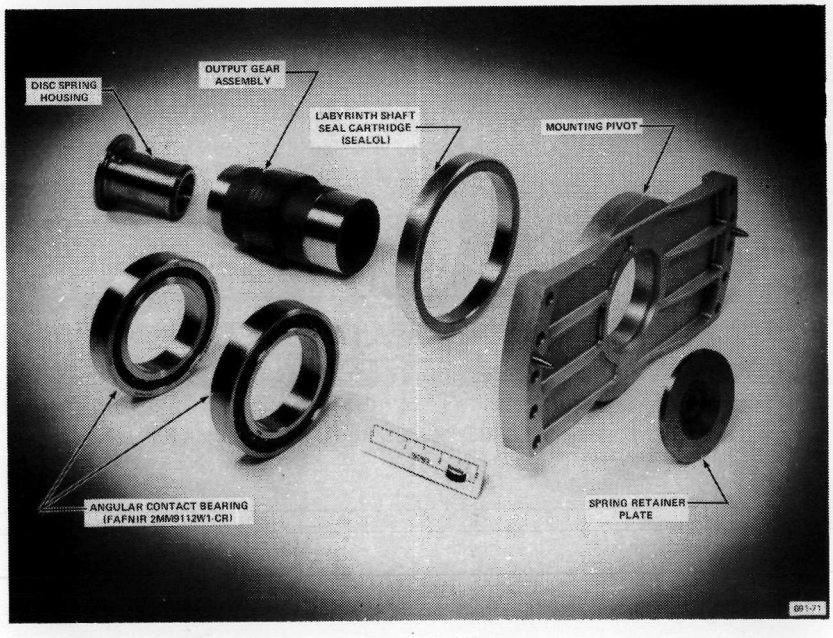

Figure 4-7 - Exploded View of Output Shaft, Mounting Pivot, and Bearing Preload Assembly

4.3 BREADBOARD ACTUATOR MODEL EH-818-U1 MECHANICAL DESIGN

The mechanical configuration for Model EH-818-U1 Breadboard actuator is shown in Figure 4-1.

- Mesh Alighment and Fit

The differential gear mesh was closely processed through fabrication, heat treat, finish machining and final assembly to insure absolute alignment and fit. In addition to conventional gear data such as AGMA class, dimension over or between wires, tooth finish, etc. specific design data obtained from mesh layouts including tooth tip shaping, depth of engagement, etc. was provided to the gearing manufacturer. To minimize tolerance accumulation due to involute profile error, tooth spacing, etc. each mating mesh pair, orbiting and stationary, was individually lapped at final assembly. The hand lapping was continued until each mesh attained the identical eccentricity and radial dropout measured in the other meshes. The select fit rotor-ring gear was marked for proper assembly.

- Bearing Concentricity and Internal Clearances

To insure bearing bore alignment the bores were jig ground into the ground gears at the same time and within the same basic machining setup. This procedure insured bore concentricity. The bearings were identified as datum diameters to which all gearing and pilot diameters were machined.

- Torsional Stiffness and Hysteresis

Torsional stiffness was obtained by (1) proper material selection, (2) minimizing the number of joints and components, (3) minimizing the length of the member of torsion, (4) designing each cross-section for maximum polar moment of inertia, (5) identically lapping the meshes to the same eccentricity and radial dropout, (6) minimizing radial deflections due to mesh loads, (7) reducing the mesh friction by increasing the load distribution, (8) increasing the mesh face width to reduce the contact stress, (9) optimizing the output gear pitch diameter to reduce the mesh load, and (10) minimizing the radial internal clearance in the assembly (pilots, etc.).

- Weight and Envelope Volume

The EH-818-U1 Dynavector motor weight is 56 pounds and the unit is 8.0 inches in diameter x 4.0 long.

4.3.1 Component Description

- Rotor-Ring Gear Assembly

The 818:1 rotor ring internal gear was fabricated from high strength, gall and wear resistant 18 Ni 350 maraging steel. This material has the capacity to operate at fatigue bending stress levels of ±100,000 psi and at temperatures between -65 degrees and 600°F when in the age hardened state (R_c 51-55).

The gears were nitrided to improve wear life. The depth of case penetration was 0.004/0.006 inch; the resulting surface hardness R_c 66-67; and the core is R_c 50-55 min. A process specification, "Combined Gas Nitriding - Aging Process for 18 N_i 350 Type Maraging Steel," for fabrication and heat treat of maraging steel has been established and is presented in Appendix E of Volume II.

The rotor laminates were stamped from 0.014 inch thick M-19 steel sheet stock, insulation coated and vacuum bonded into an assembly. The I.D. was lightly ground (to minimize stresses) for a shrink interference fit to the rotor ring gear blank. The laminate and rotor ring gear were finished machined and heat treated as an assembly to insure mesh concentricity with the rotor O.D. During the nitriding-age hardening cycle the rotor O.D. was masked to prevent carbon formation buildup in the electro-magnetic circuit. A light grind of the rotor O.D. and light mesh lap after heat treat was completed as required.

- Output Shaft

To insure alignment and torsional rigidity, the output gear was fabricated as a two piece tapered assembly. The material was type 18 N_i 350 maraging steel and the heat treat was similar to that described for "Rotor-Ring Gear." The wall cross section were determined from a torsional and bending stress analysis and are of adequate thickness to insure optimum torsional and bending rigidity at rated conditions over the required life duty cycle.

- Stator Laminate and Housing S.A.

The eight pole stator was fabricated from stamped 0.014 inch thick M-19 steel sheet stock, insulation coated and vacuum bonded into an assembly. The stator O.D. and was lightly ground (to minimize stresses) for a shrink interference fit to the outboard ground gear assembly. The stator I.D. was machined (after shrink fit) concentric to the outboard ground gear bearing bore to provide 0.001/0.002 running clearance with the orbiting rotor ring gear. (The stator coils, wire size AWG 25, 650 turns, were installed prior to shrink fit.)

- Outboard Ground Gear

The outboard ground gear was fabricated from an 18 Ni 350 grade maraging steel and the heat treat was similar to that described for "Rotor Ring Gear." During fabrication and heat treat, the bearing bore was the datum reference diameter to which the gearing, stator assembly and aligning dowels were machined.

- Inboard Ground Gear Assembly

The inboard ground gear material, fabrication and processing was identical to the outboard ground gear.

- Output Shaft Bearings

The output shaft bearing are series 9112 and series 211W Precision Class 7 angular contact Bearings. The bearings are preloaded to approximately 1200 pounds. (A precision class 7 bearing is machined to within 0.0003 inch runout between the races.) A Dupont grease, Krytox® was used to pack the bearings prior to assembly.

- Labyrinth Seal

The output shaft of the actuator was sealed with a preassembled cartridge type "Sealol - Mini Maze® seal." The seal is made from two precision, dissimilar metal rings that are permanently and perfectly matched (outer aluminum ring is cast around the inner steel ring). V-shaped grooves with controlled gap between the groove faces provide torturous flow path for the fluid media. Seal assembly requires an interference fit between both the outer and inner diameter and the mating output and inboard ground gears.

- Bearing Preload Mechanism

The bearing preload mechanism consists of a disc spring, ground at assembly bearing preload ring, and disc spring housing. The disc spring housing was designed to slide on the output gear as the bearing is preloaded. Its threaded end adapts to an assembly fixture and the entire preload mechanism rotates at output speed.

4.3.2 Factors Affecting Actuator Design Material Selection

- Materials

The following material combinations for the rotor ring gear and the output gear members were evaluated:

Rotor Ring Gear

(1) 9310 steel - carbonitrided

(2) Nitroloy N steel - hardened and nitrided

(3) Nitroloy N steel - nitrided only

(4) 18 Ni 350 Maraging Steel

(5) Composite S.A. - M-19 steel laminates bonded together and close fit on a gear member that is to be fabricated from one of the materials described in Items (1) through (4).

Output Gear

(1) 1020 steel - carbonitrided

(2) Nitroloy N steel - hardened and nitrided

(3) Nitroloy N steel - nitrided only

(4) 18 Ni 350 maraging steel age hardened and nitrided.

The mechanical properties of materials were readily available whereas their electromagnetic properties were not. Therefore, a series of magnetic tests to measure field strength as a function of ampere turns have been conducted on the candidate material samples listed above and are presented in Figure 4-8. The samples were tested in an annealed state and as shown, 1020 steel exhibits the best magnetic properties and maraging steel the worst. As a result, a composite rotor containing M-19 steel laminate bonded to maraging steel gear was selected and successfully test in the breadboard design.

- Heat Treat

For optimum wear resistance, gears fabricated from the candidate materials required a hardened case. Carburizing was considered and rejected because it increases the carbon content of the parent material and high carbon steels are poor electromagnets. Nitriding is preferred because the presence of carbon is minimized and a thinner case depth can be specified. Metallurgy has indicated that Nitroloy N with its low carbon content should maintain good electromagnetic properties and develop a 0.005/0.006 inch case depth. All nitriding grade steels contain aluminum and for maximum surface hardness, (R_C 70 approximately), they should be quenched and tempered prior to nitriding. If a lower surface hardness is acceptable, R_C 58 to 60, the quench and temper cycles can be omitted. Omitting the hardening cycle improves the materials magnetic properties because the grain size rearrangement common during hardening does not occur.

The nitriding process produces a brittle white layer which is undesirable. The white layer formation must be controlled specifying a "floe process" nitriding procedure. This process by controlling the rate of nitrogen formation and hardening of the material controls the amount of white layer surface formed - usually 0.0001 to 0.0003 inch maximum.

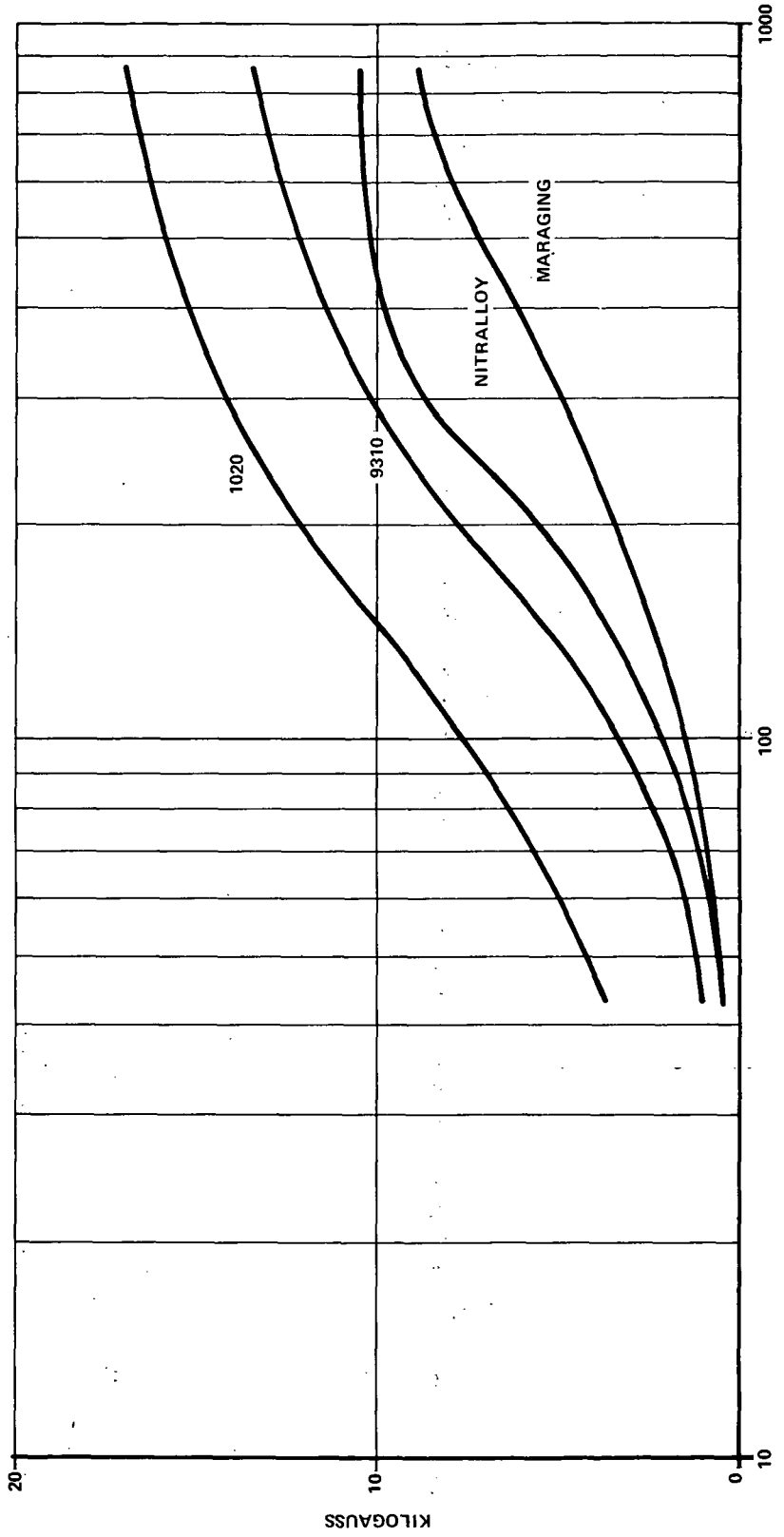

Figure 4-8 - Magnetic Curves of Candidate Gear Materials

Low carbon steel, such as AISI 9310, cannot be nitrided because it does not contain aluminum. It can, however, be carbonitrided, and the amount of carbon in the carbon-ammonia gas used to harden the steel can be minimized to reduce carbon impregnation during heat treat. As in nitriding, the steel will possess better electro-magnetic properties after heat treat if the quench and temper cycle is omitted prior to carbon nitriding.

18 Ni 350 maraging steel is a high strength tough material, but it has poor electromechanical properties. It cannot, therefore, be used to fabricate a one piece rotor ring gear. When bonded to a M-19 laminated steel ring, the resulting rotor ring gear composite provides the best features of both materials. That is, good magnetic characteristics coupled with high wear resistance at the gear surface.

- Summary

The breadboard design was fabricated using nitrided maraging grade steels for all gearing and structural (except stator housing) members. Nitroloy N, although acceptable, was not stable during sample part heat treat. As a result, it became evident that a finish grid would be required. The rotor ring gear cannot be finish ground because of insufficient space for grind wheel run-out at the step diameter where the ground meshes junction with the output mesh.

4.3.3 Gear Mesh Design

Model EH-818-U1 overall transmission ratio is 818:1. Mesh design parameters are shown in Table 4-1.

Table 4-1 - Mesh Design Parameters

Transmission ratio	818:1
Eccentricity (inch)	3/64
Diametral pitch	64
Difference in number of teeth	6
No. teeth (output gear)	179
No. teeth (ground gear)	186
No. teeth (output gear) (orbiting)	185
No. teeth (ground gear) (orbiting)	192

- Transmission Ratio

The overall transmission ratio is sized at 818:1 to minimize the magnitude of the reflected inertia to the output, which is a function of the ratio squared.

- Eccentricity

The 3/64 inch motor eccentricity was selected for optimum motor torque performance.

- Diametral Pitch

The 64 diametral pitch was selected from mesh layout for optimum rolling action.

These interrelated constraints, ratio, eccentricity, diametral pitch, require that the difference in number of teeth between meshes be 6.

- Mesh Wear Characteristics

The mesh wear characteristics are determined by the PV value of the mesh, where P is defined as the hertz contact stress, psi, and V is the sliding velocity, ft/min.

A detailed mesh wear analysis is presented in Appendix C of Volume II. The results are summarized as follows:

Total Number of Teeth Driving the Load	16
Most Highly Loaded Teeth	11 & 12
P Valve (psi)	67,800 and 62,010
$\mathring{X}$ Value (ft/min)	7.04 & 7.71
Maximum PV Value	477,000 psi ft/min

4.3.4 Transmission Ratio Analysis

The transmission ratio analysis is determined as follows:
Required: T.R. is to be 818:1 and eccentricity, e, at 3/64 inch.
Given:

$$e = \frac{\Delta N}{2\ DP} \qquad (4\text{-}1)$$

where

ΔN = difference in number of teeth between meshes

DP = diametral pitch

Solve for N from (4-1) gives;

$$\Delta N = 2\ (DP)\ e$$

$$= (2)\ (64)\ (3/64)$$

$$\Delta N = 6 \text{ teeth}$$

NOTE: $3 < \Delta N < 6$ provides a good working mesh with a large wrap angle without extreme tooth modifications.

Let

$$N_4 = 179 \text{ teeth (No. teeth on output gear)}$$

and

$$\Delta N = 6$$

then

$$N_3 = 179 + 6 = 185 \text{ teeth (No. of mating teeth on ring gear)}$$

The transmission ratio solution which satisfies the mesh design shown in Figure 4-1 is:

$$T.R. = \frac{N_2\ N_4}{N_1\ N_3 - N_2\ N_4} \qquad (4\text{-}2)$$

$$N_4 = 179$$

$$N_3 = 185$$

T.R. 818

Substituting: in (4-2) to find N_1 gives;

$$818 = \frac{179\ N_2}{185\ N_1 - 179\ N_2}$$

and given

$$N_2 = N_1 + 6$$

then:

$$818 = \frac{179\ (N_1 + 6)}{185\ N_1 - 179\ (N_1 + 6)} = \frac{179\ N_1 + 1074}{6\ N_1 - 1074}$$

Solving for N_1

$$6\ N_1 - 1074 = \frac{179}{818}\ N_1 + \frac{1074}{818}$$

$$N_1 \left(6 - \frac{179}{818}\right) = 1074 \left(1 + \frac{1}{818}\right)$$

$$N_1 \left(\frac{4908 - 179}{818}\right) = 1074 \left(\frac{819}{818}\right)$$

$$N_1\ (4729) = (819)\ (1074)$$

$$N_1 = \frac{(819)\ (1074)}{4729}$$

N_1 = 186 (No. teeth in stationary ground gear)

given

$$N_2 = N_1 + 6$$

then

$$N_2 = 192 \text{ (No. mating teeth in orbiting ring gear)}$$

And the pitch diameters are found from N/DP

$$N_1 = \frac{186}{64} = 2.90625$$

$$N_2 = \frac{192}{64} = 3.00000$$

$$N_3 = \frac{185}{64} = 2.89063$$

$$N_4 = \frac{179}{64} = 2.79688$$

4.3.5 Actuator Stiffness and Mechanical Hysteresis

The factors which determine the effective actuator stiffness include:

(1) material
(2) number of joints and components
(3) length of torsion member
(4) section polar inertia
(5) mesh fit
(6) radial deflections
(7) mesh friction
(8) mesh contact stress (face width)
(9) tooth loading and deflection
(10) internal clearances

- Material

The primary material used in the breadboard design was high strength 18 Ni 350 maraging steel.

- Number of Joints and Components

One mechanical joint between the ground gears is required, three mesh joints lapped as one unit, (output and two ground gears) are required between the orbiting and stationary members.

- Length of Torsional Members

The longest torsional member is the output gear and is 6.1 inches. Its section inertia was designed for maximum torsional (solid shaft) rigidity.

- Section Inertia

The sectional inertia of all torsional members was designed for maximum torsional rigidity and bending stiffness.

- Mesh Fit

The meshes was hand lapped to fit as one joint and their radial play was limited to 0.002 inch maximum.

- Radial Deflection

The section modulus of all load carrying members was designed to insure minimum radial deflections (less than 0.001 inch).

- Mesh Contact Stress

The stall torque mesh contact stress is 110,000 psi maximum for the most highly loaded tooth.

- Internal Clearances

The EH-818-U1 design was machined as a unit assembly whenever possible, concentricities between mating halves (pilot diameter, bearing diameters, etc.) were controlled to within 0.0002 inch. The total cumulative concentricity error (runout) did not exceed 0.0006 inch TIR at the output shaft when the unit is run at rated condition.

- Torsional Analysis

A torsional analysis of Model EH-818-U1 breadboard actuator design is presented in Appendix B of Volume II. A summary of component torsional displacement (windup) at 1200 in-lb torque is presented below.

Description	Windup, Arc-Minutes
Output gear	1.10
Outboard ground gear and flange	0.071
Rotor ring gear	0.014
Inboard ground gear	0.108

The cummulative actuator windup to ground is 1.22 arc minutes.

- Output Gear Beam Deflection Analysis

At rated conditions the radial deflection of breadboard Model EH-818-U1 is 1×10^{-4} inch.

- Mesh Hysteresis

Test (Section 6) results obtained during power on hysteresis testing of breadboard Model EH-818-U1 at 1200 in-lb load conditions indicate a 3 arc-minute windup. Of this, 1.2 arc-minutes are attributed to structural windup (shaft, rotor, ground gear, etc.) and 1.8 to the differential mesh interface.

- Bearing Life

The bearing life analyses are presented in Appendix A of Volume II. At rated conditions and with a 1130 pound spring preload the following B-10 life has been predicted.

Outboard Bearing #2MM9112

B-10 life = 2.5×10^6 hours

Inboard Bearing #2MM211W1

B-10 life = 7.3×10^6 hours

4.4 FLIGHTWEIGHT ACTUATOR MODEL EH-818-U2

The mechanical configuration for Model EH-818-U2 flightweight actuator design is shown in Figure 4-4.

The mechanical design characteristics, including component description, material selection, transmission ratio analyses and results, mesh wear (PV) characteristics, are identical to breadboard actuator Model EH-818-U1 described in Section 4.3. Design modifications incorporated into the flightweight configuration and not discussed in Section 4.3 are as follows.

- Pivot and Mounting Flange

An aluminum output pivot and a mounting flange were designed and fabricated to satisfy flightweight configuration installation requirement shown in Figure 4-4. To minimize overall weight and eliminate the torsional windup of a long output gear, these aluminum members were designed for a shrink fit assembly to the mating steel components.

The design parameters which defined the amount of interference fit required at the dissimilar metal joints were:

1. capacity to transmit 5000 in-lbs at 158°F
2. capacity to withstand the induced tangential stress which occur at -40°F operation.

A detailed analysis is presented in Appendix F of Volume II and the results are summarized below.

Output Pivot	
Required 70°F assembly diametral interference	0.0039 inch
Tensile stress at -40°F	18,450 psi

Mounting Flange	
Required 70°F assembly diametral interference	0.0052 inch
Tensile stress at -40°F	13,200 psi

- Output Shaft Bearings

The flightweight actuator's inboard bearing was changed from Series 211W to Series 9112. (The outboard bearing, Series 9112, remains the same size). This modification was incorporated with NASA approval to facilitate assembly and optimize the actuators weight and volume.

- Torsional Analysis

A complete torsional analysis of the flightweight design is presented in Appendix B of Volume II. A summary of component torsional displacement is presented below:

Description	Windup-arc Minutes
Output gear	0.41 arc minutes
Outboard ground gear	0.189 arc minutes
Rotor ring gear	0.065 arc minutes
Inboard ground gear	0.189 arc minutes

The total cumulative actuator windup to ground at 1200 in-lbs output torque is 0.680 arc minutes. This design value is 56 percent the design value of the breadboard design.

- Mesh Hysteresis

Test results obtained during power on hysteresis testing of flightweight Model EH-818-U2 (Section 6) at 1200 in-lb load conditions indicate a 4 arc minute (nominal) windup. Of this, 0.68 arc minutes are attributed to structural windup and the 3.3 arc minutes difference is attributed to mesh interface and reduced stator torque capacity, a result of changing the stator length from 2.6 inches to 1.8 inches.

- Bearing Life

The bearing life analyses are presented in Appendix A of Volume II.

At rated conditions and with a 1130 pound spring preload, the following B-10 life has been predicted. For Inboard and Outboard Brg. No. 9112 the B-10 Life = 2.5×10^6 hours.

- Stator Assembly

Correlation analyses of the test data and the breadboard electrical stator design indicated that the performance requirements could be satisfied with a shortened stator configuration on the flightweight actuator design Model EH-818-U2 providing the coil wire size was increased from #25 wire to #22 wire. A larger wire diameter reduces the induced back emf at rated speed thereby allowing more current to flow through the stator pole. As a result, the output torque is increased even though the pole face area is reduced with the shortened stator. Analyses indicated the stator length could be reduced from 2.60 inches to 1.80 inches without loss of performance. This modification would result in a substantial weight saving. It was predicted, and later confirmed, that the flightweight actuator design (including aluminum mounting flange and output pivot mounting) weight would be 35 pounds which is 62.5 percent of the 56 pound breadboard actuator weight.

4.5 ACTUATOR ELECTRICAL DESIGN ANALYSES

The electrical design equations which are derived in this section are based on the electromagnetic circuits described in Section 3.2.3. MKS units are used for most of the derivations. The design equations are then converted to IPS units (inches-pounds-seconds).

The following simplifying assumptions are made for the design equations.

- The air gap length is constant across a pole face. The value at the center of the pole face is used for the constant value.
- Flux density is constant across a pole face.
- The effect of flux fringing can be neglected.

The nomenclature used in the electrical design equations is as follows:

A_p = pole face area, in^2

B_a = air gap flux density, gausses

F = force, lb

g = air gap length, cm

H_i = magnetizing force of iron, oersteds

i = current, amps

L_i = length of iron in magnetic circuit, cm

N = number of turns

c = minimum air gap, in.

e = eccentricity, in.

θ = angular displacement from minimum air gap, deg

$\mathcal{R}$ = reluctance, ampere turns/weber

μ_o = permeability of space

η_t = torque efficiency

4.5.1 Electrical Design Equations

The torque equation may be derived as follows; the air gap length is approximately given by

$$g = c + e\ (1 - \cos\ \theta) \tag{4-3}$$

Substituting for g in the equation which relates the reluctance to the air gap [reference equation (3-3)] gives;

$$\mathcal{R} = \frac{g}{\mu_o\ A_p} = \frac{c + e}{\mu_o\ A_p} - \frac{e\ \cos\ \theta}{\mu_o\ A_p} \tag{4-4}$$

$$\frac{d\ \mathcal{R}}{d\ \theta} = \frac{e}{\mu_o\ A_p}\ \sin\ \theta \tag{4-5}$$

The ideal torque developed on the armature by a single pole is given by

$$T_a = \frac{1}{2}\ \phi_a^{\ 2}\ \frac{d\ \mathcal{R}}{d\ \theta} \tag{4-6}$$

where ϕ, the magnetic flux crossing the pole face, is given by

$$\phi_a = B_a\ A_p \tag{4-7}$$

Substituting equations (4-5) and (4-7) into (4-6) gives

$$T_a = \frac{B_a^{\ 2}\ A_p}{2\ \mu_o}\ e\ \sin\ \theta$$

$$T_a = F\ e\ \sin\ \theta \tag{4-8}$$

where

F = force developed by the single pole.

The total output torque for four active poles is given by

$$T_o = \eta_t R e (F_1 \sin \theta_1 + F_2 \sin \theta_2 + F_3 \sin \theta_3 + F_4 \sin \theta_4) \quad (4\text{-}9)$$

$$T_a = \eta_t F_r e \sin \theta_r \quad (4\text{-}10)$$

where

F_r = resultant force vector, pounds

θ_r = angle of resultant force vector from the point of minimum air gap, degrees

η_t = torque efficiency

If the force is in pounds and the eccentricity is in inches, the torque calculated by equations (4-9) or (4-10) will be in-lb.

Converting the pole force [reference equation (3-5)] to IPS units (in-lb-sec) gives, for the force developed by one magnetic pole,

$$F = 5.78 \times 10^{-7} B_a^2 A_p, \text{ lb}$$

Test results indicate that the actual force is about 65 percent of the theoretical force. Using a 0.65 correction factor gives

$$F = 3.75 \times 10^{-7} B_a^2 A_p, \text{ lb} \quad (4\text{-}11)$$

Test results indicate that the coupling efficiency of a coil is about 65 percent. Using this efficiency factor, and converting units, from the analysis of Section 3, equation (3-9) becomes

$$B (2.54 g) = 0.65 \times 0.4\pi Ni \quad (4\text{-}12)$$

The relationship between the flux density at the pole face, and in the core at the center of the coil, is given by

$$B_a = \frac{A_c}{A_p} B_c \qquad (4\text{-}13)$$

where

A_c = cross-sectional area of core, in^2

B_c = flux density in core, gauss

The flux density in the core cannot exceed the saturation value of the magnetic material. The flux density in the air gap will be somewhat lower than the saturation value for the magnetic material, if the pole face area is larger than the area of the core.

- Summary of Electrical Design Equations

Force of a single pole

$$F = 3.75 \times 10^{-7} B_a^{\,2} A_p, \text{ lb} \qquad (4\text{-}11)$$

Air gap flux density

$$B_a = \frac{A_c}{A_p} B_c, \text{ gauss} \qquad (4\text{-}13)$$

Ampere turns (saturation neglected)

$$B_a (2.54\ g) = 0.65 \times 0.4\pi\ Ni \qquad (4\text{-}12)$$

Motor output torque

$$T_o = \eta_t R e (F_1 \sin \theta_1 + F_2 \sin \theta_2 + F_3 \sin \theta_3 + F_4 \sin \theta_4), \text{ in-lb.} \qquad (4\text{-}9)$$

The equations summarized above are theoretical. In order to size the stator for actual operating conditions, tests were conducted on several electromagnet configurations to establish a correlation between the theoretical equations and actual performance. The theoretical equations were modified to include empirical correction factors as follows;

$$B_a\, g = K_1\, (0.4\pi\, Ni - H_i\, L_i) \qquad (4\text{-}14)$$

$$F = K_2 \times 5.78 \times 10^{-7}\, B_a^{\,2}\, A_p \qquad (4\text{-}15)$$

The empirical factor K_2 was found to be 0.65 for all configurations tested. K_1 was found to be highest when the coils are as close to the air gap as possible. For this configuration K_1 equals 0.65 for flux density values up to about 11,000 gausses, and decreases for higher values. Since the peak air gap flux will be 11,000 gausses for this motor, a constant value of 0.65 can be used for K_2.

4.5.2 Stator Torque Characteristics

The following analysis shows how the torque performance of the breadboard actuator was predicted from the analysis of a selected stator design.

For a stator length of 2.6 inches and pole core width of 0.9 inch, the pole core area is;

$$A_i = 0.9 \times 2.6 = 2.34\ in^2$$

Similarly, the pole face area is;

$$A_p = 1.325 \times 2.6 = 3.45\ in^2$$

When the core is saturated, the flux density in the core should be about 16,000 gauss. The flux density at the pole face is then

$$B_p = \frac{A_i}{A_p} \times B_s = \frac{2.34}{3.45} \times 16{,}000 = 11{,}000\ \text{gauss}$$

At rated speed and torque the magnetizing force is

$$Ni = 630 \text{ turns} \times 0.9 \text{ amp} = 567 \text{ ampere turns}$$

The air gap flux density, B_a, is given by

$$B_a = \frac{K_1}{2.54\ g} (0.4\pi\ Ni - H_i\ L_i) \leq 11{,}000 \text{ gauss}$$

where the air gap length is given by [reference equation (4-3)]

$$g = c + e\ (1 - \cos\theta), \text{ in.}$$

and

c = clearance = 0.005 in.

e = eccentricity = 0.048 in.

H_i = magnetizing force loss in iron, oersteds

L_i = length of iron, cm

K_i = empirical factor determined by test (0.65)

The calculated flux density curve is shown in Figure 4-9. The output torque was calculated by two methods. The first method considers the flux density as constant over the pole face, and equal to the value at the center of the pole.

The force developed by a pole has been determined by test to be given by equation (4-11)

$$F = 3.75 \times 10^{-7}\ A_p\ B_a^2, \text{ lb.}$$

The poles are active from zero to 180 degrees. The four active poles are considered to be at 0, 45, 90, and 135 degrees. From Figure 4-9. the air gap flux densities are

$$B_{a1} = 11{,}000 \text{ gauss}$$

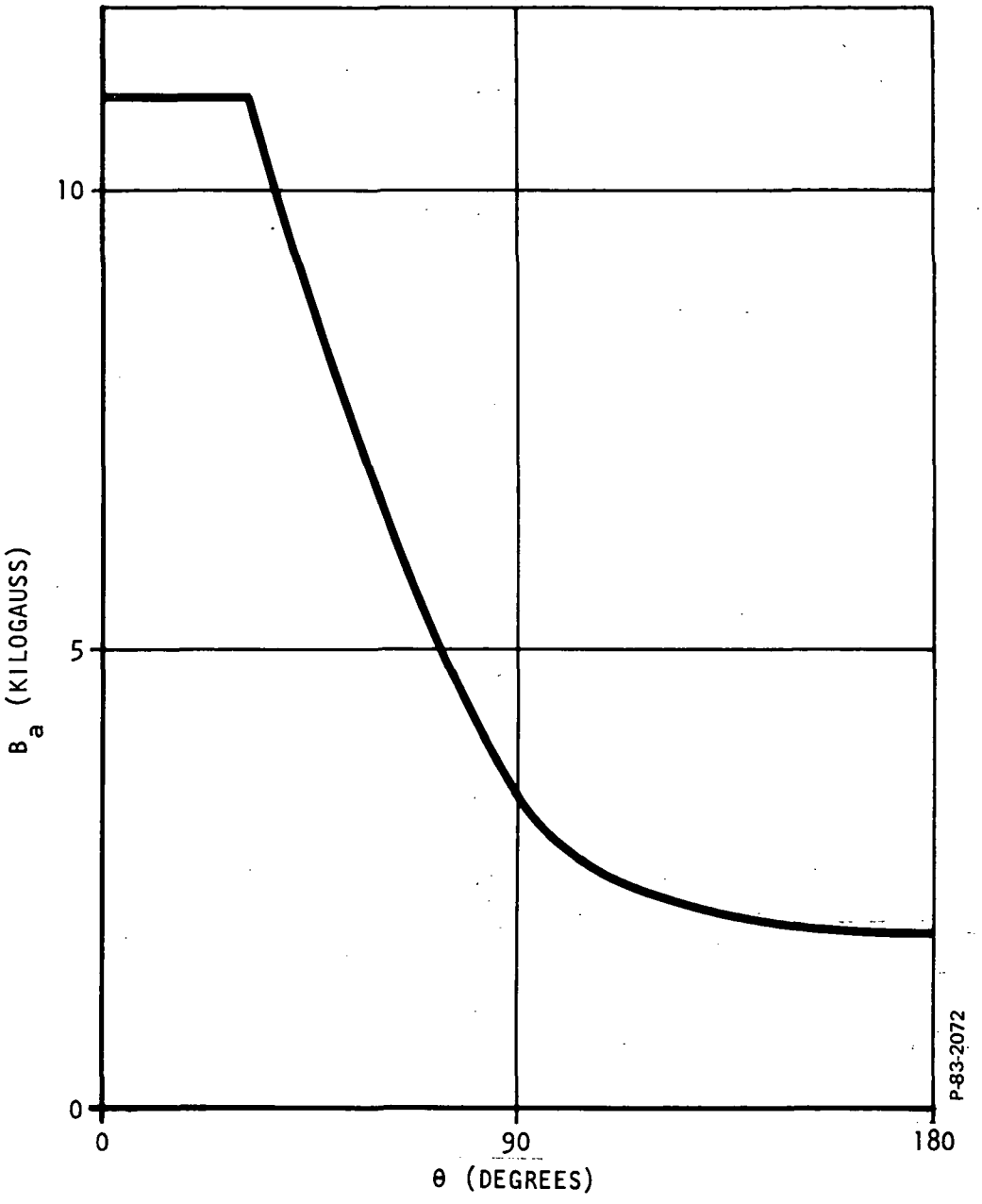

Figure 4-9 - Theoretical Air Gap Flux Density

$$B_{a2} = 8{,}900 \text{ gauss}$$

$$B_{a3} = 3{,}300 \text{ gauss}$$

$$B_{a4} = 2{,}100 \text{ gauss}$$

The force vectors are then

$$F_1 = 3.75 \times 10^{-7} \times 3.45 \times (11{,}000)^2$$
$$= 1.29 \times 10^{-6} \ (11{,}000)^2 = 156 \text{ lb.}$$

$$F_2 = 1.29 \times 10^{-6} \ (8{,}900)^2 = 102 \text{ lb.}$$

$$F_3 = 1.29 \times 10^{-6} \ (3{,}300)^2 = 14.1 \text{ lb.}$$

$$F_4 = 1.29 \times 10^{-6} \ (2{,}100)^2 = 5.7 \text{ lb.}$$

The torque is given by equation (4-10) as

$$T = \eta_t \ e \ R \ \Sigma \ F \sin \theta$$

where

η_t = mechanical efficiency (0.65 percent)

R = transmission ratio (818)

Thus

$$T = 0.65 \times 0.050 \times 818 \ (102 \sin 45° + 14.1 \sin 90° + 5.7 \sin 135°)$$

$$= 2400 \text{ lb-in}$$

The torque should be the same when the four active poles are at 45, 90, 135, and 180 degrees. When these poles are at the intermediate position of 23, 68, 113, and 158 degrees

B_1 = 11,000 gauss

B_2 = 5,500 gauss

B_3 = 2,400 gauss

B_4 = 1,900 gauss

F_1 = 156 lb

F_2 = 39 lb

F_3 = 7.45 lb

F_4 = 4.65 lb

T = 234 ft-lb

The torque may be calculated by a second method which considers incremental stator areas given by

$$\Delta A = 0.8\, W_r\, \Delta\theta \qquad (4\text{-}16)$$

where

W = stator width, in.

r = radius, in.

$\Delta\theta$ = incremental angle, radians

The torque resulting from the force developed by a single incremental area is

$$\Delta T = \eta_t \, e \, R \left[3.75 \times 10^{-7} \, \Delta A \, B_a^{\,2} \sin \theta \right] \qquad (4\text{-}17)$$

The output torque is obtained by summation of the incremental torques. Thus

$$T = \eta_t \, e \, R \times 3.75 \times 10^{-7} \, Wr \, \Sigma \, B_a^{\,2} \sin \theta \, \Delta\theta \qquad (4\text{-}18)$$

The torque obtained by this method was 3050 lb-in.

4.5.3 Stator Fabrication Techniques

The stator and rotor laminates were made of M-19 electrical sheet steel. The laminates were stamped, annealed, and bonded with Chrysler Chemical Division Cycleweld #55-9 using a locating fixture to maintain proper alignment. An indexing notch was rotated throughout the stack to provide uniform magnetic properties.

After bonding, the outside diameter of the stator was ground. The housing then heated to 350°F and the stator inserted in the housing, using a fixture to assure correct alignment. After the shrink-fit assembly, the inside diameter of the stator was ground. The rotor laminates were assembled on the rotor with a shrink fit using a similar procedure.

Raychem No. 44/0411/22-9 hookup wires were then soldered to the magnet wires, with Essex Wire No. F 28112 sleeving covering the solder joint. The coils and hookup wire were tied with lacing cord and impregnated with Shell Compound EPON No. 828 epoxy resin and activator No. 2.

4.5.4 Stator Flux Tests

After completing the fabrication of the breadboard stator, a test armature was fabricated with the same outside diameter, cross-sectional area, and material as the motor armature. Tests were conducted to determine the flux densities in the stator and armature. Calculations were then made to predict the forces and output torque. It was concluded that the required stall torque of 200 ft-lb could be obtained with this stator.

A sensing coil was fabricated by cementing 3 turns of magnet wire to a plastic sheet. The center was cut out to permit placing the sensing coil over the stator poles. Other sensing coils were wound

on the stator and armature as shown in Figure 4-10. A Rawson type 504 fluxmeter was used to measure the magnetic flux. The change in fluxmeter reading divided by the number of turns in the sensing coil equals the change in magnetic flux enclosed by the coil. An external switch was used to switch the current on and off as required for taking flux measurements. A diode and capacitor were used to prevent switch arcing.

Coils 1 through 4 were excited with 0.9 ampere. Flux measurements were taken at the test points indicated in Figure 4-10. The flux density equals the total flux divided by the cross-sectional area of the iron, in square centimeters. The flux density values are presented in Table 4-2.

Table 4-2 - Flux Density Values (kilogauss)

B_{a1}	5.85	B_{a7}	0.045	B_{i2}	7.55
B_{a2}	8.80	B_{a8}	0.18	B_{i3}	10.20
B_{a3}	9.15	B_{s1}	13.95	B_{i4}	1.82
B_{a4}	6.30	B_{s2}	14.35	B_{i5}	3.64
B_{a5}	0.38	B_{s8}	6.30	B_{86}	2.27
B_{a6}	0.15	B_{i1}	9.30	B_{i7}	2.73
				B_{i8}	4.08

When coils 1 through 4 are excited, the armature should contact the stator at the mid point between poles 2 and 3. Figure 4-11 shows the theoretical curve of air gap flux density versus air gap length. Also shown in Figure 4-11 are the measured values of flux density at poles 1 through 4, at the calculated mean air gap lengths for these poles. The flux densities at poles 1 and 4 correlate very closely with the theoretical values. The flux densities at poles 2 and 3 are about 20 percent lower than predicted. This loss of flux is probably due to iron losses being higher than predicted. The highest flux density is in the outer ring of the stator. This flux density, and the resulting iron loss should be lowered considerably when the stator is placed in the housing, as the housing can then carry part of the magnetic flux.

The following calculations, based on the flux density curve shown in Figure 4-11 with lower saturation value, indicate that this stator is capable of producing the required 200 ft-lb stall torque.

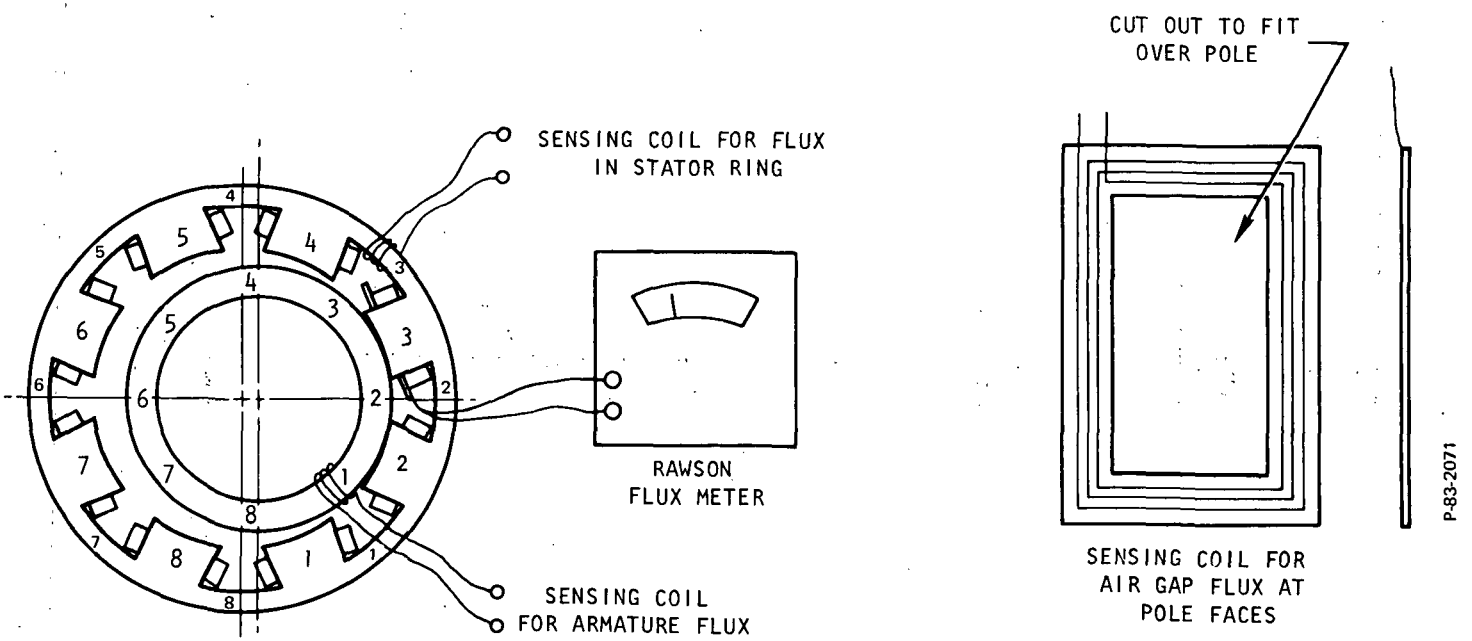

Figure 4-10 - Test Setup for Stator and Armature Flux Measurements

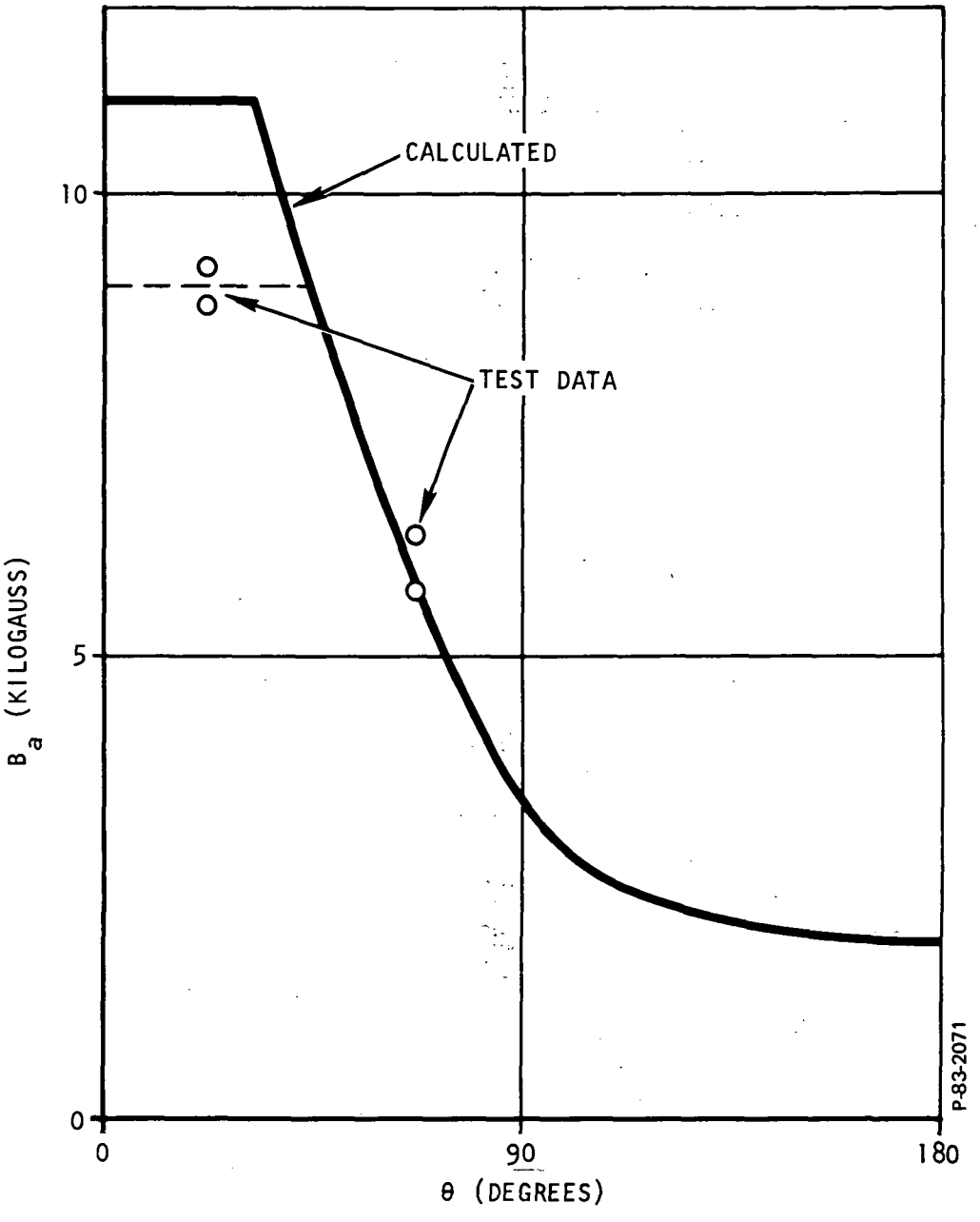

Figure 4-11 - Experimental Air Gap Flux Density

The air gap flux densities with the four active poles at 0, 45, 90, and 135 degrees, from Figure 4-11, are

$$B_{a1} = 9{,}000 \text{ gauss}$$

$$B_{a2} = 9{,}000 \text{ gauss}$$

$$B_{a3} = 3{,}300 \text{ gauss}$$

$$B_{a4} = 2{,}100 \text{ gauss}$$

The force developed by a pole has been shown by tests to be given by

$$F = 3.75 \times 10^{-7} A_p B_a^2, \text{ lb}$$

where

A_p = pole face area (3.45 in^2)

B_a = air gap flux density, gauss

The force vectors developed by poles 1 through 4 are then

$$F_1 = F_2 = 3.75 \times 10^{-7} \times 3.45 \times (9{,}000)^2 = 105 \text{ pounds}$$

$$F_3 = 14.1 \text{ pounds}$$

$$F_4 = 5.7 \text{ pounds}$$

The predicted peak torque, assuming 65 percent mechanical efficiency, is

$$T = \eta_t R_e (F_2 \sin 45° + F_3 + F_4 \sin 135°)$$

$$= 0.65 \times 818 \times 0.050 (105 \times 0.707 + 14.1 + 5.7 \times 0.707)$$

$$= 2450 \text{ in-lb}$$

$$2450 \div 12 = 204 \text{ ft-lb}$$

The minimum torque should occur when the active poles are at approximately 23, 68, 113, and 158 degrees. The calculated torque at this position is 190 ft-lb. This is 5 percent below the required torque of 200 ft-lb. However, the increased in flux expected with the housing in place around the stator, and with thestator inside diameter ground, should increase the torque to the required value.

4.5.5 Stator Coil Characteristics

The available input power at rated speed and torque is 100 watts, with 28 VDC supply. At stall, with 28 VDC supply, and continuous coil excitation, the input power will be 200 watts, at stall, the total current is

$$200 \text{ watts} \div 28 \text{ volts} = 7.15 \text{ amps}$$

The current per phase is

$$I = 7.15 \div 4 = 1.8 \text{ amps}$$

The estimated drop across the power transistors of the controller is 1.25 volts. The voltage available to the motor coils is then

$$V = 28 - 1.25 = 26.75 \text{ volts}$$

The required coil resistance is thus

$$R = V \div I = 26.75 \div 1.8 = 14.8 \text{ ohms}$$

Based on a layout analysis of the stator laminate design, the cross-sectional area of space available for coil windings is

$$A_c = 0.328 \text{ in}^2$$

The length of wire per turn is

$$L = 0.724 \text{ feet}$$

AWG 25 magnet wire was selected for the motor coils. The resistance of this wire is 32.37 ohms per 1000 feet. The required length of magnet wire per coil is thus

$$14.8 \text{ ohms per coil} \div 0.03237 \frac{\text{ohm}}{\text{ft}} = 456 \text{ feet}$$

The number of turns per coil is

$$N = 456 \text{ feet} \div 0.724 \frac{\text{ft}}{\text{turn}} = 630 \text{ turns}$$

This number of turns will provide the required flux density, as shown in the stator design calculation. The required space for this number of turns is

$$630 \text{ turns} \div 2475 \frac{\text{turns}}{\text{in}^2} = 0.254 \text{ in}^2$$

The required space for the next largest wire size (AWG 24) is greater than the 0.328 in^2 available space, therefore AWG 25 magnet wire was used for the breadboard motor coils. Since a weight reduction was necessary for the flightweight design, analyses showed the coil could be redesigned for AWG 22 wire of 450 turns, thereby reducing the stator length from 2.6 to 1.85 inches.

4.5.6 Coil Inductance Analysis

Based on the coil characteristics established in the previous section, an equation was derived for the inductance of the motor coils. This inductance can be shown to vary with air gap length, and with the permeability, or flux density, of the magnetic material. Tests were conducted to measure the inductance at various air gap lengths, with low and high magnetic flux density. The calculated inductance values were shown to correlate closely with measured values.

The theoretical response of a coil to a step voltage input at rated speed was plotted. The current reaches the required value of 0.9 ampere in 80 degrees of rotation from the position of maximum air gap. The poles at less than 90 degrees from the position of maximum air gap have little effect on the torque. Therefore, the coil response was considered to be adequate. The motor drive unit was therefore required to apply a constant voltage to the coils until they reach the required current. Pulse width modulation will then limit the current to the desired value. Provision was made for incorporating the required circuit in the motor drive unit.

Flux density equals the product of permeability and magnetizing force.

$$B_i = \mu_i H \tag{4-19}$$

where

B_i = flux density in iron, webers/m^2

H = magnetizing force, ampere turns/m

μ_i = permeability of iron

Magnetic flux equals flux density, times area

$$\phi = A_i B_i = \mu_i A_i H \tag{4-20}$$

where

A_i = cross-sectional area of iron, m^2

ϕ = magnetic flux, webers

The magnetizing force equals the ampere turns minus the air gap loss divided by the length of magnetic circuit.

$$H = \frac{1}{\ell_i} \left(Ni - \frac{g}{\mu_o A_p} \phi \right) \tag{4-21}$$

where

A_p = pole face area, m^2

g = air gap length, m

i = current, amperes

ℓ_i = length of magnetic circuit, m

N = number of turns

μ_o = permeability of space ($4\pi \times 10^{-7}$)

Combining equations (4-20) and (4-21) and rearranging terms gives

$$\phi = \frac{\mu_i A_i}{\ell_i} \left(Ni - \frac{g}{\mu_o A_p} \phi \right) \tag{4-22}$$

$$\phi = \frac{Ni}{\frac{g}{\mu_o A_p} + \frac{\ell_i}{\mu_i A_i}} \tag{4-23}$$

The flux linkages are given by

$$\psi = N \phi = \frac{N^2 i}{\frac{g}{\mu_o A_p} + \frac{\ell_i}{\mu_i A_i}}$$

Inductance equals the change in flux linkages divided by the change in current.

$$L = \frac{d\psi}{di} = \frac{N^2}{\frac{g}{\mu_o A_p} + \frac{\ell_i}{\mu_i A_i}}$$

Thus, the inductance varies with both air gap length and permeability of the magnetic material. At the instant when a coil is switched on, the air gap is at its maximum value, and the permeability is low. Thus the inductance is low. As the armature orbits, g decreases and μ_i increases, thus increasing the inductance. When the iron becomes saturated, μ_i becomes very small. Thus, at the instant of switching the coil off, inductance is low. The inductance increases as the flux density drops.

The air gap lengths of single poles are as follows:

Vector Angle (deg)	Gap (in)	Gap (m)
0	0.005	1.27×10^{-4}
45	0.0196	4.97×10^{-4}
90	0.055	1.4×10^{-3}
180	0.105	2.67×10^{-3}

The air gap length which must be used for inductance calculations is the combined, or total air gap length around the magnetic circuit.

Permeability is the ratio of flux density to magnetizing force.

$$\mu_i = \frac{B_i}{H}, \frac{\text{webers}}{m^2} \times \frac{m}{\text{amp turns}}$$

Permeability is usually given in units of gauss/oersted. The conversion of units is as follows:

$$\text{gauss} \times 10^{-4} = \text{webers}/m^2$$

$$\text{oersteds} \div 4\pi \times 10^{-3} = \text{amp turns}/m$$

$$\mu_i = B_i \text{ (gauss)} \times 10^{-4} \times \frac{4\pi \times 10^{-3}}{H \text{ (oersteds)}}$$

$$\mu_i = \mu_o \times \frac{B \text{ (gauss)}}{H \text{ (oersteds)}}, \frac{\text{webers}}{\text{amp turns m}}$$

where

$$\mu_o = 4\pi \times 10^{-7}$$

Permeability values for M19 magnetic sheet steel are as follows:

$$\mu_i = 2.5 \times 10^{-3} \text{ (very low flux density)}$$

$$\mu_i = 9.36 \times 10^{-3} \text{ (peak value)}$$

$$\mu_i = 6.3 \times 10^{-4} \text{ (at 15,000 gauss)}$$

Values of the other constants are as follows:

$$A_i = 1.52 \times 10^{-3} \text{ m}^2$$

$$A_p = 2.22 \times 10^{-3} \text{ m}^2$$

$$\ell_i = 0.2 \text{ m (except as noted)}$$

$$N = 650 \text{ turns}$$

- Maximum Air Gap - Low Flux Density

At low flux density, the return path for magnetic flux would be through the pole with minimum air gap, since this is the path of least resistance. The effective air gap is thus the sum of the maximum and minimum air gap lengths.

$$g = 2.67 \times 10^{-3} + 0.13 \times 10^{-3} = 2.8 \times 10^{-3} \text{ m}$$

The length around the magnetic circuit is

$$\ell_i = 0.52 \text{ m}$$

The inductance is then

$$L = \frac{650^2}{\frac{2.8 \times 10^{-3}}{4\pi \times 10^{-7} \times 2.22 \times 10^{-3}} + \frac{0.52}{2.5 \times 10^{-3} \times 1.52 \times 10^{-3}}}$$

$$L = \frac{4.23 \times 10^5}{10 \times 10^5 + 1.37 \times 10^5} = 0.37 \text{ hy}$$

The measured value was 0.35 henry.

- Maximum Air Gap - High Flux Density

The theoretical inductance at the maximum air gap with high flux density is 0.27 henry. No measurements were made due to the difficulty of holding the rotor at this position.

- Minimum Air Gap - Low Flux Density

The effective air gap is the sum of the values at zero and 45 degrees.

$$g = 5.1 \times 10^{-3}$$

The inductance is

$$L = \frac{650^2}{\frac{5.1 \times 10^{-3}}{4\pi \times 10^{-7} \times 2.22 \times 10^{-3}} + \frac{0.20}{2.5 \times 10^{-3} \times 1.52 \times 10^{-3}}}$$

$$L = 1.8 \text{ hy}$$

The measured value was 1.87 henry.

- Pole at 90 Degree Position - High Flux Density

At high flux density, most of the flux will circulate between adjacent poles. Therefore, the effective gap is taken to be twice the value at 90 degrees.

$$g = 2.8 \times 10^{-3}$$

The inductance is

$$L = \frac{650^2}{\frac{2.8 \times 10^{-3}}{4\pi \times 10^{-7} \times 2.22 \times 10^{-3}} + \frac{0.2}{6.3 \times 10^{-4} \times 1.52 \times 10^{-3}}}$$

$$L = 0.35 \text{ hy}$$

The measured inductance value was also 0.35 henry.

Thus, very good correlation exists between theoretical and measured values of inductance. The effective inductance will be taken to be 0.35 henry, as this value is for the mean operating position.

- Effect of Inductance

The current response of coil to a step voltage input is given by

$$I = \frac{V}{R_c} (1 - e^{-t/\tau}) \text{ , amperes} \qquad (4\text{-}26)$$

where

R_c = coil resistance, ohms

t = time, sec

τ = coil time constant (L/R_c), sec

Equation 4-26 can be expressed in terms of electrical rotation (θ) by the following substitution:

$$t = \frac{\theta}{360\ n} \tag{4-27}$$

where

n = electrical or vector speed, rev/sec

θ = electrical angle, deg

Thus

$$I = I_o\left(1 - e^{\frac{R_c}{L} \cdot \frac{\theta}{360n}}\right) \tag{4-28}$$

where, for 100 percent modulation (full on)

$$I_o = \frac{V}{R_c}$$

at the rated speed

$$n = \frac{1\ \text{rev}}{\text{min}} \times \frac{1}{60}\ \frac{\text{min}}{\text{sec}} \times 8.8\ \text{ratio} = 13.6\ \text{rev/sec}$$

$$\frac{R_c}{L} \cdot \frac{1}{360\ n} = \frac{14.8}{0.35} \cdot \frac{1}{360 \times 13.6} = 0.00865$$

The theoretical curve of current versus time is shown in Figure 4-12.

- Inductance Measurement

The test setup for inductance measurement is shown in Figure 4-13. When the switch is closed, a step voltage input is applied to the series combination of coil and resistor. The transfer function for the voltage across resistor R_1 is

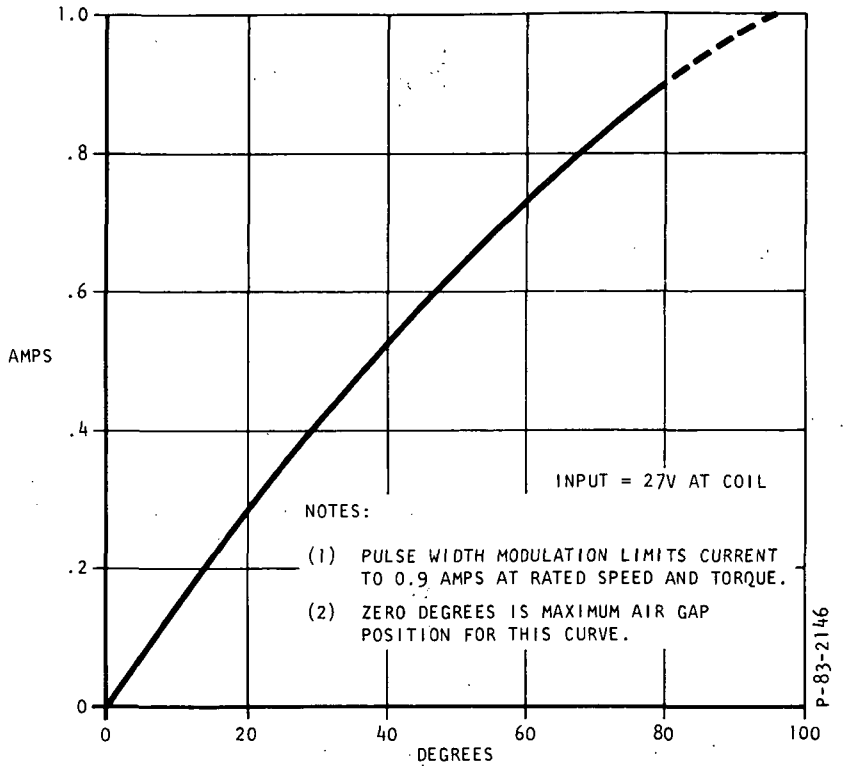

Figure 4-12 - Theoretical Response of Coil to a Step Voltage Input at Rated Speed

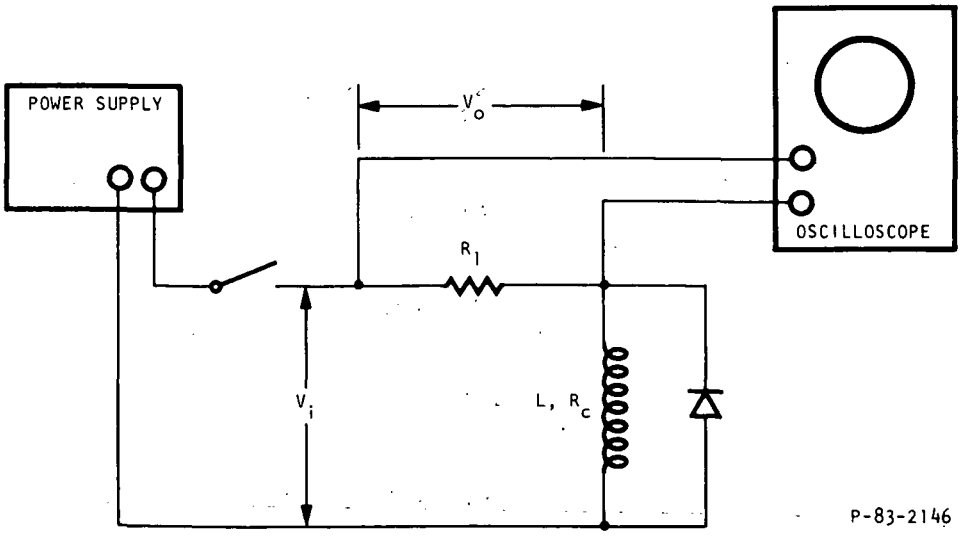

Figure 4-13 - Test Schematic for Inductance Measurement

$$V_o = \frac{R_1}{R_1 + R_c} \frac{V_i}{1 + \tau s} \qquad (4\text{-}29)$$

where

$$\tau = \frac{L}{R_1 + R_c}, \text{ sec}$$

R_c = coil resistance, ohms

V_i = input voltage, volts

τ is the time required for voltage V_o to reach 63 percent of its final value.

Plastic shims were used to establish the desired air gaps between the active pole and rotor.

- Test Results

(Zero Gap - Low Flux Density)

$$\tau = 0.075 \text{ sec}$$

$$R_1 + R_c = 25 \text{ ohms}$$

$$L = \tau \times (R_1 + R_c) = 1.87 \text{ hy}$$

(Maximum Gap - Low Flux Density)

$$\tau = 0.014 \text{ sec}$$

$$L = 0.014 \times 25 = 0.35 \text{ hy}$$

(0.054 inch Air Gap - High Flux Density)

For this test, three coils were excited with a constant current of 0.9 amperes each. The fourth coil was switched on and off for inductance measurement. The results were

$$\tau = 0.014 \text{ sec}$$

$$L = 0.35 \text{ hy}$$

4.5.7 Power Consumption Analysis

At rated speed and torque, the output power is

$$P_o = 150 \text{ ft/lb} \times \frac{2\pi}{60} \frac{\text{rad}}{\text{sec}} \times 1.357 = 21.3 \text{ watts}$$

The power loss in the coil resistance is

$$4 \text{ active phases} \times (0.9 \text{ amps})^2 \times 14.8 \text{ ohms} = 48 \text{ watts}$$

The power consumption of the motor controller and commutator was estimated to be 10 watts. The combined stator and armature iron weight is about 15 pounds. The estimated core loss at 60 Hertz, from M-19 data sheet, is

$$15 \text{ lb.} \times 2 \frac{\text{watts}}{\text{lb.}} = 30 \text{ watts}$$

The frequency at rated speed is

$$1 \frac{\text{rev}}{\text{min}} \times \frac{1}{60} \frac{\text{min}}{\text{sec}} \times 818 \text{ ratio} = 13.6 \text{ Hz}$$

The core loss varies as the square of frequency. Thus, this loss is

$$30 \times \left(\frac{13.6}{60}\right)^2 = 1.5 \text{ watt}$$

The power available at rated speed and torque is 100 watts. The power available for mechanical loss in the bearings and transmission is

$$100 - (21.3 + 48 + 10 + 1.5) = 19.2 \text{ watts}$$

The required mechanical efficiency is thus

$$\frac{21.3}{21.3 + 19.2} \times 100 = 53\%$$

4.6 FREQUENCY RESPONSE ANALYSES FORMAT

The block diagram of the motor and inertia load is shown in Figure 4-14. The transfer function is

$$\frac{T}{T_c} = \frac{J}{\partial T/\partial\theta} \frac{S}{1 + \frac{J}{\partial T/\partial\theta} S + \frac{\tau J}{\partial T/\partial\theta} S^2} \qquad (4\text{-}30)$$

For frequency response, the transfer function becomes

$$\frac{T}{T_c} = \frac{1}{\tau} \frac{\frac{\omega}{\omega_n} S}{1 + 2\zeta \frac{\omega}{\omega_n} S + \left(\frac{\omega}{\omega_n}\right)^2 S^2} \qquad (4\text{-}31)$$

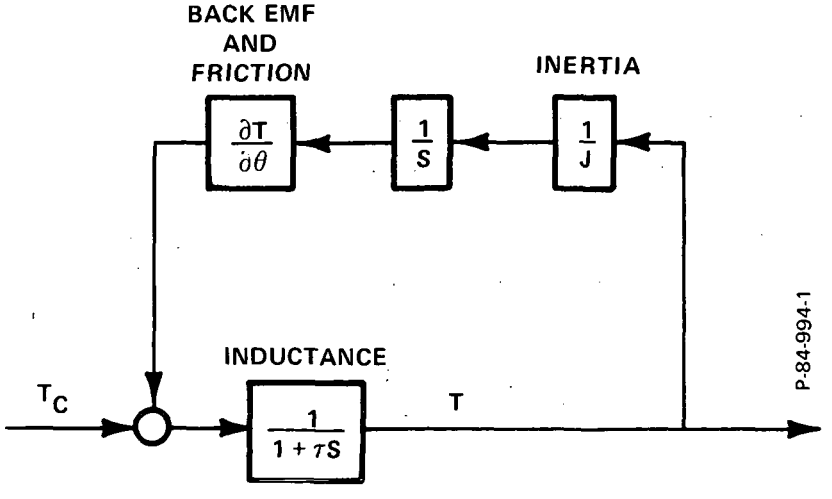

Figure 4-14 - Block Diagram - Electric Dynavector Motor with Inertia Load

The amplitude is given by

$$A = \frac{1}{\tau} \frac{\frac{\omega}{\omega_n}}{\sqrt{\left[1 - \left(\frac{\omega}{\omega_n}\right)^2\right]^2 - \left(2\zeta \frac{\omega}{\omega_n}\right)^2}} \tag{4-32}$$

The phase angle is given by

$$\phi = 90 \text{ deg} - \tan^{-1}\left[\frac{2\zeta \frac{\omega}{\omega_n}}{1 - \left(\frac{\omega}{\omega_n}\right)^2}\right] \tag{4-33}$$

To simplify the analysis, consider the damping ratio to be unity.

$$\zeta = 1.0$$

Then, at the natural frequency

$$\omega = \omega_n$$

$$\phi = 90 \text{ deg} - 90 \text{ deg} = 0 \text{ deg}$$

$$A = \frac{1}{2\tau}$$

The phase angle is +90 degrees at very low frequency, zero degrees at the natural frequency, and -90 degrees at very high frequency. The amplitude ratio is zero at very low frequency. This is because it takes very little torque to oscillate an inertia load at very low frequency. The amplitude ratio reaches its peak value at the natural frequency and decreases with further increase in frequency.

Breadboard actuator Model EH-818-U1 frequency response tests were conducted with inertia loads of 2.0 and 20.0 slug ft^2. The frequency response curves are shown in Figure 4-15.

The expected ratio of the two natural frequencies is

$$\frac{\omega_{n2}}{\omega_{n1}} = \sqrt{\frac{J_1}{J_2}} = \sqrt{\frac{2}{20}} = 0.32$$

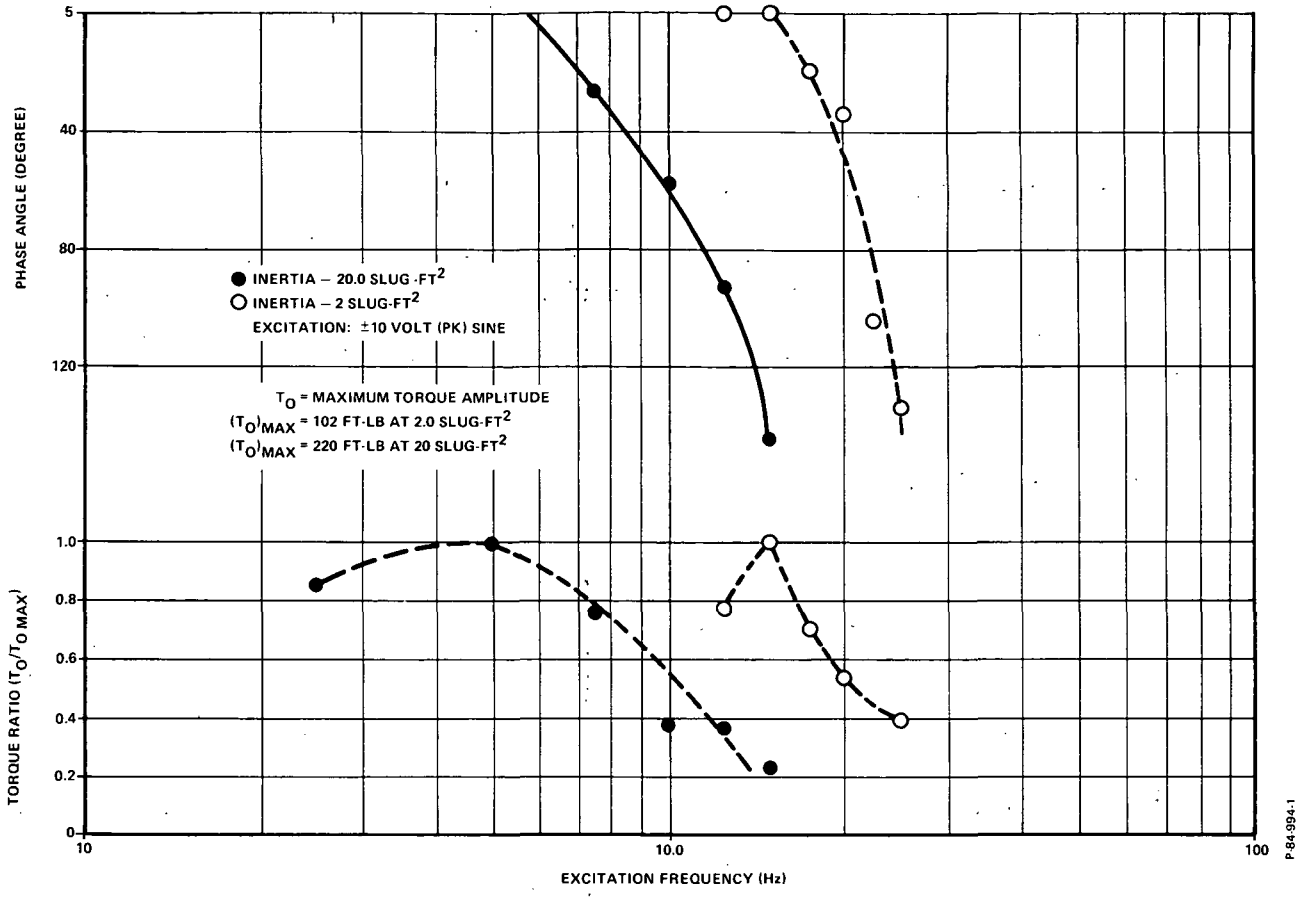

Figure 4-15 - Inertia Load Frequency Response

The peak amplitude ratio occurred at 15 hertz with 2.0 slug-ft^2 inertia and at 4.75 hertz with the higher inertia. The ratio is

$$\frac{4.75}{15} = 0.32$$

The shape of the test curves correlates well with the transfer function below the natural frequency. At higher frequencies, the motor has greater phase lag than predicted by theory, due to higher order effects which are impractical to analyze. The effect of inertia on natural frequency is the same as predicted by theory.

The frequency at which 90 degrees phase lag occurs does not decrease as much as the natural frequency does when the inertia is increased. This is because the higher order effects are less significant at lower frequencies.

The natural frequency for any load inertia can be calculated from

$$\omega_n = 4.75\sqrt{\frac{20}{J}} \text{ , Hz} \qquad (4\text{-}34)$$

The frequency at which 90 degrees phase lag occurs can be approximated from the general shape of the curves shown in Figure 4-15 as discussed in the following example calculation for the flightweight gimbal inertia.

Assume the flightweight actuator Model EH-818-U2 is required to drive a 500 slug-ft^2 inertia load. Determine the natural frequency solving (4-34) for ω_n and approximation of the 90-degree phase frequency. Given

$$J = 500 \text{ slug-ft}^2$$

then

$$\omega_n = 4.75\sqrt{\frac{20}{500}}$$

$$\omega_n = 0.95 \text{ hertz}$$

Based on the characteristic curves of Figure 4-15 the 90-degree phase shift point would occur at a frequency no less than 2.5 Hertz. This is determined as follows.

From Figure 4-15 the ratio of the 90-degree phase shift frequency to natural frequency for the 20 slug-ft^2 test curve is;

$$\frac{\omega}{\omega_n} = \frac{12.5}{4.75} = 2.63$$

Therefore the 90-degree phase shift for an inertia load of 500 slug-ft^2 will be at least

$$\omega = 2.63\ (0.95) = 2.5 \text{ Hertz}$$

As discussed above this is a conservative estimate and the actual frequency value should exceed 2.5 Hertz.

4.7 MODEL EH-818-U2 OUTPUT INERTIA

The moment of inertia of the total actuator when reflected to the output shaft is expressed by:

$$I_o = \frac{W}{g}(e)^2 + \frac{I_G}{(R_r)^2}(\text{Ratio})^2 + \Sigma I \text{ (output shaft, bearings, seal, etc.)} \quad (4\text{-}35)$$

Where the following nomenclature and values are used:

W = weight of rotor (3.6 pounds)

g = 386 inch/sec^2

R_r = transmission ratio of rotor to ground gear

e = eccentricity (0.0468 inch)

Ratio = overall actuator ratio (818:1)

I_g = inertia of rotor (0.0284 in-lb-sec^2)

ΣI = output shaft, bearings and seal inertia (0.283 in-lb-sec^2)

The value of R_r is found by:

$$R_r = \frac{N_2}{N_1 - N_2} = \frac{192}{192 - 186} = 32$$

The value of I_g is found by considering the rotor as a tubular ring of outside radius, r_o = 1.95 inches and inside radius, r_i = 1.52 inches

$$I_g = \frac{1}{2}\frac{W}{g}\left(r_o^2 - r_i^2\right) = \frac{1}{2}\ \frac{3.6}{386}\ (1.95^2 - 1.52^2)$$

$$= 0.0284 \text{ in-lb-sec}^2$$

Substituting the above values into equation (4-35) gives

$$I_o = \left[\frac{3.6}{386}(0.0468)^2 + \frac{0.0284}{(32)^2}\right](818)^2 + 0.283$$

$$I_o = 32.47 \text{ in-lb-sec}^2 = 2.7 \text{ ft-lb-sec}^2$$

SECTION 5

CONTROLLER DESIGN

The Model EH-818-U1 and U2 Electric Dynavector motors can be operated in either stepping of self-commutated modes. The controllers for both modes of operation are described in this section.

The basic function of a control unit for an electric stepper motor, or electronically commutated motor, is to switch the motor windings, or coils, on and off in the correct sequence. The stepper motor control unit has a single input consisting of pulses supplied from a function generator, or other source. Logic circuitry is used to convert the input pulses to switching signals for the motor coils. The control unit for self-commutation has several input signals, one from each commutator sensor, and has different logic circuitry from the stepper motor unit. Otherwise, the two types of control units are the same. The output signal from the logic section is amplified and used to drive power transistors for switching the motor coils.

5.1 STEPPER CONTROLLER

The stepper controller, which was obtained from Harmonic Drive Division, United Shoe Machinery Corporation, Beverly, Mass., is a Responsyn Driver Module, Model HDUM-A-MM4. This unit consists of two circuit boards.

The Model HDUM-A-MM4 driver is a solid state translator for converting input "step" pulses to logical switching of current to 8 windings (or phases) of a digital step motor. The schematic is shown in Figure 5-1 and 5-2, and the wiring diagram in Figure 5-3.

The built-in logic turns "on" phases, 4 at a time, in the sequence shown in Table 5-1 - Specifications, in response to input "step" pulses. Pulses to terminals #20 produce logic switching in the forward direction (reference Figure 5-3). Pulses to terminal #22 produce logic switching in the reverse direction. Each input pulse produces one motor "step."

When power is first applied to a driver-motor system, logic switching may not be in correct sequence. A maximum of 8 input pulses are required to bring the system to correct sequence.

All solid state circuitry is of the silicon type for long life in the presence of high temperatures. However, several modifications were made by Bendix to assure the reliability of the controllers. For example, transistors Q1, Q2, Q3, and Q4 were replaced with 2N2605 transistors.

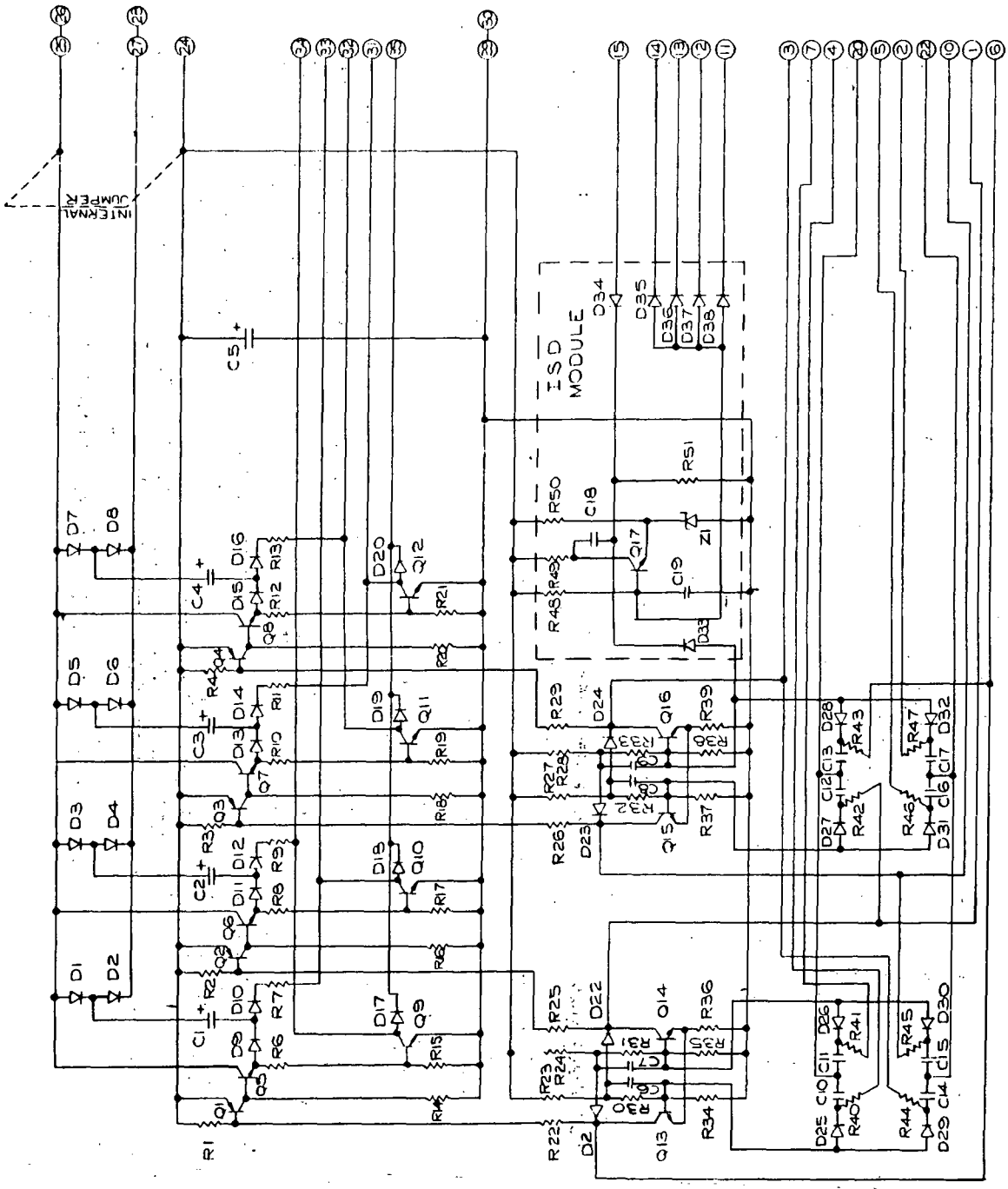

Figure 5-1 - Stepper Controller Wiring Diagram - Board A

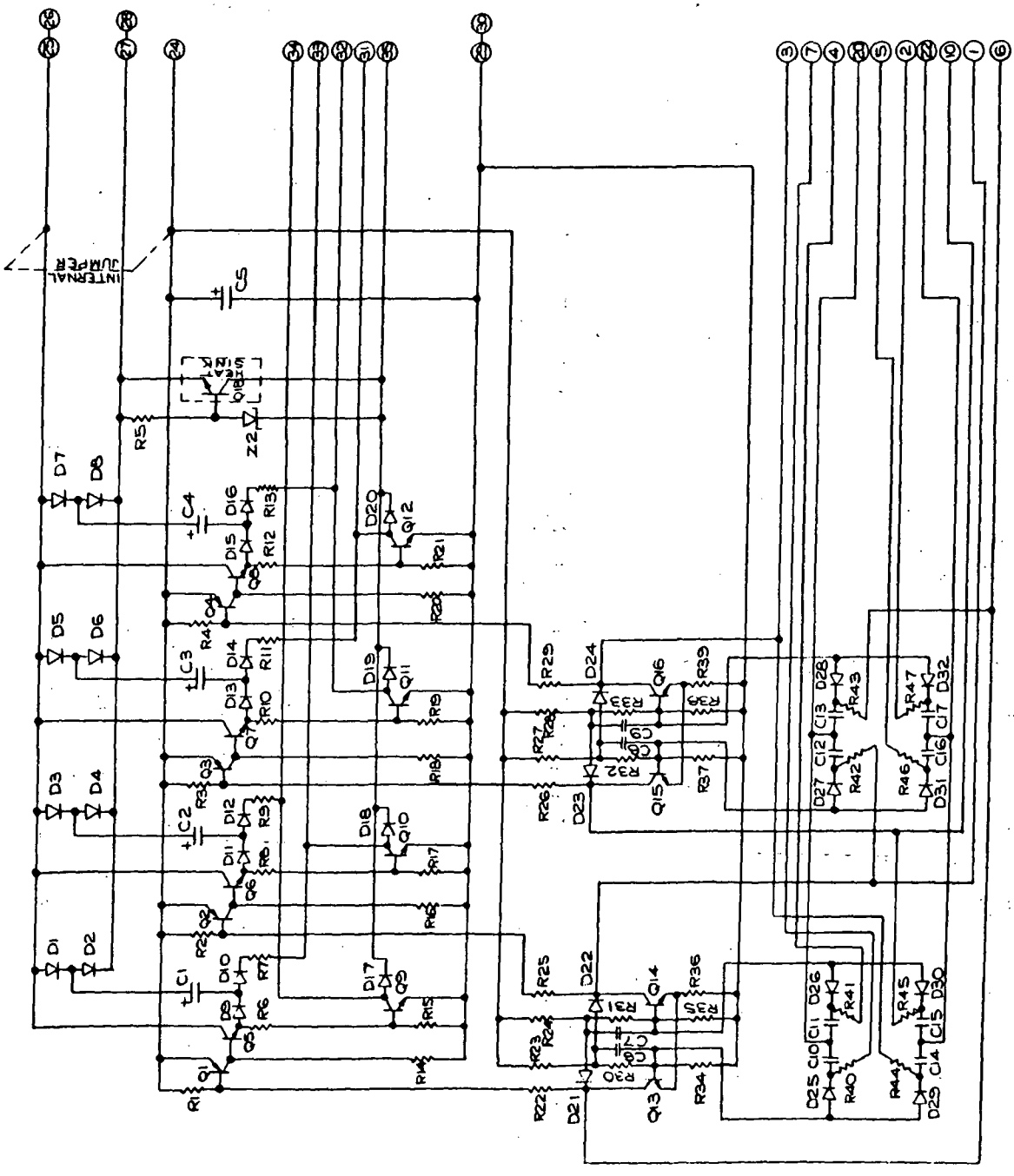

Figure 5-2 - Stepper Controller Wiring Diagram - Board B

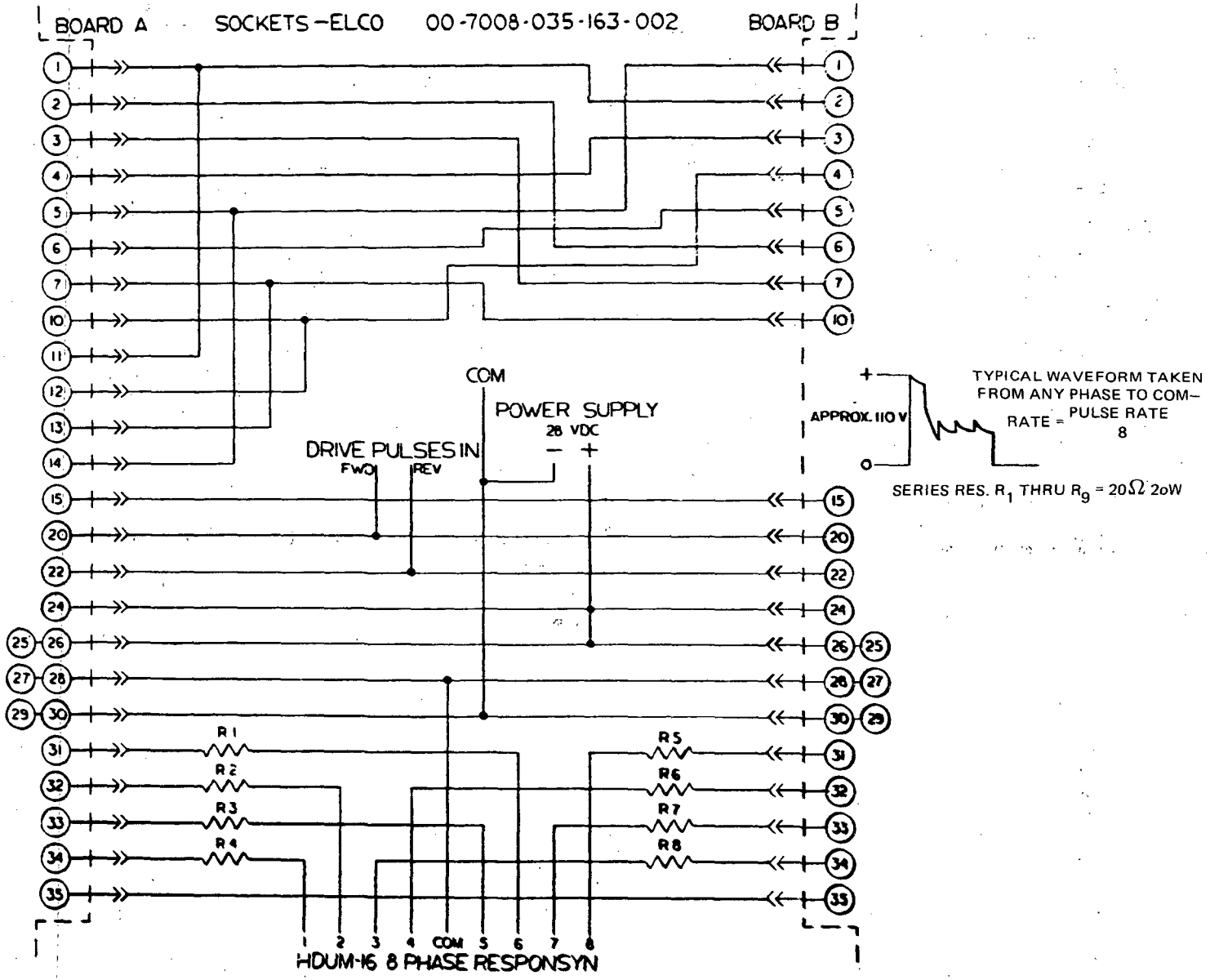

Figure 5-3 - Stepper Controller External Wiring Diagram

Table 5-1 - Specifications - Stepper Controller

INPUT TRIGGER PULSES	Amplitude: 8-10 volt Polarity: Negative Rise Time: <1 microsecond Duration: >20 microseconds Rate: 4,500 pps max.
OUTPUT LOGIC	Phases: 8 Sequence:- 1, 2, 3, and 4; 2, 3, 4, and 5; 3, 4, 5, and 6; 4, 5, 6, and 7; 5, 6, 7, and 8; 6, 7, 8, and 1; 7, 8, 1, and 2; 8, 1, 2, and 3; 1, 2, 3, and 4, etc; (4 phases on at a time), forward or reverse.
CURRENT PER PHASE	1.2 amps maximum
SUPPLY VOLTS	28 volts dc @ 5 amps maximum
"TURN OFF" SPIKE SUPPRESSION	Internal. No external spike suppression circuitry required.
CIRCUITRY	All solid state. Silicon semiconductors used throughout.
COOLING	Convection under most conditions. Forced air cooling for sustained hi-speed operation or operation in confined space.
DIMENSIONS	Circuitry mounted on 2-printed circuit cards 10' x 4-1/2". Circuitry 2" thick maximum each board.
CONNECTORS	Elco plug on each board. Mates with Elco 00-7008-035-163-002 socket.

P-84-994-1

Performance was improved by replacing 100 mfd capacitors C1, C2, C3, and C4 on both circuit boards with 500 mfd capacitors. These capacitors provide a surge of current at higher voltage to aid coil turn on. The circuit normally used in the Responsyn control unit to decrease coil turn on time is shown in Figure 5-4. This circuit provides a voltage pulse equal to twice the supply voltage each time a coil is switched on. The higher voltage helps to build up the current faster.

Initially, transistor Q11 is on. Transistors Q5 and Q9 are off. The collector of Q11 is thus at ground potential. The negative side of Capacitor C is connected through diode D10 and resistor R7 to the collector of Q11, and thus is at ground potential. The positive side of C is at +28 volts. At the instant when Q11 is turned off, Q5 and Q9 are turned on. The negative side of C charges through Q5 and D9 to +28V. Since the voltage drop across the capacitor cannot change instantly the voltage at the positive side of C jumps to +56 volts, or twice the supply voltage. Capacitor C then discharges through Coil 1 thus decreasing the turn on time.

The circuit modification used for surge suppression, and to decrease coil turn off time is shown in Figure 5-5. Q17 is normally off. When Q9 is turned off, voltage V1 increases until the breakdown voltage of zener diode Z1 is reached. Current flows through the base of Q17 thus turning on Q17 and allowing current to circulate around coil 1 through Q17. As soon as V1 drops below the breakdown voltage of Z1, Q17 shuts off and current in coil 1 stops.

The photos of Figures 5-6 and 5-7 show the stepper controller units SN/1 and SN/2 that were delivered with the flightweight actuators.

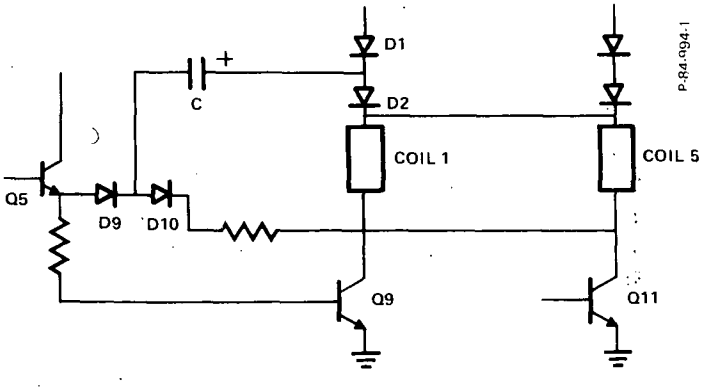

Figure 5-4 - Circuit for Reducing Coil Turn on Time in Stepper Controller

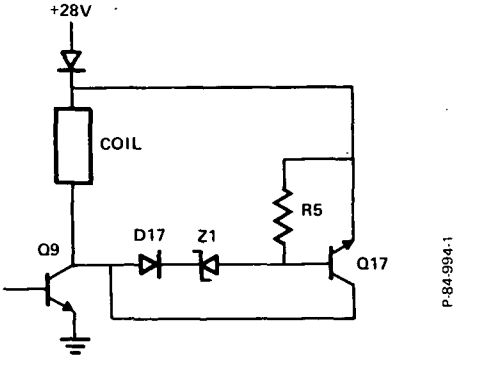

Figure 5-5 - Circuit Used to Limit Surge Voltage and Provide Rapid Coil Turn Off In Stepper Controller

Figure 5-6 - Photograph of Stepper Controller

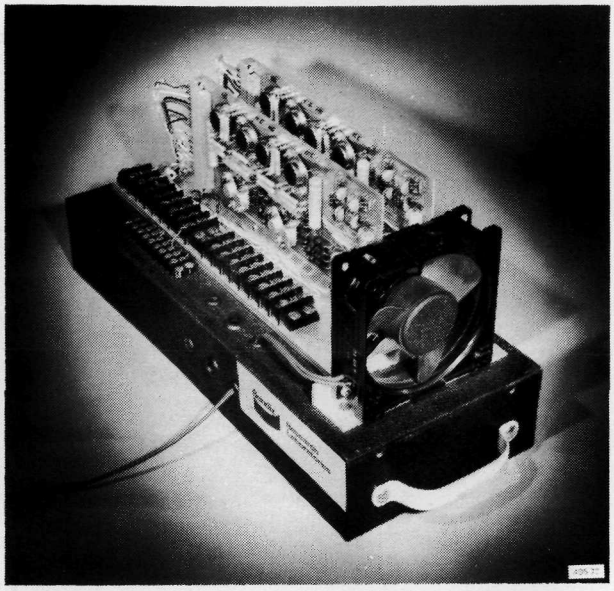

Figure 5-7 - Photograph of Stepper Controller - Cover Removed

5.2 BREADBOARD SELF-COMMUTATED CONTROLLER

The Self-Commutated Controllers were designed and fabricated by Bendix Research Laboratories. The first controller was fabricated in a breadboard type configuration to facilitate controller testing and modifications during tests with actuator model EH-818-U1 (breadboard unit). Two self-commutated controllers were also built by Bendix for consignment use by NASA during the life testing of the two flightweight actuators (Models EH-818-U2).

5.2.1 Description of Breadboard Drive Unit

The breadboard drive unit is functionally similar to the final version, but packaging and certain features such as adjustments and test points have been designed to make the breadboard unit more convenient and flexible for use in initial test and evaluation of the motor. A photo of the breadboard drive unit is shown in Figure 5-8.

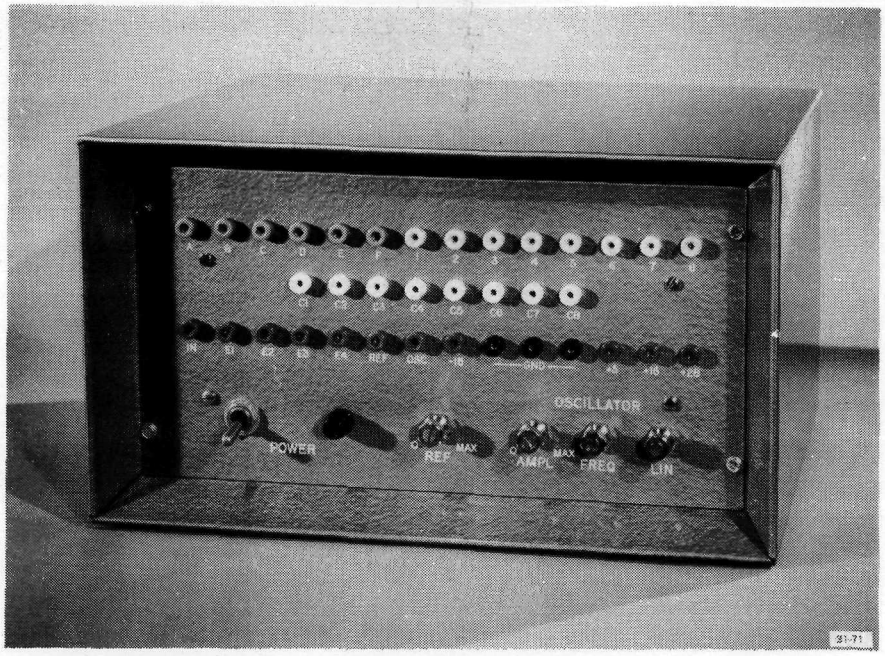

Figure 5-8 - Photograph of Breadboard Self-Commutated Controller

Figure 5-9 consisting of two sheets (drawing C2176995) is a detailed schematic diagram of the unit.

Digital logic circuits (D1, D2, D3, D4 and D5) convert the four commutator input signals (A, B, C, and D) and the direction control signals (E, $\overline{E}$) to a set of eight coil control signals, implementing the logic design concept.

Pulse-width modulation is accomplished by combining a variable dc control signal, a dc "reference" signal and a saw-tooth waveform of constant amplitude and frequency, at the input of A6. When the combined input reaches a specific value, the level detector output will switch from zero to a positive voltage level of about 5 volts, compatible with digital logic circuits. The resultant output is a series of pulses of constant frequency, determined by the saw-tooth wave, and whose non-zero pulse-width is proportional to the variable dc control signal level. The pulse-frequency of the pulse-width modulator, which is determined by the saw-tooth oscillator, has been set at about 1000 pps; however, a frequency control is provided in the breadboard unit which gives considerable latitude in the range of frequencies which can be used. The dc "reference" signal establishes the threshold of operation of the pulse-width modulator and can be used to in part compensate for deadband in the motor.

Operational amplifier A2 and two analog gates (comprised of a single CAG13 integrated circuit module) serve as an absolute value

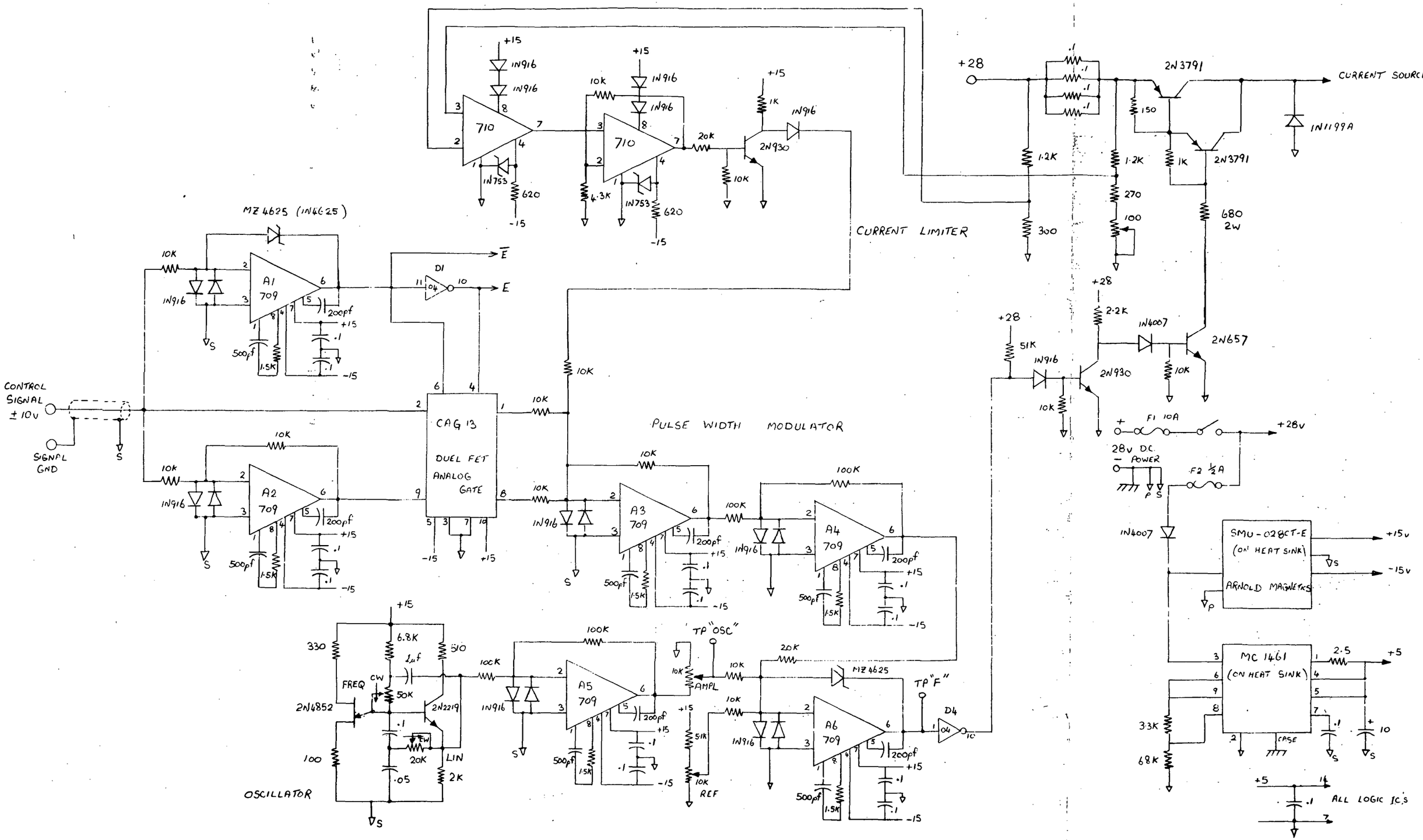

Figure 5-9 - Wiring Schematic Breadboard Self-Commutated Controller (1 of 2)

"Page missing from available version"

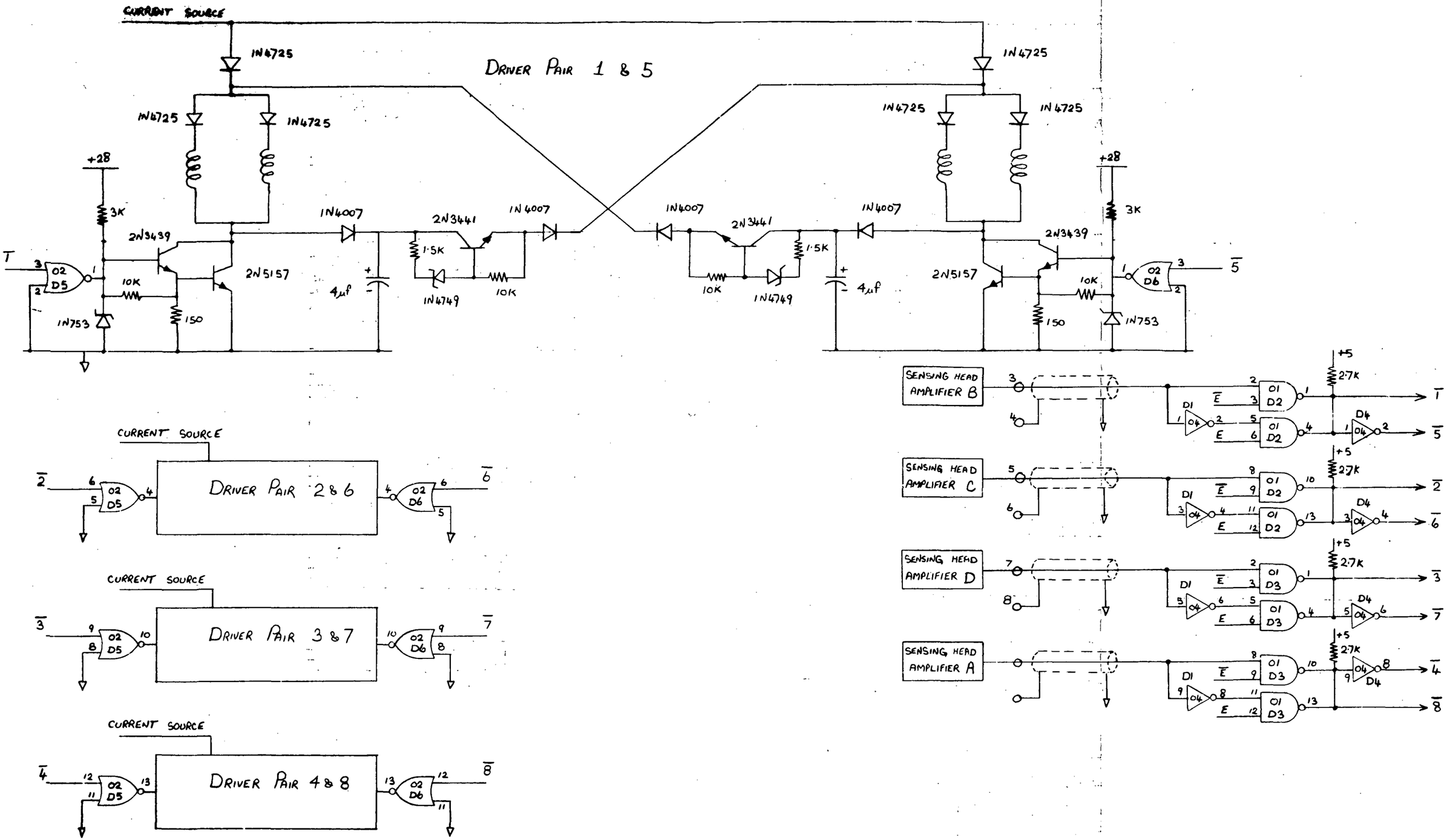

Figure 5-9 - Wiring Schematic Breadboard Self-Commutated Controller (2 of 2)

"Page missing from available version"

circuit, providing a dc signal for the pulse width-modulator, having a magnitude proportional to that of the control signal, but always of negative polarity.

To increase the flexibility and convenience of the breadboard system, two integrated circuit operational amplifiers, A3 and A4, have been included between the analog gates and the pulse-width modulator. These were placed there to permit addition of current feedback and to permit shaping of the current versus input signal (to linearize torque) if either of these features is found to be needed. Each of these amplifiers is wired as a unity-gain inverter.

Operational amplifiers A1 serves as an input signal polarity or zero-crossing detector to provide the direction control signals (E, $\overline{E}$) required for the digital logic and to control the analog gates.

A dc-to-dc converter and regulator module converts the +28 vdc to $\pm$15 vdc for tha analog circuits, while an integrated circuit regulator provides +5 vdc for the digital logic circuits. These permit the entire system to function from a single +28 vdc external power source but allow simpler and more conventional analog circuits to be used than which would be required if the analog circuits were designed to work from only positive dc supply voltages. For convenience, the breadboard drive unit is equipped with a power switch, indicator lamp, and fuses.

The drive unit makes extensive use of commerically available analog and digital integrated circuit modules.

To facilitate access for measurement or revisions during testing of the electric Dynavector motor, the breadboard drive unit is assembled on a flat rectangular circuit board and a similar sized aluminum heat-sink plate. These together with a control and test point panel and a connection panel are assembled as a hinged module which can be fanned open for easy access to all components and connections. This assembly is housed in a small cabinet suitable for table-top use. When mounted in the cabinet, the front panel contains the power switch, the pilot light, the adjustments provide for the pulse-width modulator, and test-point jacks to permit monitoring all significant points in the drive unit. The fuses and all connections are located at the rear of the unit. A flightweight version of the drive unit could employ a compact annular ring packaging configuration designed to fit around the motor, becoming an integral part of the final motor configuration. The connections between the motor (commutator circuits and coils) and the drive unit will then be permanently wired. Only terminals or connectors for external connection of power and control signal will then be provided.

5.2.2 Use of the Breadboard Drive Unit

This section outlines the use of the breadboard drive unit. The breadboard drive unit can be safely operated with or without the motor coils connected to the coil driver outputs.

- Connections

All connections to the breadboard drive unit are made at the rear of the unit.

- Power

Connect 28 vdc to TB1, the two-terminal barrier strip, observing the polarity indicated. The 28 volt supply used must be capable of providing at least 10 amps, the current drawn by the drive unit when the motor is being operated at maximum power. Two fuses are provided at the rear of the drive unit. All current from the 28 volt supply flows through F1, and 10 amp fuse. F2, and 0.5 fuse, protects the low-power analog and digital circuits.

- Input of Control Signal

The variable control signal should be connected to the binding posts at the rear of the unit. The signal should be connected to the red terminal, and the signal-ground or return path to the black terminal. The unit is designed for a reversible polarity control signal with a nominal full scale value of $\pm$10 vdc.

- Commutator Signals

The signals from the commutator circuits should be connected to terminals 1 through 8 of barrier strip TB2. A signal ground terminal is provided adjacent to each commutator signal terminal so that shielded leads or twisted pairs of leads may be used in making the connections. The commutator signals must be compatible with TTL logic circuits, and must not exceed +5 vdc or be less than 0 vdc. Voltage levels exceeding these limits may damage the logic circuits in the drive unit.

- Motor Coils

The motor coils are to be connected to TB2 terminals 10 through 18. The coils must be connected in the proper sequence to yield desired motor rotation. Neither end of any coil is at ground. A ground connection is provided at TB2 terminal 9 for use in grounding the case of the motor if desired. This connection is recommended for safety, but is not necessary for motor operation.

The drive unit may be safely operated with any number of the motor coils connected, or with no coils connected (no load). It may also be operated with from 1 to 8 resistive dummy loads.

- Pulse-Width Modulator Adjustments

With the exception of the POWER on-off switch, all of the controls on the front panel of the drive unit are adjustments associated with the pulse-width modulator, which serve to establish

the gain and threshold characteristics of the drive unit with respect to the analog input or control signal. It is expected that most or all of these adjustments will be eliminated in the final drive unit design, and fixed parameters will be incorporated base on values established during test and evaluation of the first motor using the breadboard drive unit.

All of the controls were set during checkout of the breadboard drive unit, to settings which may be near optimum. Hence, they may require no further attention. The following paragraphs serve as a guide to the approach to use, however, in the event that further adjustment is felt to be necessary. These front panel controls are the only adjustment provided; there are no controls inside the unit.

- FREQ

The FREQ control adjusts the frequency of the saw-tooth oscillator which determines the pulse frequency of the pulse-width modulator. It has been set to about 1000 pulses per second, about 10 times the stepping rate of the motor when operating at rated speed. To set some other frequency, connect an oscilloscope to the "OSC" test point and turn the FREQ control until the desired frequency is obtained. The frequency range should be limited to that which yields a sharp saw-tooth waveform.

- LIN

The LIN control serves to adjust the linearity of the saw-tooth waveform, which in turn affects the "linearity" of pulse width versus input signal amplitude. Connect an oscilloscope to the "OSC" test point and adjust for best linearity of the observed waveform.

- AMPL

The AMPL control adjusts the amplitude of the saw-tooth waveform which is fed to level-detector amplifier A6. This has the effect of adjusting the "gain" of pulse-width versus analog control input signal. This control has been set so that 100 percent conduction (pulse always "on", maximum power to motor) occurs at about $\pm$9.0 volts input.

To reset this parameter, connect an oscilloscope to test point "F", establish a known value of control signal at the input, and adjust the AMPL control for the desired percent of condition. The waveform at "F" will be a square wave varying between about 0 and +5 volts. "Conduction" or motor operation occurs during the +5 volt portion of the wave.

There is some interaction between the results of the AMPL control and those of the REF control discussed in the next paragraph. Hence, when the AMPL control is set, the REF control must normally also be readjusted.

- REF

The REF control serves to establish the minimum value of input signal required to cause conduction (+5 volt level at test point "F") or the amount of conduction for a zero-value input signal. It thus serves to establish the threshold of operation of the unit, and can be used to, in part at least, compensate for deadband in the motor. At checkout this control was adjusted to yield a very slight conduction for zero input. Readjustment may be accomplished in one of two ways.

(1) Connect an oscilloscope to test point "F". Set the input signal to zero volts (or ground the input), and adjust the REF control to give some desired percent conduction.

(2) Set the input to a desired threshold value and adjust the REF control so that the motor just begins to move.

- Normal Operation

When all necessary connections have been made, and the pulse-width modulator has been adjusted, the unit is ready for initial use without making any further adjustments, and normal operation becomes very simple:

(1) Turn the POWER switch ON.

(2) Adjust the external control signal to yield desired motor operation.

5.3 CIRCUIT DESCRIPTION AND ALIGNMENT PROCEDURES FOR FLIGHTWEIGHT ACTUATOR CONTROLLER

This section describes the two self-commutated controllers built by Bendix for consignment to NASA for life testing of the flightweight actuators.

The controllers are essentially a laboratory built piece of hardware and not intended for severe environments. The input power supply is +28 volts dc, and 115 volts ac (for the cooling fan). There are eight potentiometers associated with the circuit, four located outside the box, and four trimpots are located inside. Procedures for adjustment are described. Circuit schematics are shown in Figure 5-10 (sheets 1 and 2 BRL drawing C2176996). Also described is a schematic of a sequencing logic circuit that has been used to operate the actuator as a stepper motor. The controller was designed primarily for self-commutating actuator operation, the ability to operate as a stepper motor was an added feature to facilitate adjustment of potentiometers and to aid in checkout.

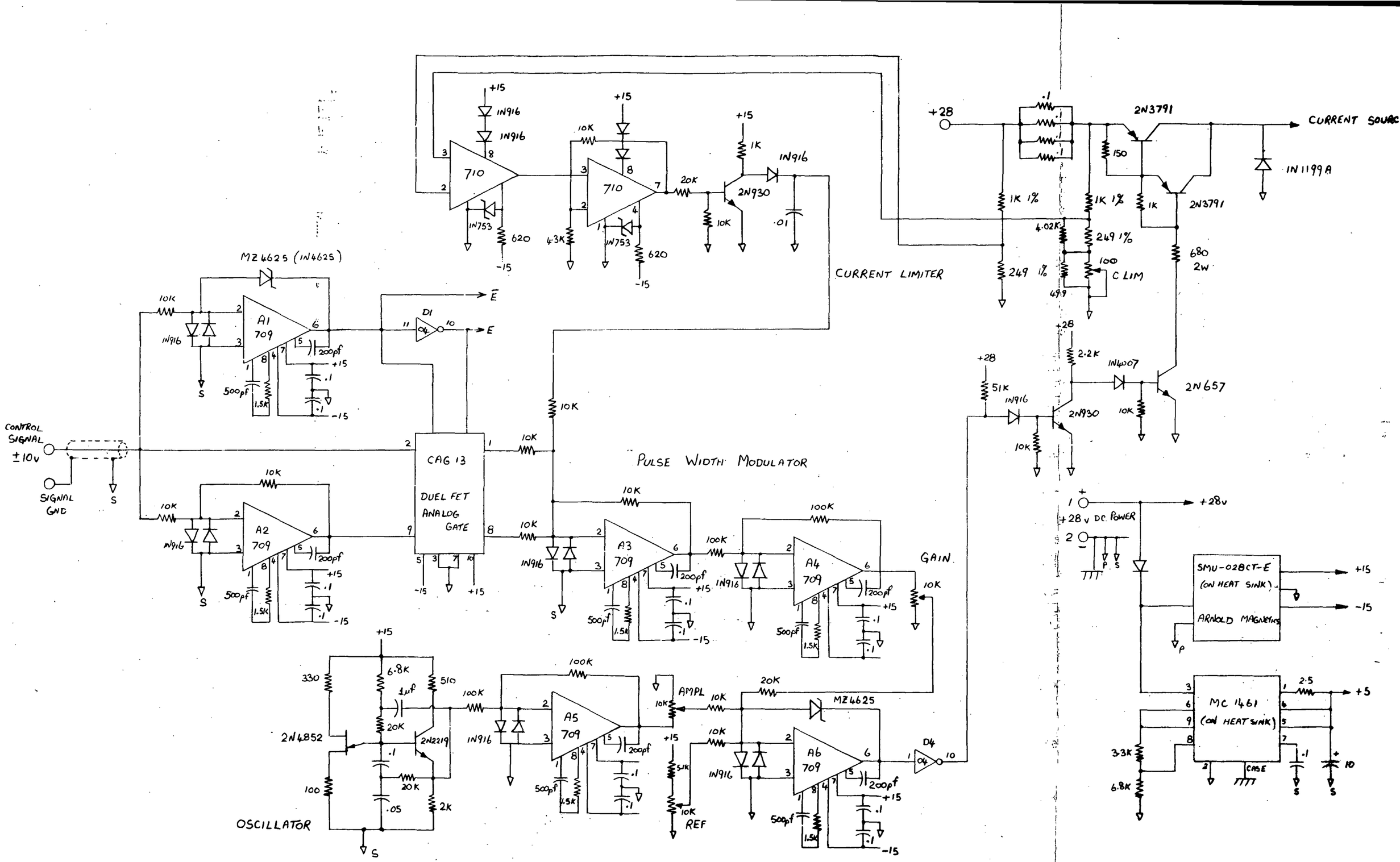

Figure 5-10 - Wiring Schematic Flightweight Self-Commutated Controller (1 of 2)

"Page missing from available version"

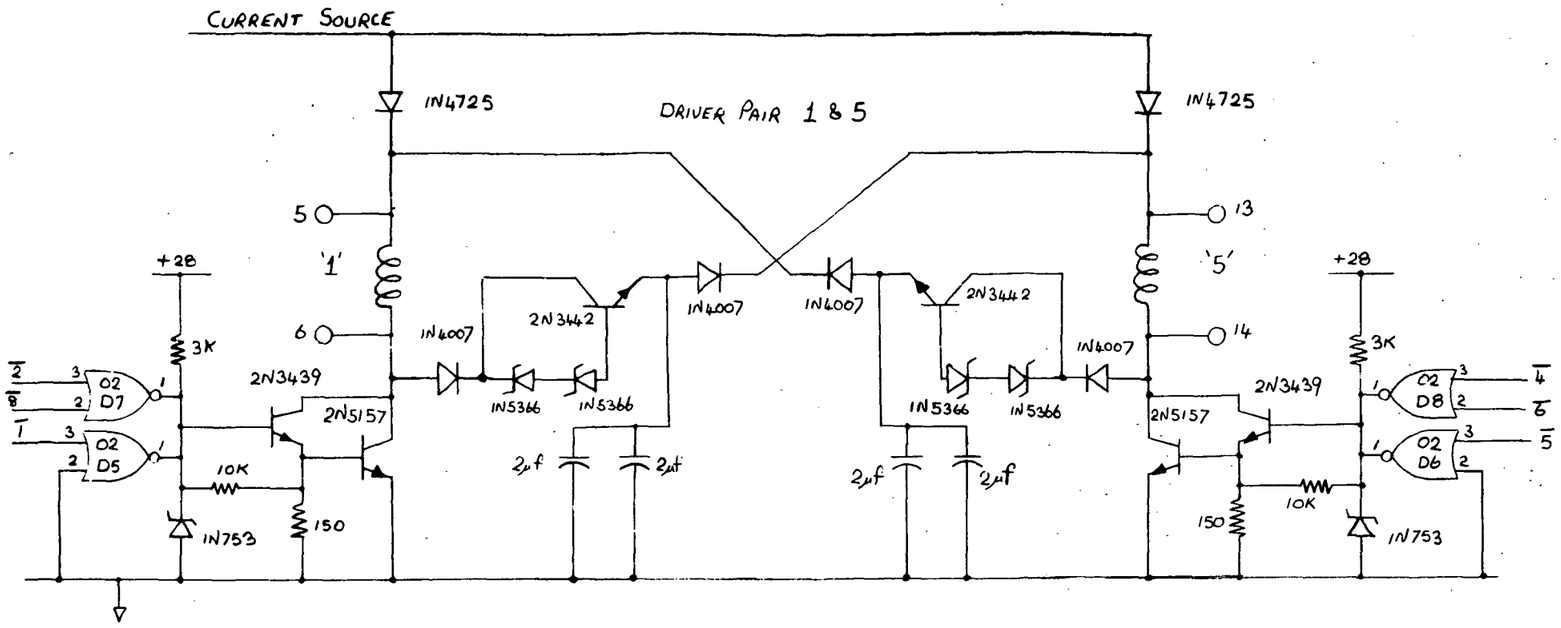

PIN No.	MODE CONNECTION		
	STEPPER		SELF COMM.
	CW	CCW	
1	FF1	FF4	to 14
2	INTERNAL GND		
3	FF2	FF3	12
4	NC	NC	NC
5	FF3	FF2	10
6	NC	NC	NC
7	FF4	FF1	8
8	OPEN		7
9	NC		NC
10	OPEN		5
11	NC		NC
12	OPEN		3
13	INTERNAL +5v.		
14	OPEN		1

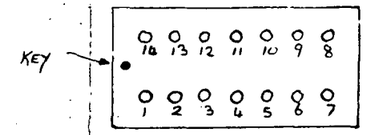

STEPPER MODE SOCKET

Figure 5-10 - Wiring Schematic Flightweight Self-Commutated Controller (2 of 2)

"Page missing from available version"

5.3.1 Power Driver Circuits

The power drivers are arranged in four pairs. Driver inputs are derived from digital logic gates controlled by the commutating sensor amplifiers and also by the control input signal. The control input signal polarity determines the direction of actuator rotation. A DUAL FET ANALOG GATE (Type CAG13) senses the input signal polarity and generates a logic signal E or $\overline{E}$ (exclusive OR). This in turn changes the driver switching sequence. For each driver pair, either one or the other is always on (but not both together). The power transistor 2N5157 is controlled by a driver 2N3439 in the Darlington configuration. Switching a coil OFF causes an induced voltage to be generated at the collector. When this voltage has climbed to +80 volts the energy transfer network begins to conduct and power is transferred to the opposite coil (which has just been switched on). The transfer network consists of the 2N3442, a four microfaced high voltage capacitor, and blocking diodes. The 2N3442 starts to conduct when the two IN 5366 zener diodes reach the zener voltage region (40 volts each). The voltage transient at the collector can reach over 400 volts depending on actuator load conditions. The energy transfer network allows the storage energy in the coil that is switched off to be used in powering the coil just coming on.

5.3.2 Proximity Sensor Amplifiers

Four proximity sensors labeled A, B, C and D are located inside the actuator and are adjacent to the rotor. The eccentric motion of the rotor with respect to sensors during actuator rotation causes pulse sequential signals to be generated. The sensor consists of a piece of ferrite with a winding. The coil together with capacitor C_f at the amplifier input form a tuned circuit. The 709 amplifier allows sustained oscillation until the sensor gap is reduced below a certain critical level (determined by the trimpot setting). The amplifier output is buffered in the complementary transistor stage and then demodulated in the diode, capacitor, resistor network. The output voltage is divided down to drive the logic circuit.

5.3.3 Pulse Width Modulator

The control signal is inverted in a unity gain amplifier A2. Amplifier A1 detects input signal polarity and controls switching of the DUEL FET ANALOG GATE. Hence the control signal, irrespective of polarity, is summed in amplifier A3 together with current limiter information. The signal is again inverted and buffered in A4. Output level of A4 is adjusted by the GAIN potentiometer. The oscillator circuit output is buffered in unity gain amplifier A5. The output level is adjusted by AMPL potentiometer. Control signal and oscillator signal are summed at the input of A6. The dc level is controlled by REF potentiometer. The output of A6 is a pulse width modulated signal at oscillator frequency. The amount of modulation is proportional to

input control voltage, and is further controlled by the current limiter circuit. The output signal of A6 controls the series regulator power transistors 2N3791. The collector outputs serve as the current source for the power driver circuits.

5.3.4 Current Limiter

The input power supply is taken through a precision 0.025 ohm power resistor. A resistor divider network on either side of this is used to detect a critical voltage drop. This voltage drop is proportional to the maximum current of the controller (10 amperes). Potentiometer C LIM provides some adjustment to this value. The current limit is detected on the 710 comparator amplifier which then feeds into another 710 comparator which is connected up in a Schmitt trigger configuration to provide hysteresis. The output is buffered by a 2N930, and a 0.01 capacitor provides memory to prevent oscillation when in the current limit mode. The limiter signal is summed with the control signal at the input node of A3.

5.3.5 Procedure for Setting up Proximity Sensor Amplifiers

The controller is set up in the stepper mode by removing the 14 pin jumper pad and replacing with an external drive cable connected to a sequencing logic network which in turn is driven by an external oscillator. The external sequencing logic is shown in Figure 5-11 and the connector pin numbers are shown in Figure 5-10.

The external oscillator is set to a frequency of 300 pulses per second (300 Hz), and the input controller voltage is set to maximum. With these conditions the actuator should now rotate at a speed of 300 steps per second. Assuming that the actuator direction is set for clockwise (as viewed from the output shaft flange) the next step is to connect an oscilloscope probe to the output of the amplifier demodulator circuit. There are four test points in the controller box for this purpose, and each amplifier has an identification letter. The oscilloscope probe should be connected to amplifier A, and trimpot potentiometer 'A' should now be adjusted until there is a square waveform on the oscilloscope, the waveform should resemble that shown in Figure 5-12. There will be some horizontal jitter in this waveform due to the actuator, but adjustment should be made as close as possible to a 50 percent On-Off duty cycle. The next step in the setting up procedure is to do the same thing with the output from the demodulator circuits of amplifiers B, C and D. The four waveforms should be in a phase relationship as shown in Figure 5-12. When the controller is connected back into the self-commutating mode, the actuator should now operate correctly.

5.3.6 Procedure for Adjusting Power Modulator

The pulse width modulator circuit enables the controller to operate in a variable duty cycle mode in order to reduce dissipation and to control actuator speed.

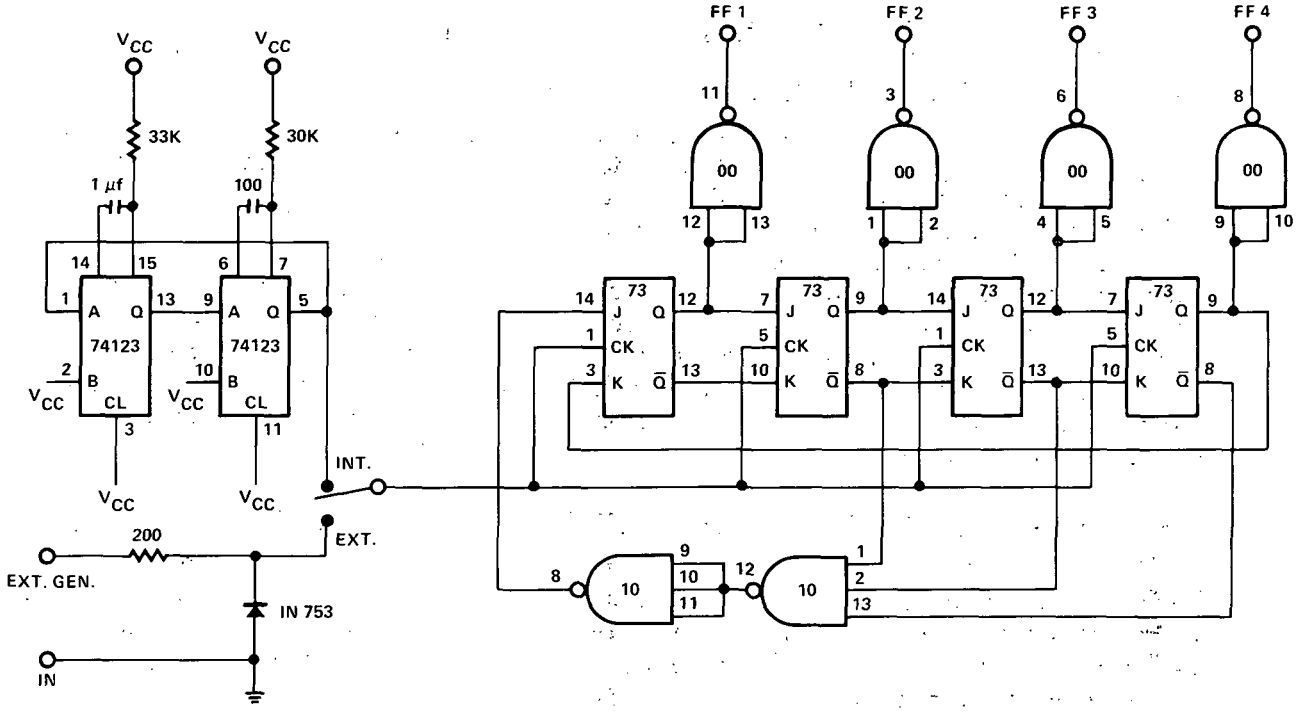

Figure 5-11 - External Sequencing Logic (Self-Commutated Controller)

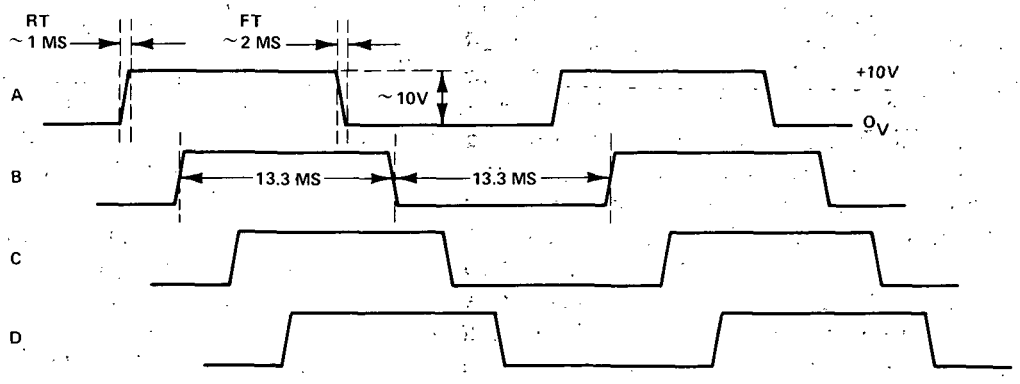

Figure 5-12 - Demodulator Output Waveforms

The oscillator generates a frequency of around 3 KHz, and the output is fed into a circuit to generate a ramp voltage. A detector circuit determines the amount of ON-OFF time that is associated with a given input voltage, and the three potentiometers marked GAIN, AMPL, and REF enable a range of control to be set up for a given input voltage. The input control signal is presently set up so that with zero input voltage the actuator will turn slowly, and with an input voltage of plus or minus eight and a half volts the actuator will operate at maximum power. Different relationships between input voltage and degree of modulation can be obtained by suitable adjustment of the three potentiometers. The method that has been used is as follows.

(1) AMPL potentiometer is adjusted to give a five volt peak-to-peak signal (reference Figure 5-13).

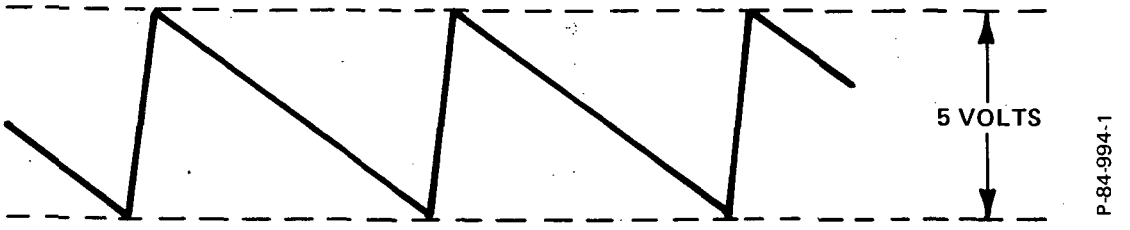

Figure 5-13 - AMPL Potentiometer Adjustment

(2) With zero voltage input, the REF potentiometer is adjusted to give a slight amount of modulation (reference Figure 5-14).

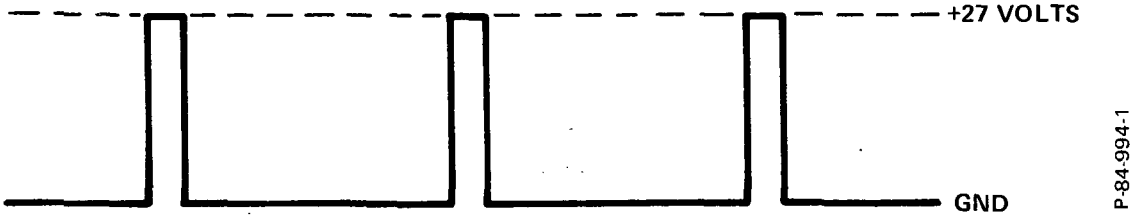

Figure 5-14 - REF Potentiometer Adjustment

The oscilloscope is connected to the cathode end of the IN1199A located on the hinged lid. This is the driver current source.

(3) The gain pot is adjusted to establish the desired relationship between control signal and percent modulation.

The relationship has been initially set so that with eight and a half volts input control signal the modulation is 100 percent (as viewed on an oscilloscope connected to the driver current source).

5.3.7 Procedure for Setting up Current Limiter

The controller current limiter has been set up to cause current limiting at the 10 ampere level. If adjustment is necessary the procedure is as follows.

The controller is set up for stepper mode operation by removing the 14 pin jumper pad and replacing with an external drive cable and sequencing logic network. The input frequency is set at 10 Hz and the control voltage is adjusted for maximum modulation (100 percent). It does not matter whether the actuator is in C.W. or C.C.W. direction. In this mode the actuator coils are taking full current. The input current to the controller should be monitored with a current meter. The meter used to do this adjustment was an H.P. Model 428B with type 248A-21A current probe. The current limiter potentiometer is adjusted until the current reading is 10 amperes, the potentiometer is then locked off.

5.4 PROXIMITY SENSOR DESCRIPTION

Electro-Products proximity sensors and Mini-Prox drivers were used for commutation of the Breadboard Electric Dynavector Motor. A schematic of the Mini Prox is shown in Figure 5-15 and a photo of the driver circuit modules in figure 5-16.

The power consumption of the Mini Prox driver was decreased from 0.90 watts to 0.34 watts by changing R17 from 1.0K to 10K ohms, changing R18 from 470 to 1.1K ohms, and removing the indicator lamp bulb. In addition, a zener diode was used to limit the output of each Mini Prox unit to 5 volts. A higher voltage could damage the motor drive unit.

The proximity sensor is a coil of inductance L. The loop consisting of the proximity sensor and capacitor C_1 is a resonant circuit with natural frequency

$$f = \frac{1}{2\pi\sqrt{L\ C_1}}$$

The current in the proximity sensor is normally oscillating with frequency f. When metal is moved close to the proximity sensor, the induced eddy currents in the metal increase the effective resistance of the coil, thus damping out the oscillations. Potentiometer R_3 also provides damping and is used to adjust the set point, or distance at which oscillations cease. The LC circuit is connected to the input of operational amplifier IC-1. The feedback through R1 furnishes the energy to sustain the oscillations.

The output of the rectifier formed by D1, D2, and C7 is about 5 volts dc when in oscillation. This voltage drives the output signal to zero. When the oscillations cease, the rectifier output is zero, and the driver output is 10 volts.

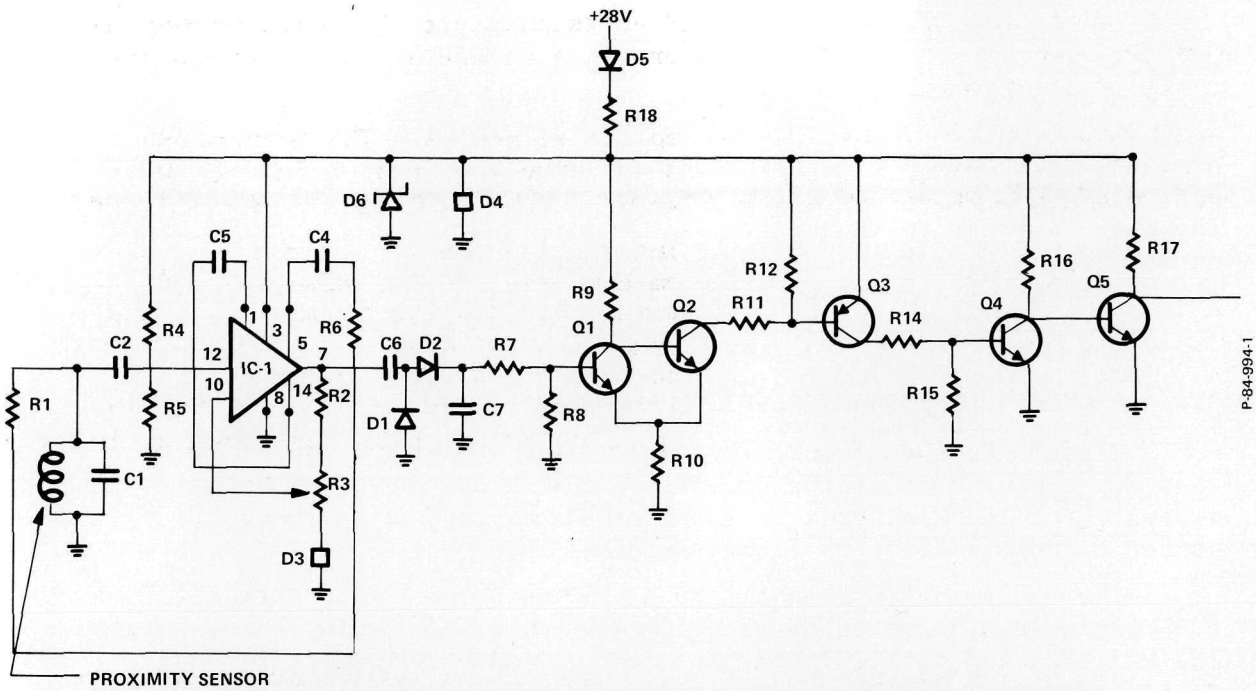

Figure 5-15 - Driver Circuit for Proximity Sensor

Figure 5-16 - Photograph of Commercial Sensor - Driver Circuit Modules

Zener diode D6 reduces the 28 volts supply to 12 volts as required for the operational amplifier and provides an output that does not vary for a range of supply voltage.

Metal film resistors were used for R1 and R2. The temperature coefficient of metal film resistors is quite low, thus reducing the effect of temperature on this unit.

An alternate breadboard proximity sensor driver circuit was fabricated by Bendix using stockroom components. The schematic is shown in Figure 5-17 This circuit was tested using a commutator test fixture. Test results at room temperature were about the same as results with the Mini-Prox driver. The circuit was sensitive to temperature changes at first. The use of metal film resistors for the two 20K ohm resistors appeared to eliminate or greatly reduce the temperature problem.

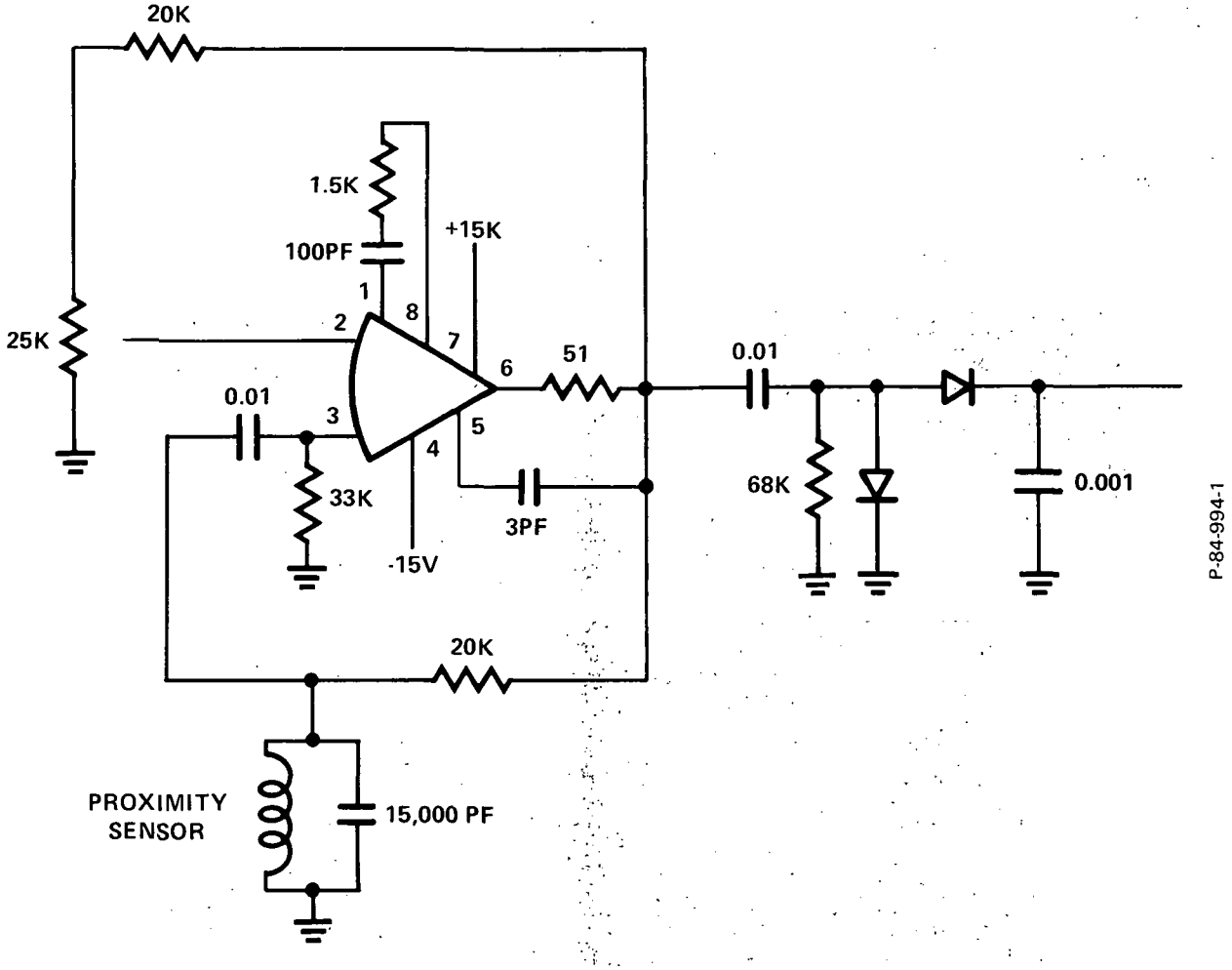

Figure 5-17 - Breadboard Proximity Sensor Driver

SECTION 6

SUMMARY OF TEST RESULTS

Both the breadboard unit and the two flightweight units were tested in the stepper and self-commutated control modes. Torque-speed-current data were recorded for all tests. In addition, backlash, stiffness and hysteresis tests were conducted on the units. Also a series of frequency response tests were conducted on the breadboard unit. Stepping mode response tests were conducted by Bendix. The results of the self-commutated response tests, conducted by Avco, Lowell, Mass., have been used to predict the performance of the unit to drive an inertia load of 500 slug-ft^2 and are discussed in Section 4.6.

6.1 BREADBOARD ACTUATOR MODEL EH-818-U1 PERFORMANCE TEST

- Stepper Mode Tests

The stepper mode tests were conducted using both a Responsyn 8-Phase Controller and the Bendix self-commutated set-up to run in the stepper mode.

Torque speed performance data for the Responsyn Controller was obtained as follows:

(1) Set the power supply current limiter at 10 amperes and the voltage supply at 28 volts dc.

(2) Adjust the driving frequency to the desired stepping rate. Example: 104 cycles/sec = 1 rpm output revolution.

(3) Record all data (current, no-load speed, voltage, etc.).

(4) Using a torque wrench and an in-line torque cell, load the actuator until the unit loses synchronous step. Record torque. Relieve the load torque slowly until the actuator drives the load without slipping. This value is the maximum torque the actuator is capable of driving without losing its step. Record all data.

(5) Repeat in opposite direction steps (1) through (4) and record all data.

This method of measuring torque speed performance data provides the most accurate results. Several load devices including friction clutches, were tried and found to be unsatisfactory because the coefficient of friction fluctuates between static and dynamic values at very low speeds.

The wiring schematic for the Responsyn Controller set-up is shown in Figure 6-1. Table 6-1 summarizes the performance characteristics at a supply voltage of 26.5 volts.

Table 6-1 also shows the performance characteristics of the breadboard unit with the Bendix self-commutated controller set-up to run in the stepper mode.

Table 6-1 - Model EH-818-U1 Performance Comparison at 26.5 Volts Supply

Parameter	Specification	Controller A(1)	Controller B(2)
Stall torque	2400 lb-in.	2400 at 65 step/sec	2400 at 50 step/sec
Rated torque	1800 lb-in.	1800	1800
Speed at rated torque	105 steps/sec (1 rpm)	80	75
Stall current	7.15 amps	8.0 amps	8.0 amps (motor only)
Current at rated torque	3.57 amps	6.0 amps	6.0 amps (motor only)
No-load speed	Not specified	350 steps/sec	650 steps/sec
No-load current	Not specified	1.3 amps	Not measured

(1) Bendix self-commutated controller. Current is total drawn by controller and motor.

(2) Responsyn stepper controller. Current is for motor only.

- Self-Commutated Performance Tests

The breadboard actuator performance tests conducted with the Bendix self-commutated controller are presented in Figures 6-2 and 6-3. At the rated 1 rpm operating point the actuator developed 1500 in-lb output torque and at stall, the actuator developed 2100 in-lb output torque. These data points were approximately 15 percent below the test results obtained in the stepper mode.

Because of delivery commitments, further development testing of the self-commutated controller and actuator was not possible, and the unit was delivered to Avco Corporation, Massachusetts for endurance life testing.

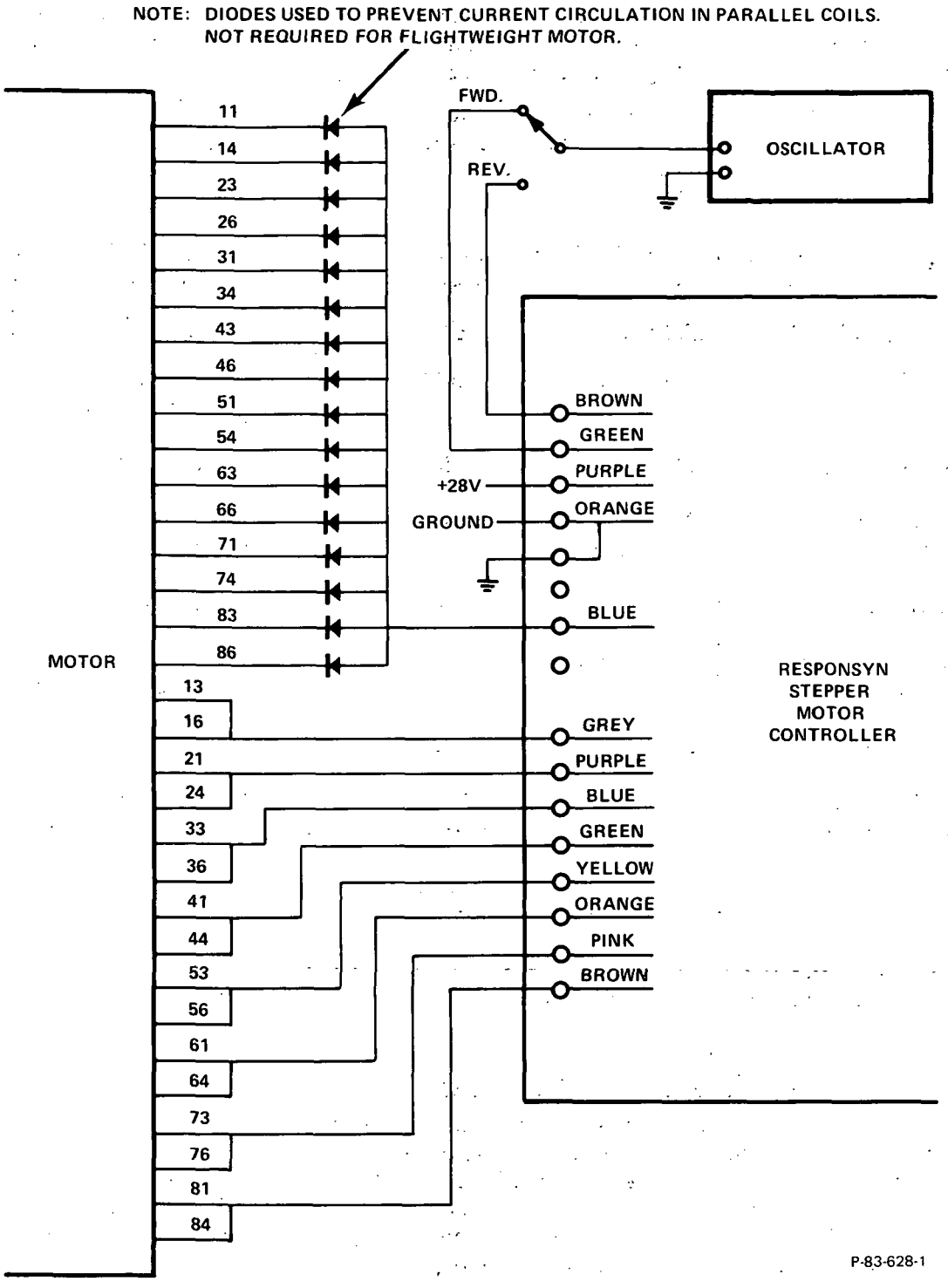

Figure 6-1 - Wiring Diagram - EH-818-U1 Motor - Stepping Mode

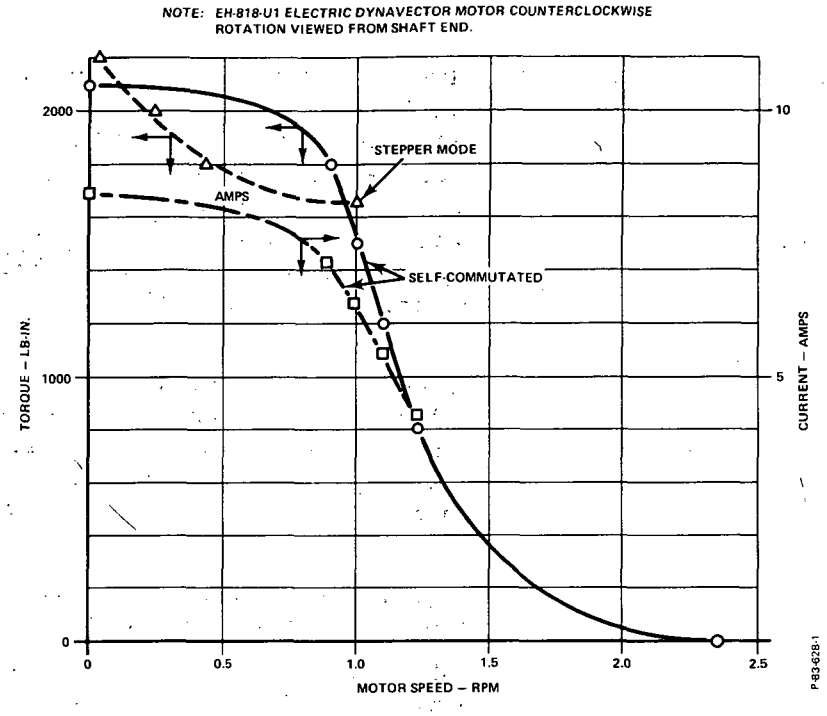

Figure 6-2 - Torque - Speed Curve (EH-818-U1)

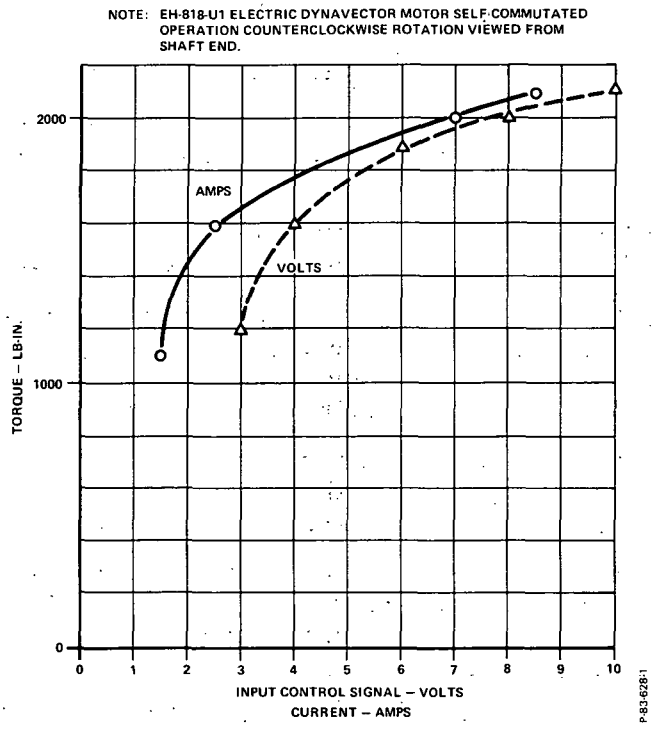

Figure 6-3 - Torque Versus Control Voltage and Current (EH-818-U1)

Shortly thereafter, Bendix discovered the performance evaluation tests were conducted with a wiring error in the self-commutated controller current limiting circuit. Analysis indicated that the error would reduce the torque producing current in the stator coils. To correct this condition, Bendix personnel visited Avco to alter the current limiter circuitry to (1) prevent high frequency oscillations from occurring and (2) to linearize the torque output versus control voltage characteristic, and (3) to set-up the controller for self-commutated operation.

The oscillating condition of the current limiter was corrected by adding memory to the circuit. Adding capacitance to the output of the limiter ensured that whenever the current limit was detected, the series switch would be held open for approximately 100 μsec. This limits the effective frequency of the limiter to that of the pulse width modulator.

The torque-control voltage characteristic was linearized to some extent by varying the parameters of the pwm circuit.

Upon completion of the above two steps, a set of data was taken for stepper operation as is shown in Table 6-2 and Figure 6-4. Then the proximity switches were balanced and the control connected to operate in a self-commutated manner. The data from self-commutated operation, as shown in Table 6-3 and Figure 6-5, indicates that the actuator developed the required stall and rated torque.

- Backlash, Stiffness and Hysteresis Tests

The breadboard actuator was tested for backlash, stiffness and hysteresis on the test fixture shown in Figure 6-6, and the tests were run as follows:

(1) Four coils selected at random were energized to 28 volts dc and the power supply current limiter was set at 10 amperes.

(2) A 1800 in-lbs back driving load torque was applied to the actuators output shaft using a 3600 in-lb rated torque wrench. A 5000 in-lb rated torque cell positioned between the torque wrench and actuator shaft recorded the actual applied torque.

(3) A 0.0001 inch-per-division calibrated dial indicator placed 4 to 6 inches from the shaft centerline was used to record the actual deflections for each applied load.

(4) Starting at zero torque and gradually applying a clockwise torque, the beam deflection and applied torque was measured at 200 in-lb intervals until the 1800 in-lb load point was reached.

(5) The load was gradually reduced through zero torque and then continued to 1800 in-lb on the counterclockwise direction. And, as in (4), both deflection and torque were recorded at 200 in-lb intervals.

Table 6-2 - Stepper Data (CCW Rotation) as Recorded at Avco, 30 August 1971

Control Volts	Current (Amps)	Torque (lb-in) Run	Torque (lb-in) Stall	Pulse Rate (pps)
2	1.6	200	250	10
3	3	700	750	10
4	4.3	1100	1150	10
5	5.6	1450	1500	10
6	6.9	1800	1850	10
7	7.7	2000	2050	10
8	8.5	2050	2100	10
9	8.7	2200	2250	10
10	9.5	2400	2450	10
10	6.5	1700	1800	105 (1 rpm)

P-83-746-1

Table 6-3 - Self-Commutated Data (CCW Rotation) as Recorded at Avco, 30 August 1971

Control Volts	Current (amps) After Limiter	Current (amps) Before Limiter	Torque (lb-in) Run	Torque (lb-in) Stall
2	1.5	0.8	250	300
3	3	1.2	800	900
4	4.4	1.8	1200	1250
5	5.2	2.5	1550	1600
6	5.7	4	1800	1900
7	6.4	5.8	2100	2200
8	7	6.5	2100	2200
9	7-8	7.5	2200	2300
10	8-10	8.8	2350	2500

P-83-746-1

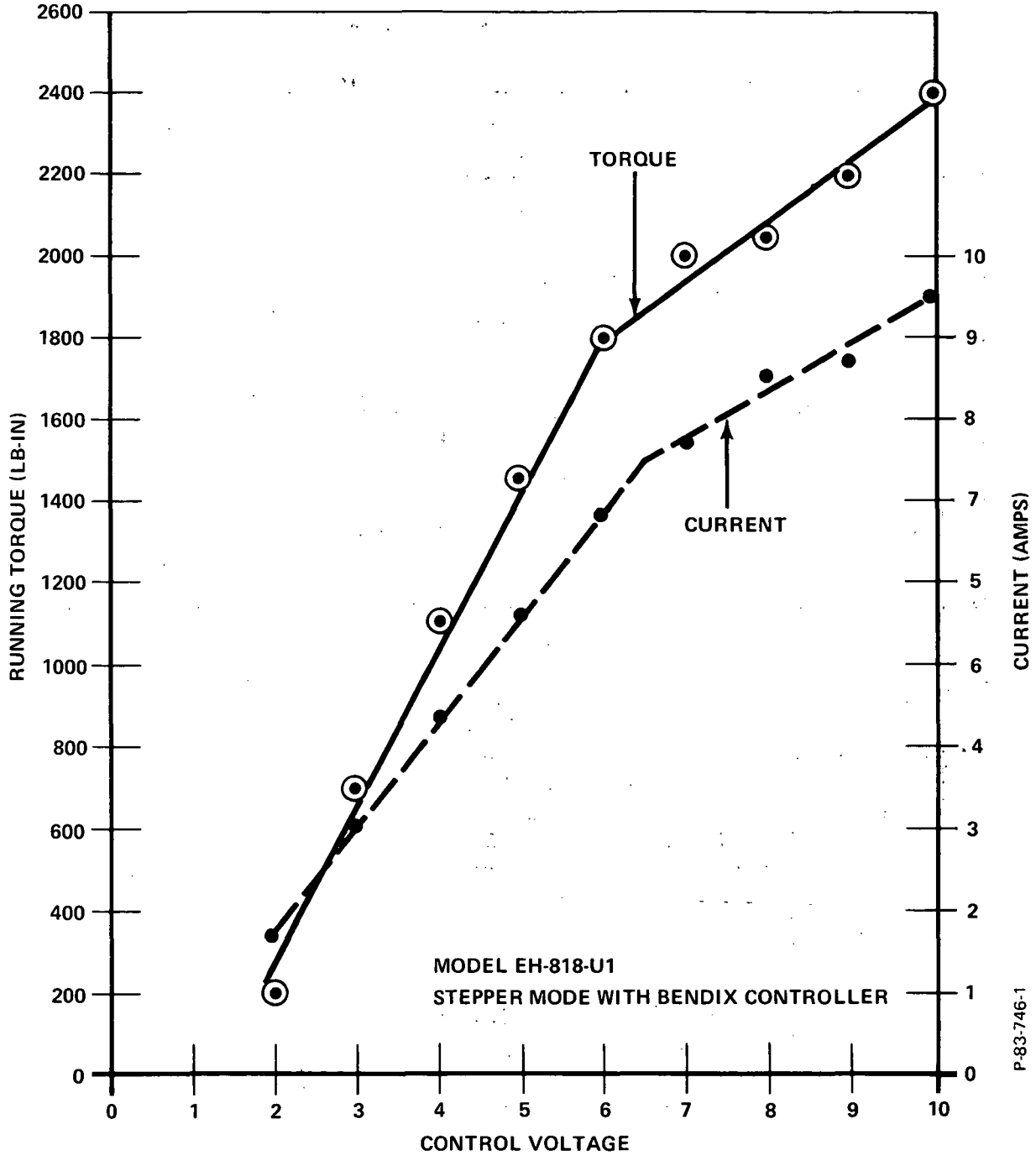

Figure 6-4 - Running Torque and Current Versus Control Voltage in Stepper Mode (Model EH-818-U1)

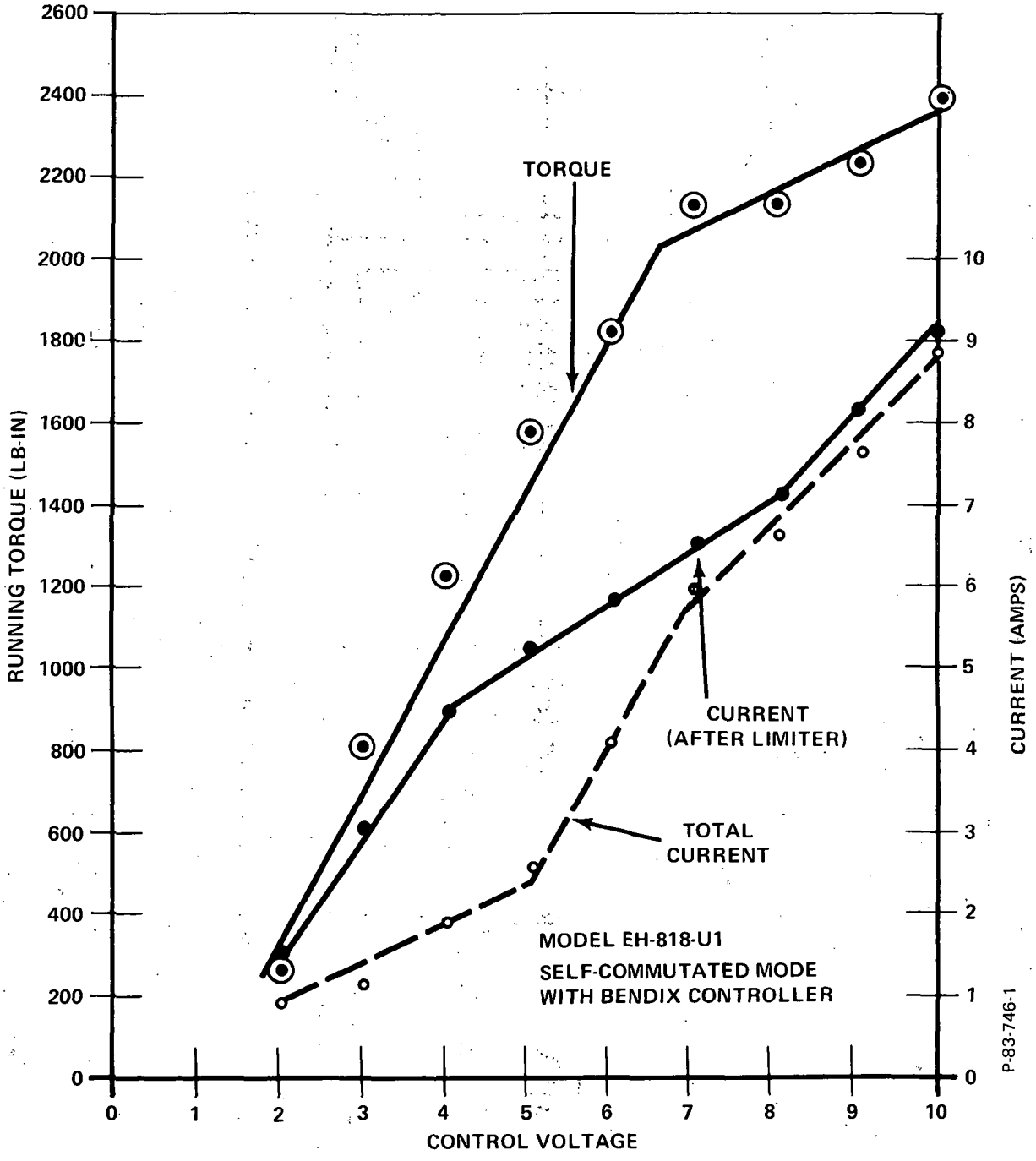

Figure 6-5 - Running Torque and Current Versus Control Voltage in Self-Commutated Mode (Model EH-818-U1)

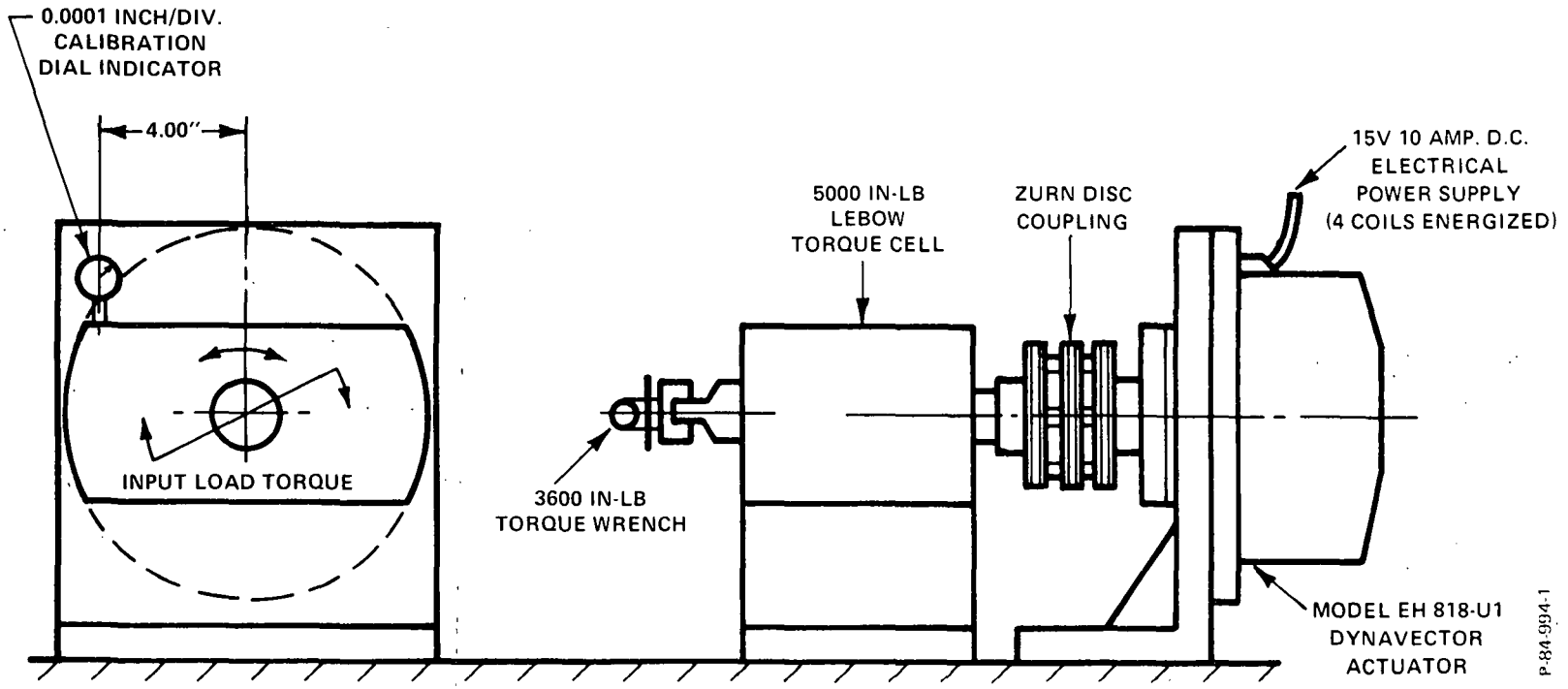

Figure 6-6 - Mechanical Stiffness and Hysteresis Test Schematic

(6) The "loop" was completed by again reducing the counterclockwise direction until 1800 in-lbs were recorded. At this point, the test was complete.

(7) Starting in a counterclockwise direction, items (1) through (6) were repeated.

Several tests were run and the average values were used after converting the results to arc-minutes, to plot the torque-deflection curves shown in Figures 6-7 and 6-8. These tests were run with a bearing preload value of 1100 pounds.

As shown in Figures 6-7 and 6-8, the initial slope line originating at the zero (start) position defines the actuators stiffness characteristics. As shown in the figures, it passes through the 3 arc-minute position at 1200 in-lb applied torque. These test results show the actuators stiffness characteristics to be 400 in-lb/arc-minutes (1.375×10^6 in-lb/radian) which is the minimum allowable stiffness defined in the design specification. The continuity of the curve through the zero torque position indicates that the actuator does not have any backlash when the coils are energized. The absence of backlash is attributed to the large number of contacting teeth sharing the load.

The 1.0 arc-minute hysteresis band at zero torque occurs as the rotor ring gear moves its mesh position to either side of top dead center to support the applied load. Mesh friction effects prevent the rotor from returning to its absolute original start position as the load is removed. Also, with four coils energized, the rotor is initially in a position with its eccentricity axes aligned between the two energized poles at the minimum air gap position. As the load torque is applied, the rotor mesh point rotates to support the load. It swings from a position between the poles toward a position in line with a pole. As the relative air gap is reduced, the rotor becomes attracted to that pole by its increased field strength. Relieving the applied load does not perfectly recenter the rotor as the combined effects of stator attractive force and mesh friction effects slightly bias the rotor position. This characteristic exists for all designs where complete load reversal is to be experienced. The hysteresis band at zero load torque would be reduced to 0.3 arc-minutes if only unidirectional loading (0 to +1800 in-lbs) were applied.

- Frequency Response Tests

The objectives of these tests were to determine the closed-loop frequency response and dynamic stiffness of Model EH-818-U1 with an inertia load and position feedback. A further objective was to examine the test results for hysteresis effects.

The test circuit used is shown in Figure 6-9, and the Analog-to-Digital Converter in Figure 6-10. The frequency response test results are shown in Figures 6-11, 6-12, and 6-13. The response to a $\pm$ 1/2-degree

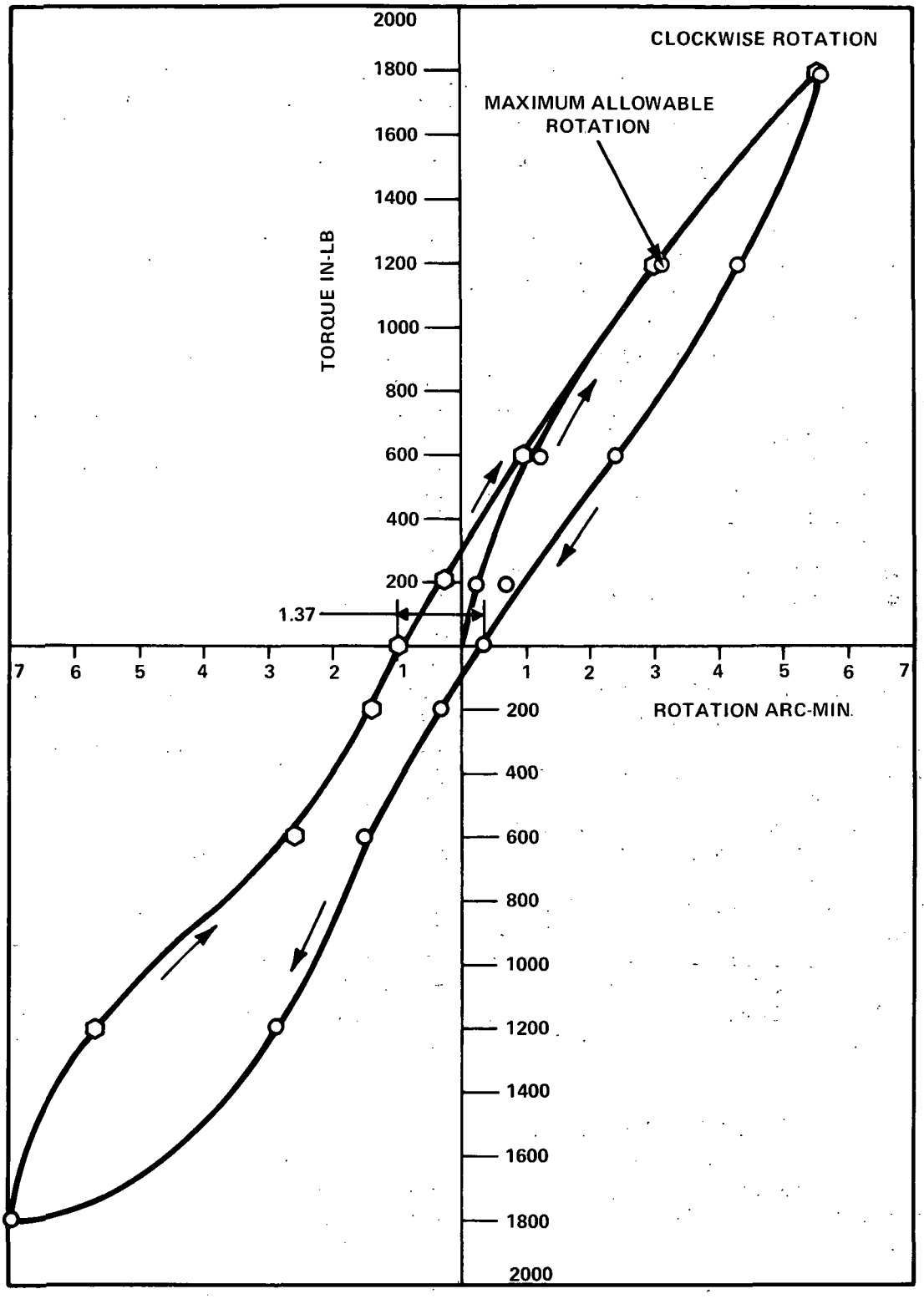

Figure 6-7 - Model EH-818-U1 Stiffness and Hysteresis Curve (CW Rotation)

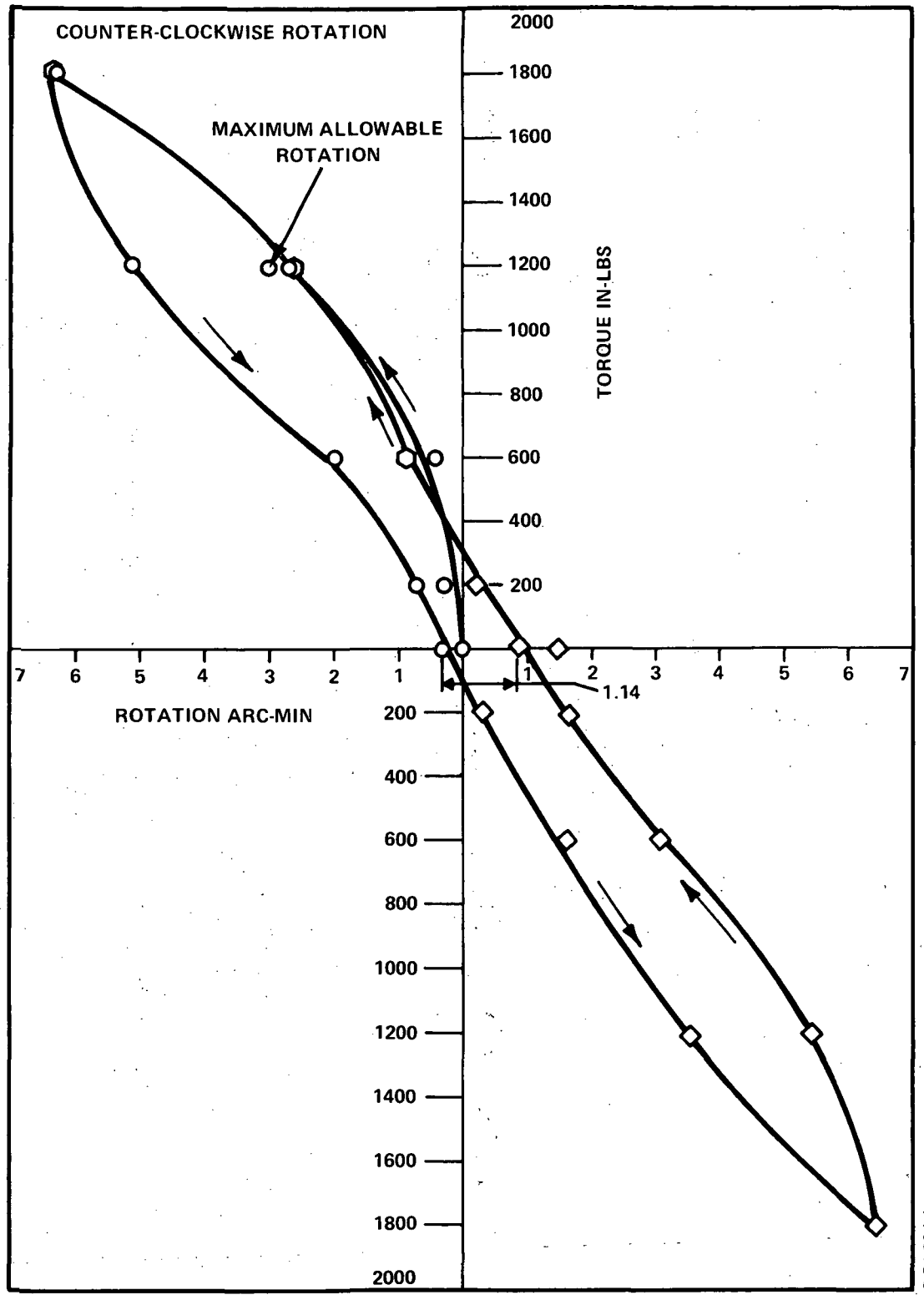

Figure 6-8 - Model EH-818-U1 Stiffness and Hysteresis Curve (CCW Rotation)

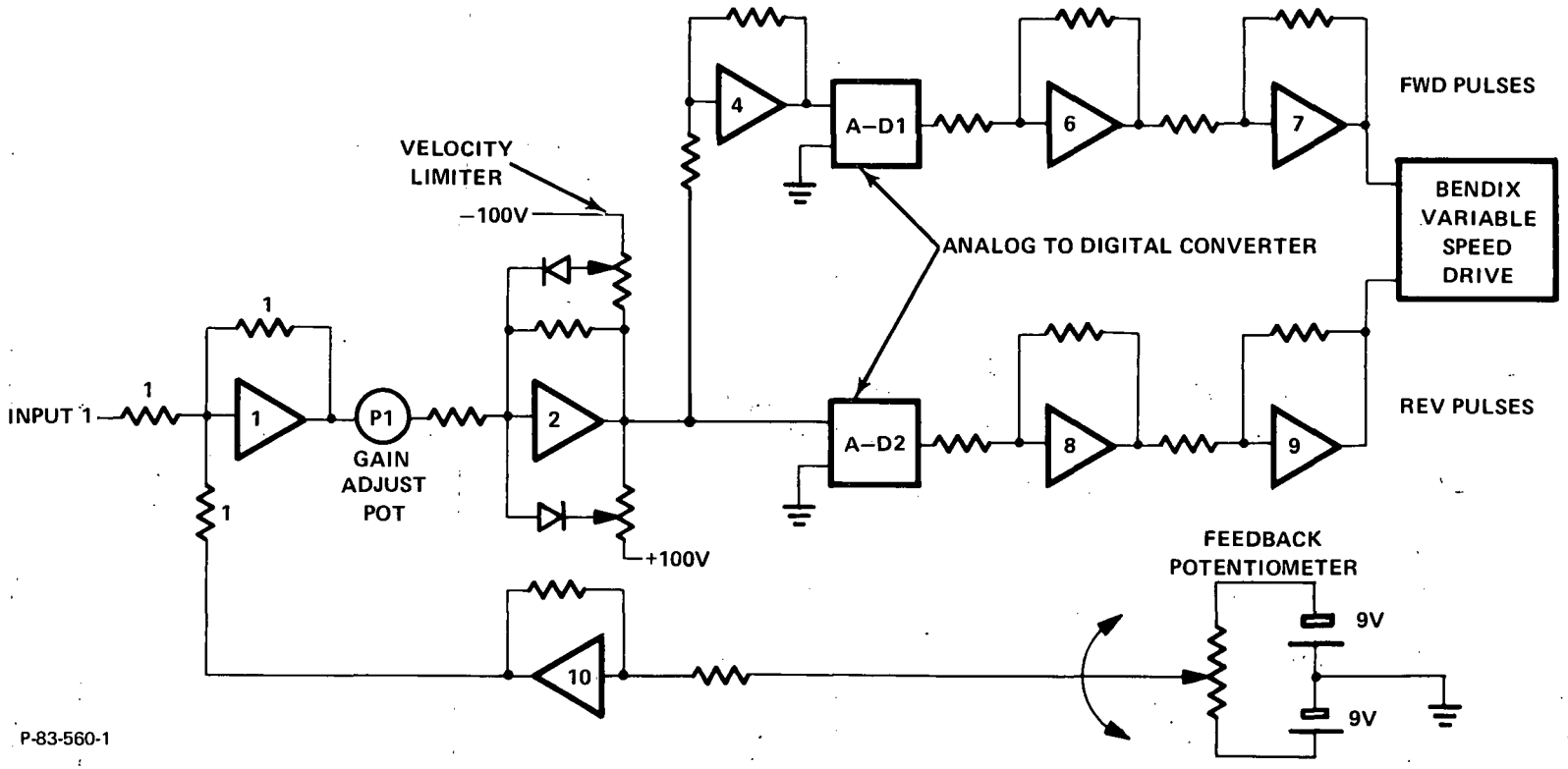

Figure 6-9 - Analog Computer Schematic - Closed Loop Tests

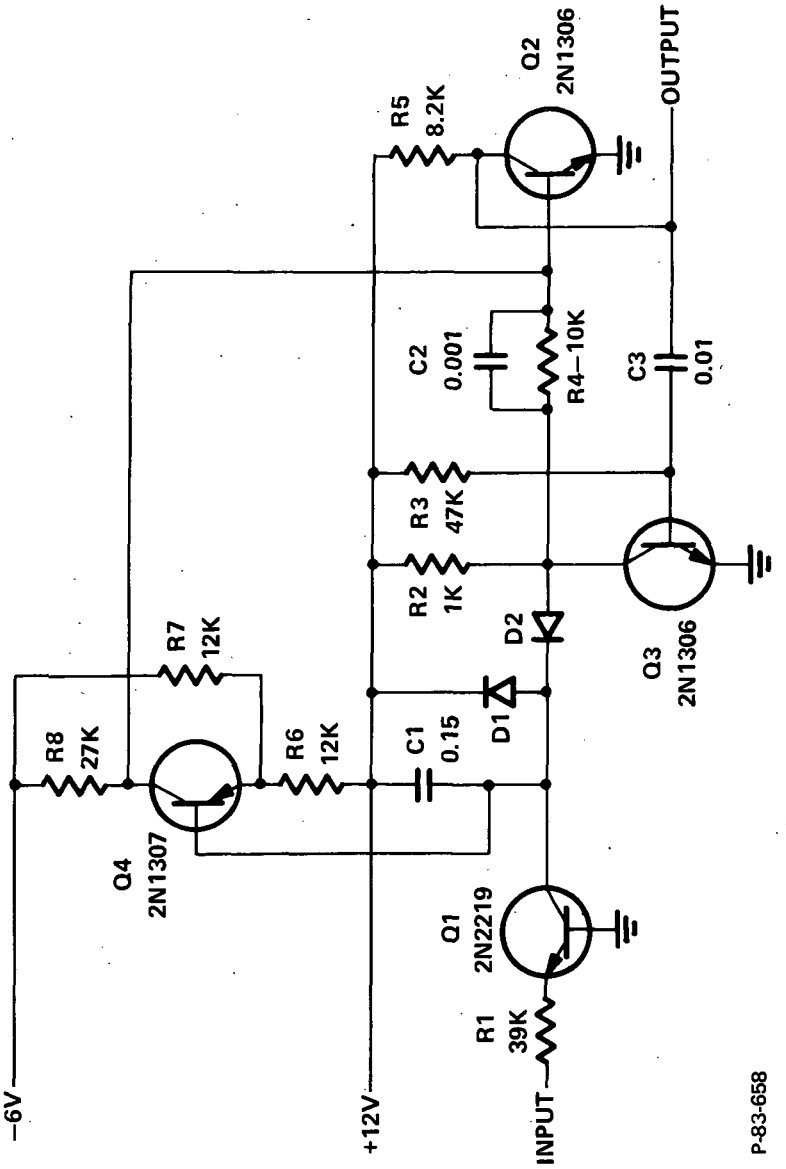

Figure 6-10 - Analog-to-Digital Converter Schematic

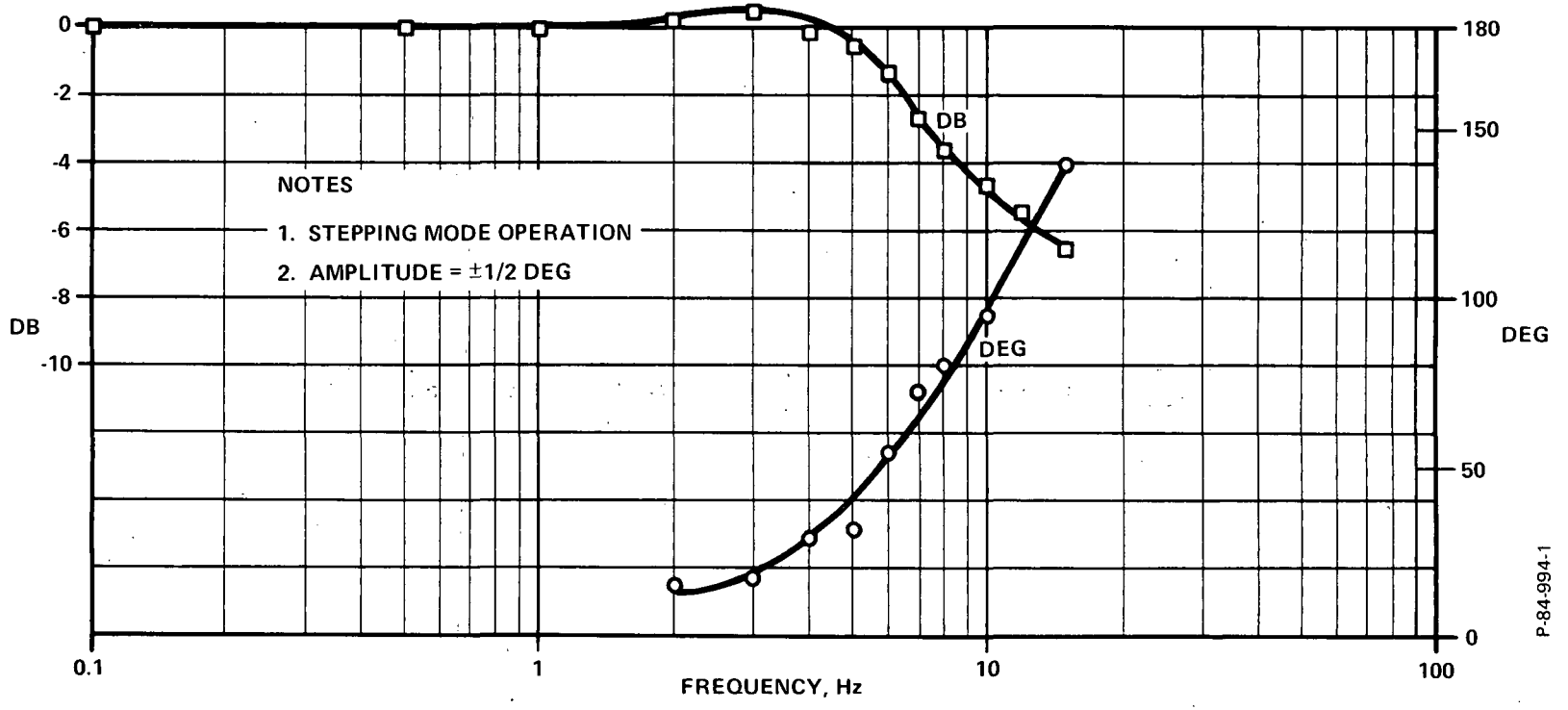

Figure 6-11 - Frequency Response (Model EH-818-U1 at ±0.5 degree amplitude)

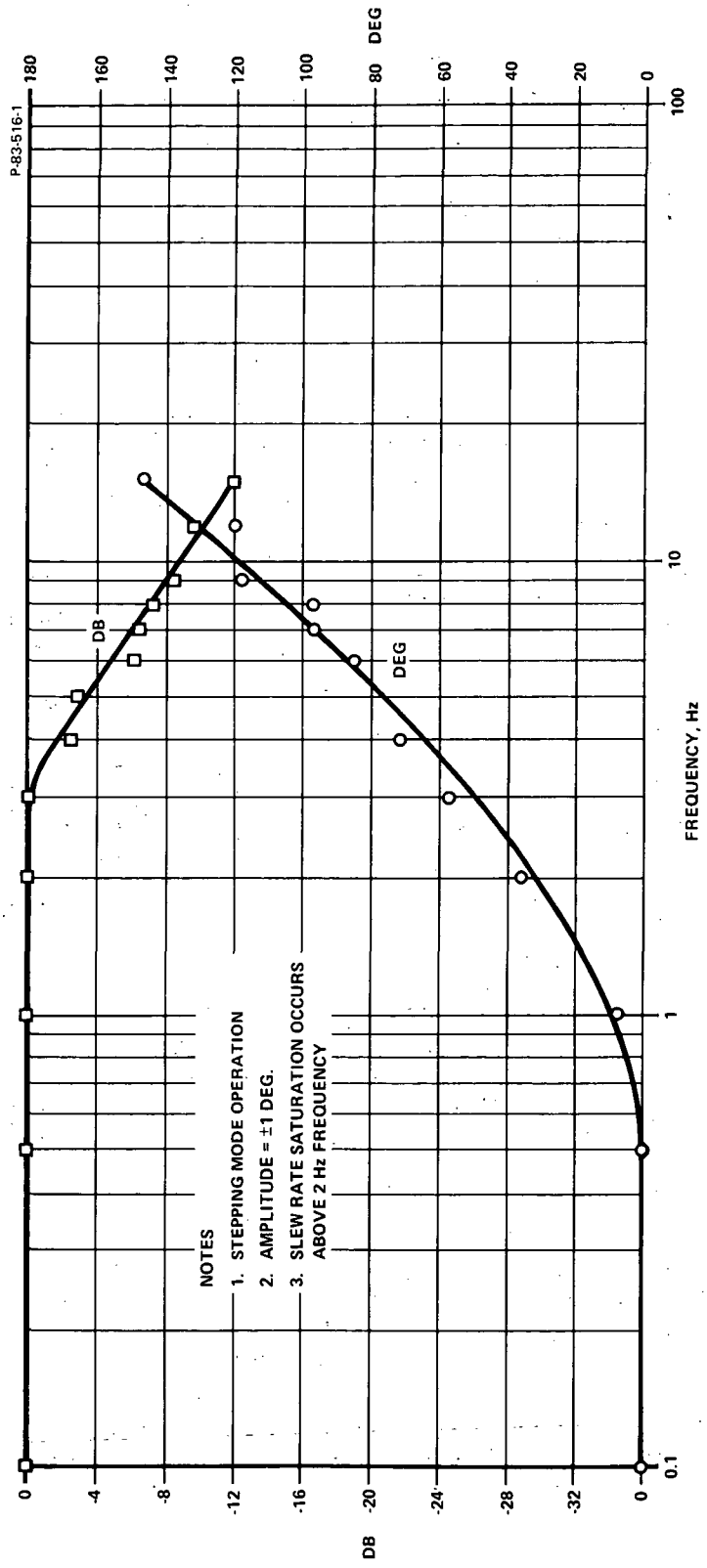

Figure 6-12 - Frequency Response (Model EH-818-U1 at ±1 degree amplitude)

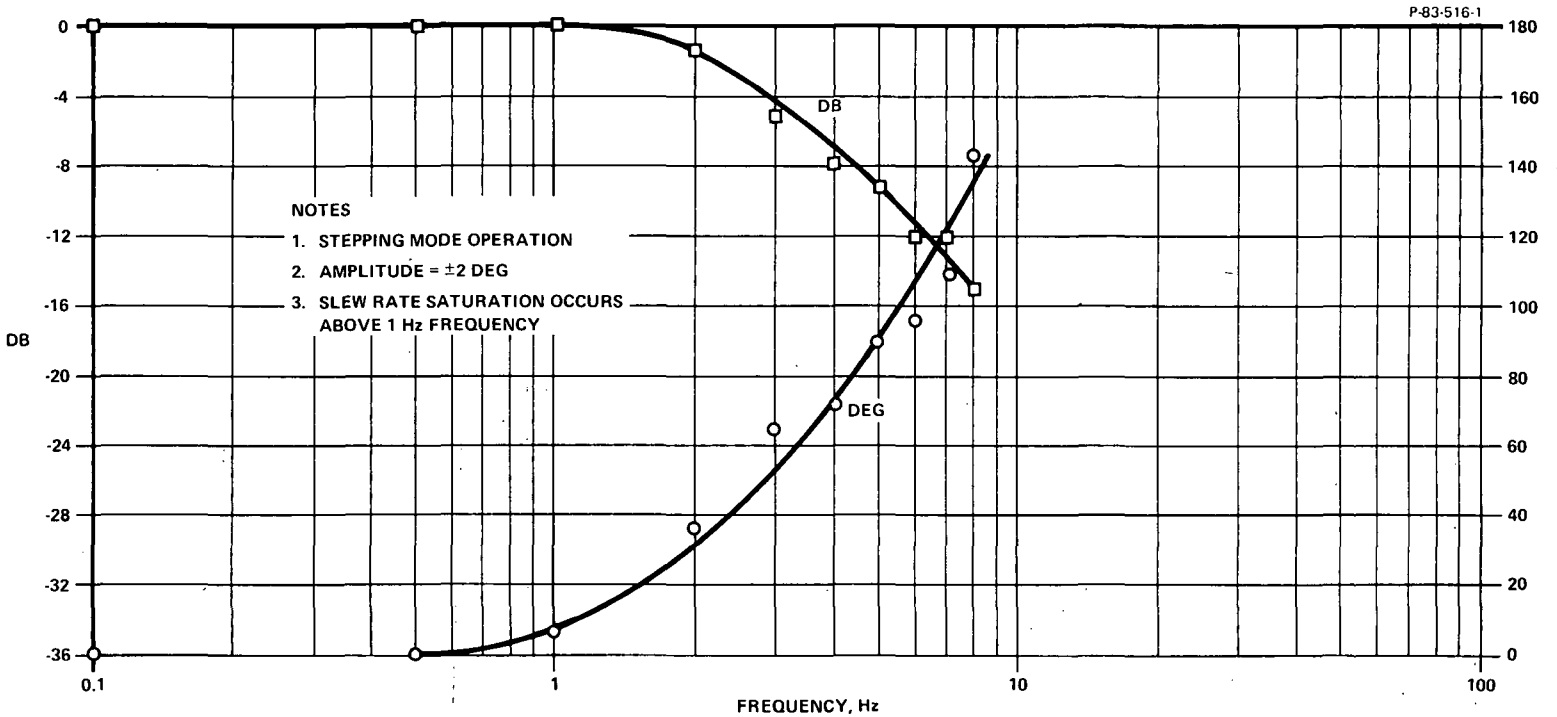

Figure 6-13 - Frequency Response (Model EH-818-U1 at ±2 degrees amplitude)

amplitude input shows a 90 degree phase lag at 9.4 hertz and is 3 db down at 7.3 hertz. The response decreases with larger amplitudes due to slew rate saturation. The effect of saturation is to lower the gain as the frequency is increased, thus reducing the response. Typical sinusoidal and step response waveforms are shown in Figures 6-14 and 6-15.

6.2 FLIGHTWEIGHT ACTUATOR MODEL EH-818-U2 SERIAL No. 1 TEST SUMMARY

The Serial No. 1 Actuator was tested in both stepper and self-commutated control modes. Torque-speed-current data were recorded for all modes. In addition, backlash, stiffness and hysteresis tests were conducted on the unit. A frequency response analysis to predict the performance when driving a flightweight gimbal inertia is presented in Appendix G. The stepper controller wiring schematic is shown in Figure 6-16.

- Torque-Speed Tests

The torque versus speed and current versus speed test results for the Actuator (S/N-1) with stepper controller (S/N-1) are presented in Table 6-4. The self-commutated tests were run with the self-commutated controller (S/N-1) and the results are presented in Table 6-5.

- Discussion of Test Results

At rated condition, Actuator (S/N-1) developed 1100-1200 lb-in. output torque in the stepper and self-commutated operating mode. At stall, the unit developed 2200-2000 lb-in., respectively. These values are 64 percent the required torque at rated conditions and 87.5 percent the required torque at stall. The loss in torque output is attributed to the shortened stator design and temperature effects on coil resistance.

It is recommended that subsequent design include a longer stator configuration and that the stator housings incorporate cooling fins to increase its radiation surface. In addition, an investigation of coil winding arrangements, series versus parallel, is required to optimize the actuators motor performance.

- Mechanical Backlash, Stiffness and Hysteresis Tests

The Actuator (S/N-1) was tested for backlash, stiffness and hysteresis on the test fixture shown in Figure 6-17. The fixture is similar to the breadboard actuator test fixture shown in Figure 6-6. A linear variable differential transformer LVDT was added with instrumentation to provide an analog output of load versus deflection on an X-Y plotter. A description of the test set-up and procedure follows:

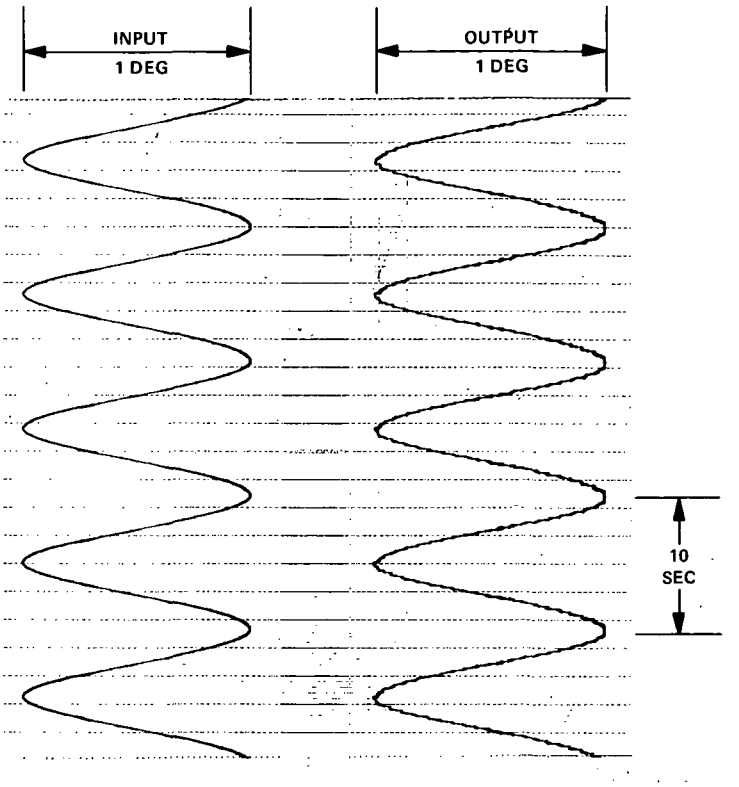

Figure 6-14 - Waveforms During ±1 Degree Response Test

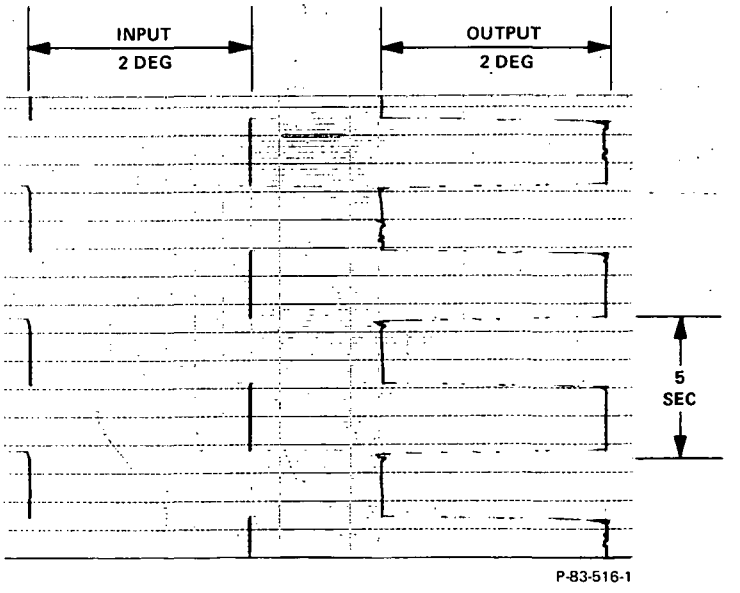

Figure 6-15 - Waveforms During ±2 Degrees Response Test

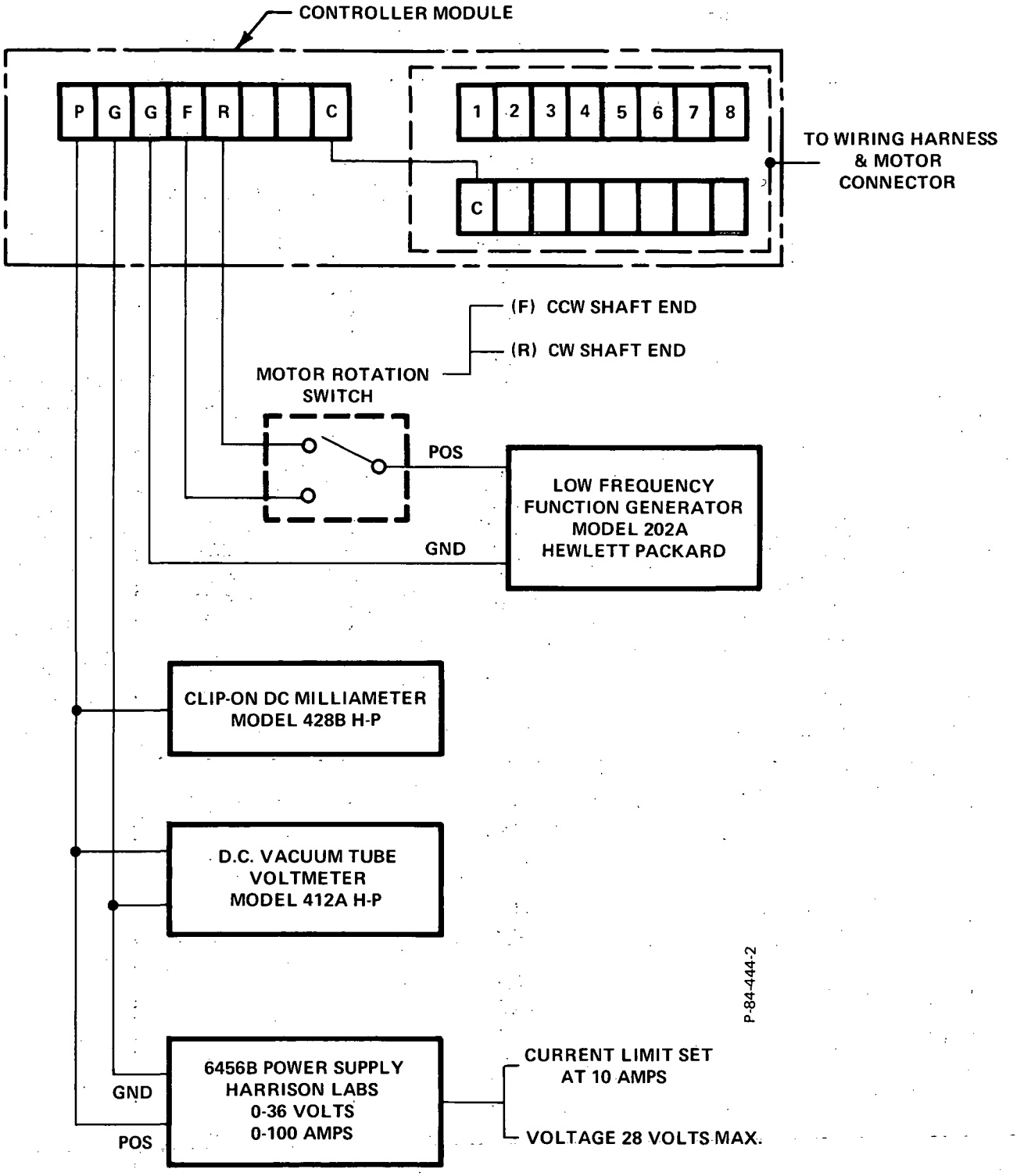

Figure 6-16 - Dynavector Drive Stepper Control - Test Schematic

Table 6-4 - Actuator (S/N-1) Stepper Torque - Speed Tests

Performance Test No. 1 - Actuator at Room Temperature

Voltage (Volts)	Pulses/ Sec	Stall Torque (in-lb)	Current (Amps)	Rotation
28	5	2200	10.0	CW
28	25	2000	9.2	CW
28	45	1800	8.2	CW
28	75	1600	6.5	CW
28	105	1200	5.2	CW
28	150	600	3.5	CW
28	200	300	2.5	CW
28	250	200	2.1	CW
28	300	200	2.0	CW
28	5	2000	10.0	CCW
28	25	1900	9.2	CCW
28	45	1800	8.1	CCW
28	75	1600	6.5	CCW
28	105	1300	5.5	CCW
28	150	700	4.1	CCW
28	200	600	3.1	CCW
28	250	400	3.0	CCW
28	300	200	2.5	CCW

Maximum No-Load Speed CW and CCW was 420 pps.

Performance Test No. 2 - Actuator Housing at 123°F with an Ambient at 70°F

Voltage (Volts)	Pulses/ Sec	Stall Torque (in-lb)	Current (Amps)	Rotation
28	25	2000	10.0	CW
28	50	1900	9.5	CW
28	75	1800	8.5	CW
28	100	1400	6.5	CW
28	150	750	5.0	CW
28	200	400	2.5	CW
28	250	150	2.5	CW

Maximum No-Load Speed CW was 300 pps.

Table 6-5 - Actuator (S/N-1) Self-Commutated Torque-Speed Tests

Performance Test No. 1

(1) Actuator housing at 123°F. Air ambient 70°F.

(2) Two proximity driver circuits were replaced with commercial externally packaged units. Data recorded was as follows:

Voltage (Volts)	Torque (lb-in)	Speed (rpm)	Current (Amps)	Rotation
28	1750	Stall	9.5	CW
28	1625	0.55	8.5	CW
28	1100	1.0	6.0	CW
28	800	1.2	4.5	CW
28	650	1.3	4.0	CW
28	350	1.4	3.5	CW
28	250	1.5	2.75	CW
28	No-Load	1.8	2.25	CW

The power-on tests were conducted with four adjacent coils energized to 10 amperes total input current (2.5 amperes per coil) and 15 volts dc. The load was applied with a torque wrench to the actuator shaft in both a clockwise and counterclockwise direction and the shaft windup was recorded on an X-Y plotter. The actual torque recorded on the X-axis of the X-Y plotter was the output signal of a 5000 in-lb rated Lebow torque cell. The shaft windup was measured with an LVDT, positioned 4.0 inches from the actuator centerline. Prior to each test, the LVDT was mechanically calibrated using a 0.0001-inch-per-division calibration dial indicator also positioned 4.0 inches from the actuator centerline. Its output signal was recorded on the Y-axis of the X-Y plotter as arc-minutes windup. (At 4.0-inches radius arm, inch deflection times 0.86 conversion constant equals arc-minute windup.)

The mechanical backlash, stiffness and hysteresis tests were conducted as follows:

(1) Instrumentation calibrated, checked and zeroed.

(2) Backdriving torque applied in both a clockwise and counterclockwise direction. Starting at zero, the torque was applied clockwise up to +2400 in-lbs, slowly reduced to zero and without any adjustment continued through zero position counterclockwise to -2400 in-lbs, slowly reduced through zero to +2400 in-lbs clockwise and stopped.

(3) The test was twice repeated for each direction of rotation.

(4) An X-Y plotter recorded all data.

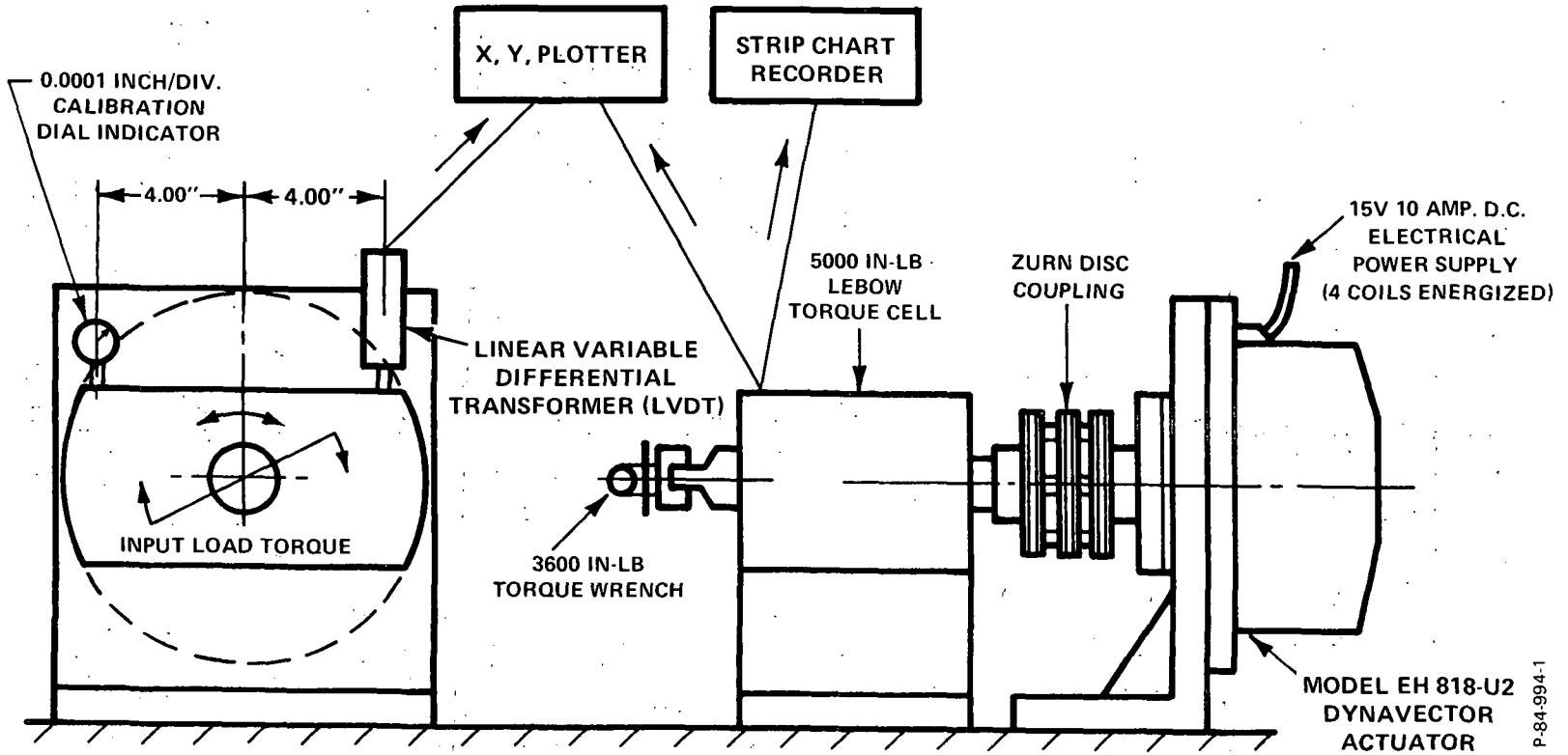

Figure 6-17 - Flightweight Actuator Model EH-818-U2 Mechanical Stiffness and Hysteresis Test Installation

The results of the first set of stiffness, backlash and hysteresis tests on Actuator (S/N-1) are summarized below. The actuator was tested in an "as received" condition from first assembly without modifications.

Input Load Direction	Power Condition	Stiffness	Hysteresis at Zero-Load	Backlash
Clockwise	On	5.9 arc-min.	1.0	1.3
Counterclockwise	On	5.2 arc-min.	1.0	1.1

The excessive backlash measured in Test No. 1 was attributed to over "lapping" the heat-treated gears (designed with a slight interference fit) during initial assembly. The recommended corrective action, based upon previous experience, was to chrome plate the mesh to fit. Consequently the following modifications were conducted on Actuator (S/N-1):

(a) 0.0003-inch-per-side hard chrome plating on all internal rotor meshes.

(b) 0.0002-inch-per-side hard chrome plating on the output gear mesh.

(c) 0.0004 inch (total) added to outboard ground gear bearing outside diameter.

The chrome plating was added to the outboard bearing outside diameter to eliminate 0.0005/0.0006-inch shaft radial deflection at 2400 in-lb load observed during test.

The test results of the (S/N-1) unit after the above modifications were as follows:

Input Load Direction	Power Condition	Stiffness	Hysteresis At Zero-Load	Hysteresis At 1200 In-Lb	Backlash
Clockwise	On	3.4 arc-min	1.1 arc-min	1.1 arc-min	0
Counter-clockwise	On	3.6 arc-min	1.3 arc-min	1.6 arc-min	0
Clockwise	Off	3.7 arc-min	1.0 arc-min	1.2 arc-min	0
Counter-clockwise	Off	4.1 arc-min	1.1 arc-min	1.3 arc-min	0

As shown, chrome plating the meshes totally eliminated the mesh backlash and increased the actuator's stiffness from 5.9 to 3.6 arc-minutes. Several tests were made and the average value recorded for stiffness in the "power on" condition was 4.0 arc-minutes.

- Discussion of Test Results

When comparing test curve (Figure 6-18) clockwise rotation to test curve (Figure 6-19) counterclockwise rotation, approximately one arc-minute additional windup and hysteresis band at -1200 in-lbs is noted. The apparent reduction in stiffness and the presence of hysteresis is attributed to a change in rotor position as the load is reversed.

In the stiffness test, four coils are energized and the rotor is allowed to go to its no-load equilibrium position. Shaft deflection is then measured as the load torque is cycled about this position. A hysteresis effect is observed in the test data. This hysteresis occurs because there are three stable equilibrium positions for the rotor as the test is conducted. One equilibrium position occurs when the rotor is located so that the minimum air gap is mid-way between the four active poles. The other two equilibrium positions are where the minimum air gap coincides with a pole center.

During self-commutated operation, the rotor is never in the positions, relative to the active poles, that are used for the stiffness test. For each set of active coils, there is only one rotor position where the minimum air gap coincides with a pole center. Therfore, the hysteresis effect observed in the stiffness test would not occur in self-commutated operation.

The stator shown in Figure 6-20(a) has coils 1, 2, 7, and 8 energized. The minimum air gap is between poles 1 and 8. If a torque is applied to the rotor, moving the minimum air gap to a point between coils 1 and 2, then released, the rotor will stop when the minimum air gap is at coil 1. If an opposite torque is applied, moving the minimum air gap to a point between coils 7 and 8, then released, the rotor will stop when the minimum air gap is at coil 8. Thus, there is a hysteresis effect in the stiffness test equivalent to the distance between coils 8 and 1. This hysteresis does not exist when the motor is operating in self-commutated mode.

Figures 6-20(b) and 6-20(c) illustrate self-commutated operation. In Figure 6-20(b), the minimum air gap is mid-way between coils 8 and 1. Coil 8 has just been switched on. Coils 1, 2, 3, and 4 are energized. The rotor will normally move until the minimum air gap is mid-way between coils 1 and 2, at which time coil 2 will be switched off and coil 5 will be switched on by the electronic commutator. Now, a load torque is applied, which stops the rotation. This torque is cycled such that the minimum air gap moves between the two commutation points. There should be no hysteresis such as indicated in the stiffness test as there is only one point where the minimum air gap coincides with a pole center (pole 1), and thus there is only one point of stable equilibrium. If the rotor is moved so that the minimum air gap coincides with another pole center, the commutator will switch the coils so that another coil set is on.

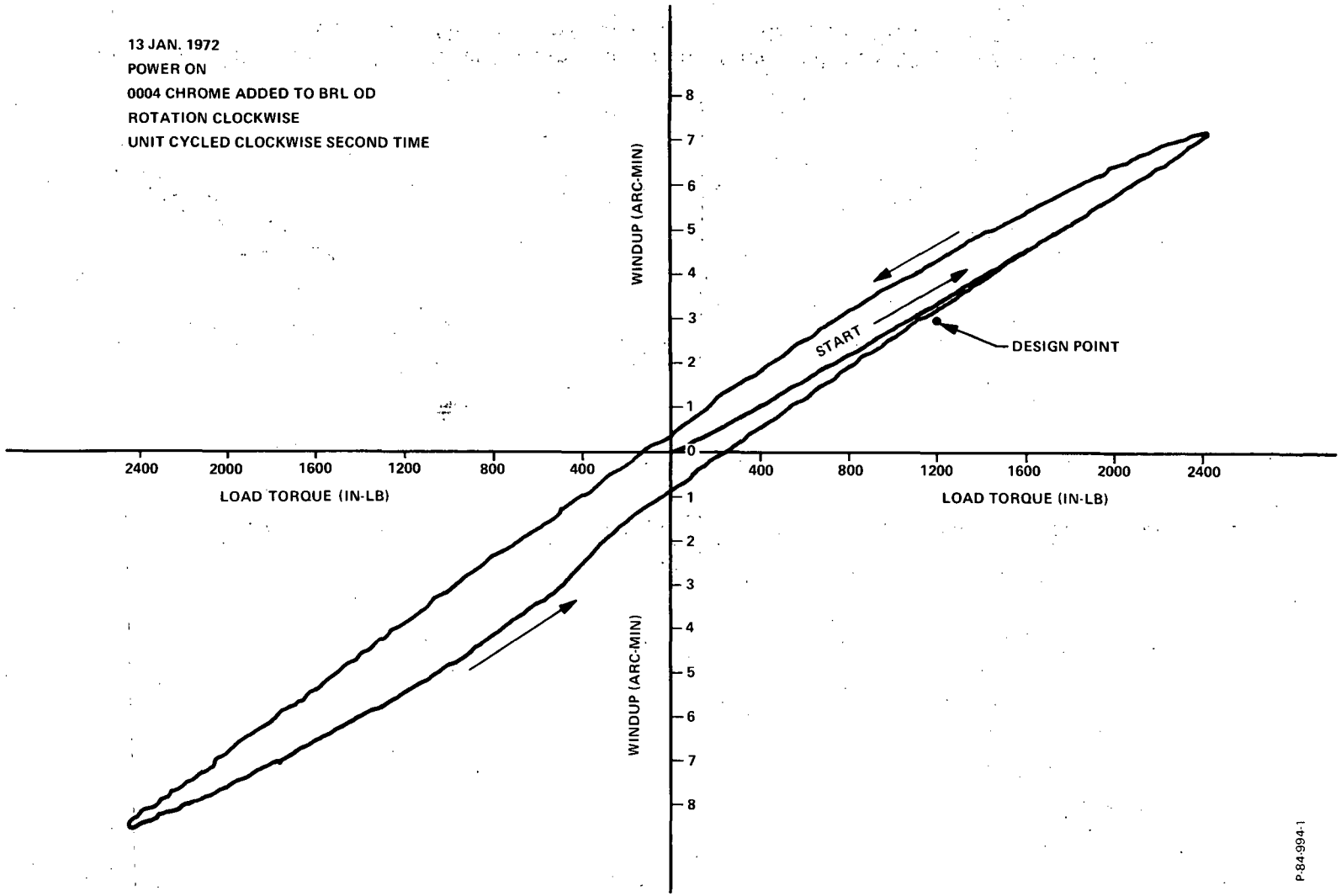

Figure 6-18 - Flightweight Actuator Model EH-818-U2 - SN/1 Mechanical Stiffness Characteristics Curve - Clockwise Rotation

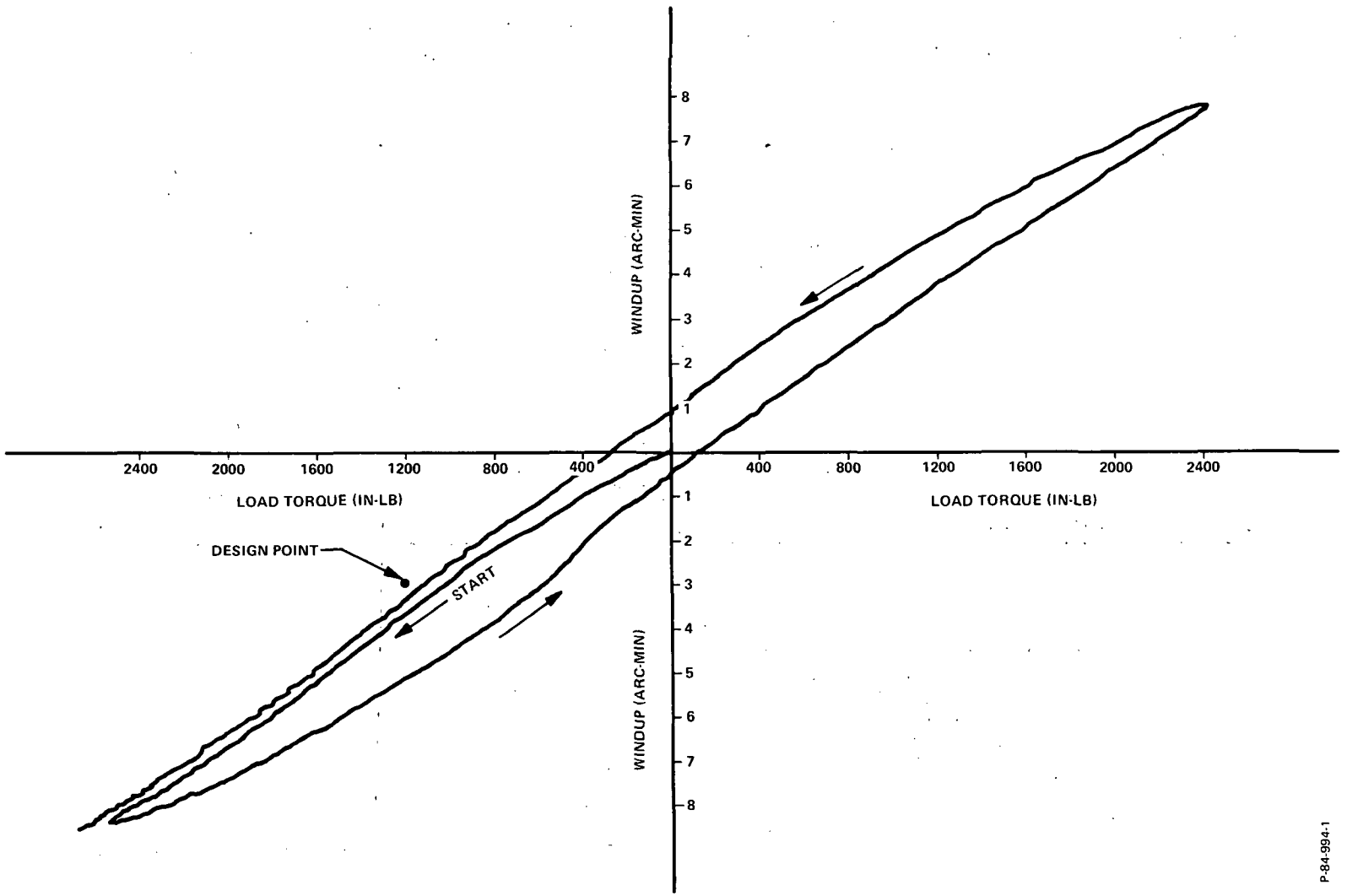

Figure 6-19 - Flightweight Actuator Model EH-818-U2 - SN/1 Mechanical Stiffness Characteristics Curve - Counterclockwise Rotation

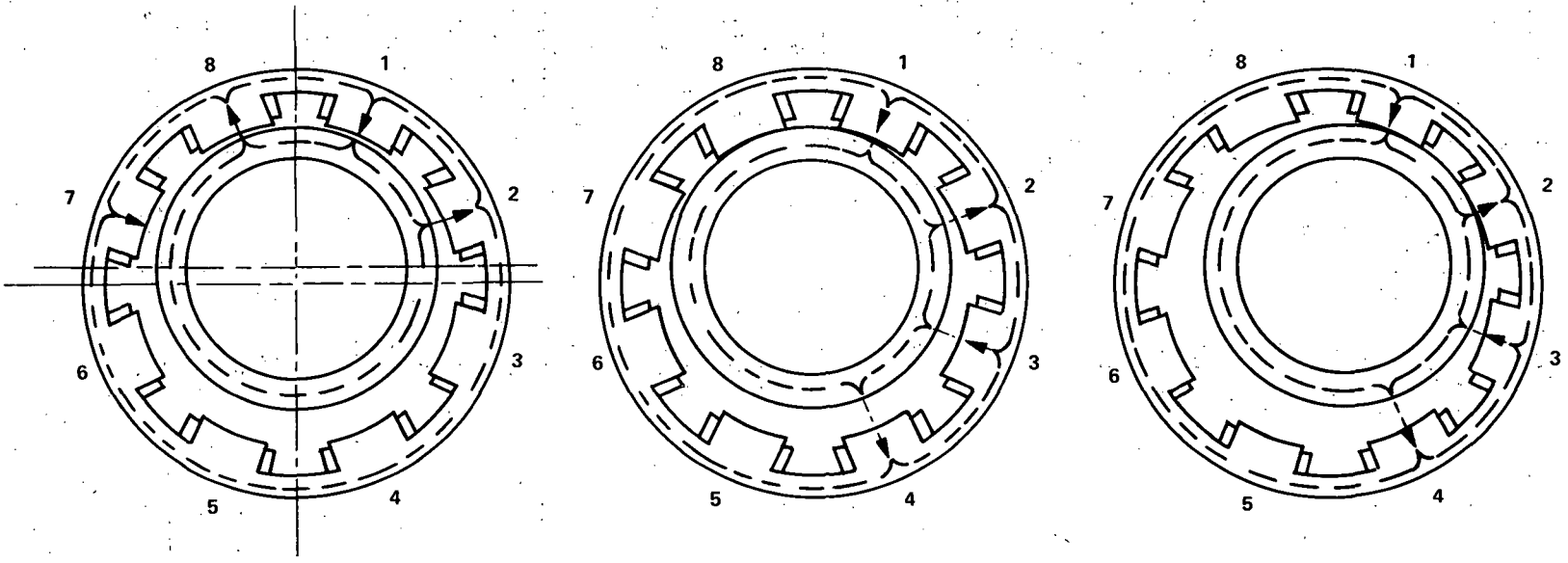

A. EQUILIBRIUM POSITION FOR STIFFNESS TEST

B. ROTOR POSITION (1) FOR SELF-COMMUTATED OPERATION – COIL 8 HAS JUST BEEN SWITCHED OFF AND COIL 4 HAS JUST BEEN SWITCHED ON

C. ROTOR POSITION (2) FOR SELF-COMMUTATED OPERATION – COIL 1 IS JUST READY TO BE SWITCHED OFF AND COIL 5 IS JUST READY TO BE SWITCHED ON

Figure 6-20 - Schematic - Rotor Positions in the Magnetic Field

- Flightweight Actuator (S/N-1) Test Summary and Conclusions

Flightweight Actuator (S/N-1) developed 1200 to 1100 in-lbs output torque and 1 rpm rated speed both in the stepper and self-commutated mode. At stall, the actuator developed 2200 and 2000 in-lbs, respectively. The reduction in output performance is attributed to reduction of stator length from 2.60 inches for the breadboard design to 1.8 inches for the flightweight design. The stator length was reduced to minimize the actuators weight. This goal was achieved. Whereas the breadboard actuator weighed 56 poinds, the flightweight actuator weighs 35 pounds.

Tests of Actuator (S/N-1) after fabrication and assembly showed 1.3 arc-minutes backlash with four coils energized to 28 volts dc and 10.0 amperes current flow. Chrome plating the meshes up to 0.0004-inch-per-side completely eliminated the backlash and increased the units stiffness from 5.9 to 4.0 arc-minutes windup at 1200 in-lbs applied load. As in the breadboard actuator tests, a 1.0 arc-minute change in stiffness characteristics and the presence of hysteresis band widths were observed. These characteristics are attributed to the fact that the rotor moves out of the stationary magnetic field as load torque is applied. As the same four coils remain energized throughout the test, the mechanical stiffness is decreased and hysteresis effects are observed. These test results simulate the operating characteristics of a stepper controlled actuator operating with power on and zero rate. When operating in the self-commutated mode, for which these units are designed, the stiffness should improve and the hysteresis minimized. Self-commutated, the actuators field and rotor phased angular positions cannot exceed one-half the distance between poles before the field is rotated by the proximity pickup sensors.

The stiffness and hysteresis tests with the self-commutated controller arrangement were not run because the controller was not available.

The reduction is stator length was not arbitrarily undertaken. Breadboard actuator performance data and electrical design studies indicated that a reduction in stator length was feasible providing the induced back emf at rated conditions could be maintained or reduced and the stall saturation current sufficiently high to develop the required torque. Breadboard tests have shown the actuator developed more than the required 2400 in-lb stall torque required. Based on these results including current flow at stall, the 1.8-inch flightweight stator length was established. Obtaining the required output torque at rated speed required that a compensating change in electrical design be made. The design changes were based upon the following relationships. Back emf, E_b, is directly proportional to the number of turns, pole face area, flux density, and operating speed. Flux density, B, is directly proportional to ampere turns and inversely proportional to air gap. The mesh design would not permit changing the air gap and the same ampere turns were required if output performance was to be satisfied.

Given that flux density and operating speed are constant, then the product of pole face area and number of turns is a constant also - for an acceptable back emf. Therefore, changing the pole face area required that the number of turns be changed from 162 turns per coil, with two coils parallel wound for the breadboard actuator design; to 450 turns per coil, series wound, on the flightweight design. To insure the ampere turns were the same, the wire sizes were increased from No. 25 wire for the breadboard design to No. 22 wire for the flightweight design. Winding the coils in series instead of parallel arrangement was based upon an equivalence analyses. The flux density of the breadboard actuators parallel winding arrangement should be equivalent to the series wound flightweight design arrangement. BRL has concluded that this area of design, series versus parallel, requires additional investigation. As it is very probable that the reduction of actuator performance, especially at rated conditions, may be attributed to the way in which the stator coils were wound.

6.3 FLIGHTWEIGHT ACTUATOR MODEL EH-818-U2 SERIAL No. 2 TEST SUMMARY

The Serial No. 2 Actuator was tested in the stepper and self-commutated control modes. Torque-speed-current data were recorded for all modes. In addition, backlash stiffness and hysteresis tests were conducted on this unit.

- Torque-Speed Tests

The torque versus speed and current versus speed test results for Actuator (S/N-2) with stepper controller (S/N-2) are presented in Table 6-6. The self-commutated tests were run with self-commutated controller (S/N-1) and the results are presented in Table 6-7.

- Discussion of Test Results

At rated condition, Actuator (S/N-2) developed 1400 in-lb output torque in the stepper and self-commutated operating mode. At stall, the unit developed 1900 in-lbs, respectively. These developed torques are 78 percent the required torque at rated conditions and 79.5 percent the required torque at stall. The loss in torque output is attributed to the shortened stator design and temperature effects on coil resistance.

- Mechanical Backlash, Stiffness and Hysteresis Test

Actuator "S/N-2 was tested for mechanical backlash, stiffness and hysteresis according to the procedures described for Actuator (S/N-2) in Section 6.2.

Table 6-6 - Actuator (S/N-2) Stepper Torque - Speed Tests

Performance Test No. 1 - Actuator at Room Temperature				
Voltage (Volts)	Pulses/ Sec	Stall Torque (in-lb)	Current (Amps)	Rotation
28	20	1900	10.0	CW
28	55	1900	10.0	CW
28	68	1800	9.0	CW
28	88	1700	8.5	CW
28	105	1500	7.0	CW
28	115	1400	6.5	CW
28	132	1150	5.6	CW
28	145	950	5.1	CW
28	165	700	4.7	CW
28	190	550	3.7	CW
28	250	370	3.0	CW
28	350	200	2.0	CW
28	470	0	1.9	CW
28	20	1650	10.0	CCW
28	45	1600	10.0	CCW
28	95	1500	7.8	CCW
28	105	1400	7.1	CCW
28	113	1250	6.4	CCW
28	124	1100	6.0	CCW
28	137	900	5.4	CCW
28	163	700	4.9	CCW
28	185	650	4.3	CCW
28	215	350	3.3	CCW
28	296	200	2.8	CCW
28	424	100	2.0	CCW
28	450	0	2.0	CCW

Table 6-7 - Actuator (S/N-2) Self-Commutated Torque - Speed Tests

Voltage (Volts)	Torque (in-lbs)	Speed (rpm)	Current (Amps)	Rotation
28	1900	0.75	8.2	CW
28	1500	0.95	7.0	CW
28	1300	1.1	5.8	CW
28	1000	1.27	4.5	CW
28	800	1.4	4.0	CW
28	600	1.55	3.6	CW
28	400	1.9	2.8	CW
28	200	2.92	2.0	CW
28	0	4.0	1.6	CW
28	1650	0.88	9.0	CCW
28	1600	0.90	7.25	CCW
28	1500	0.95	6.8	CCW
28	1400	1.01	6.5	CCW
28	1300	1.09	6.0	CCW
28	1200	1.17	5.5	CCW

The maximum no-load speed CW and CCW direction was 4 rpm.

The results of the tests, conducted with all meshes chrome plated 0.00025-inch-per-side, were as follows:

Input Load Direction	Power Condition	Stiffness	Hysteresis at Zero-Load	Backlash
Clockwise	On	4.1 arc-min	0.7 arc-min	0
Counterclockwise	On	4.2 arc-min	0.5 arc-min	0

The performance and stiffness test results for Actuator (S/N-2) are identical to those obtained for flightweight Actuator (S/N-1). As such, the summary statement and conclusions presented in Section 6.2 are applicable.

6.4 MODEL EH-818-U2 STATOR CHECKOUT PERFORMANCE TESTS

A stator performance checkout test was conducted on each stator assembly after coil winding and prior to shrink fit assembly into the stator housing. These tests were established after high voltage grounding conditions at 400 volts and above were found during initial testing of the flightweight design. The shorts occured after the prewound coils were "crush" formed over the stator poles to a configuration which prevents the coil from interfering with the proximity sensor. (It was established that "crush" shaping the coil scrapes the insulation coating off the wire at the pole piece corners.)

The problems described above were corrected by instituting the following stator assembly design modifications:

(1) Provide a large (0.060 x 45 deg-min) corner chamfer on each pole piece.

(2) Machine wind the coil directly onto the stator pole.

Initially, BRL was told by several coil winding vendors that machine winding the stator to the desired configuration was not feasible due to limited allowable clearance between the coils and the coil winding needle. Thus the technique to prewind the coil assemblies, then "crush" form them after installation, was established. Subsequent consultation with the Bendix Electric Power Division disclosed they had developed both the equipment and techniques required to satisfactorily wind the coils onto the stator assembly within the shape and installation constraints of the flightweight configuration.

The stator assembly (S/N-1) in Flightweight Actuator (S/N-1) and stator assembly (S/N-2) in Flightweight Actuator (S/N-2) were wound by the Bendix Electric Power Division to the required installation configuration. They have been electrically performance tested at Electric Power Division to the test specification outlined below. The test results for stator assembly (S/N-1) are presented in Table 6-8, and the test results for stator (S/N-2) are presented in Table 6-9.

The test procedure for stator tests is as follows:

Conduct the following electrical inspection tests 1 through 5 on each stator assembly. Record all data.

- Test No. 1 - Coil-to-Stator Shorts

  Apply 1500 volts at 60 Hz through a milliammeter to one terminal of each coil. Connect ground terminal to stator outside diameter. The current flowing from the coils to the stator shall not exceed 4.0 ma.

- Test No. 2 - Coil-to-Coil Shorts

  Apply 1500 volts at 60 Hz through a milliammeter to one terminal of each coil. Connect ground to each adjacent coil. The current flowing from one coil to each adjacent coil shall not exceed 4.0 ma. Repeat with all combinations of adjacent coils.

- Test No. 3 - High Temperature Test

  Repeat Tests 1 and 2 with the stator at a temperature of 70°C.

Table 6-8 - Stator Assembly (S/N-1) Electrical Checkout Test Results

The results of these series of five tests were as follows for stator assembly (S/N-1).

(Tests Nos. 1 & 2) - Coil-to-Stator Shorts

at 1500 volts, 60 Hz (Bendix HIPOT No. Y10)

Room Ambient		+70°C Ambient (2 Hr. Soak)	
Coil No.	Lead-to-Stator O.D. Leakage ma	Coil No.	Lead-to-Stator O.D. Leakage ma
1	0	1	0
2	0	2	0
3	0	3	0
4	0	4	0
5	0	5	0
6	0	6	0
7	0	7	0
8	0	8	0

Limit: 4.0 ma maximum

(Tests Nos. 2 & 3) - Coil-to-Coil Shorts

at 1500 volts, 60 Hz (Bendix HIPOT No. Y10)

Room Ambient		+70°C Ambient (2 Hr. Soak)	
Coil-to-Coil	Leakage ma	Coil-to-Coil	Leakage ma
1 - 2	0	1 - 2	0
1 - 8	0	1 - 8	0
2 - 3	0	2 - 3	0
3 - 4	0	3 - 4	0
4 - 5	0	4 - 5	0
5 - 6	0	5 - 6	0
6 - 7	0	6 - 7	0
7 - 8	0	7 - 8	0

Limit: 4.0 ma maximum

(Test No. 4) - Coil Resistance

at Room Ambient Kelvin Bridge No. P111

Coil No.	Res. Ohms	Coil No.	Res. Ohms
1	4.975	5	4.965
2	4.925	6	4.825
3	4.910	7	4.935
4	4.920	8	4.980

Limit: Shall not vary by more than 5 percent.

(Test No. 5) - Coil Internal Shorts

Voltage drop across each coil at 1.0 Amp., 60 Hz.

Coil No.	No. F14 Amps.	No. R89 Volts	Coil No.	No. F14 Amps.	No. R89 Volts
1	1.0	25.32	5	1.0	25.43
2	1.0	25.36	6	1.0	25.63
3	1.0	25.33	7	1.0	25.37
4	1.0	25.41	8	1.0	25.51

Limit: Shall not vary by more than 5 percent.

Table 6-9 - Stator Assembly (S/N-2) Electrical Checkout Test Results

The results of these series of five tests were as follows for stator assembly (S/N-2).

(Tests Nos. 1 & 2) - Coil-to-Stator Shorts

at 1500 volts, 60 Hz (Bendix HIPOT No. Y10)

Room Ambient		+70°C Ambient (2 Hr. Soak)	
Coil No.	Lead-to-Stator O.D. Leakage ma	Coil No.	Lead-to-Stator O.D. Leakage ma
1	0	1	0
2	0	2	0
3	0	3	0
4	0	4	0
5	0	5	0
6	0	6	0
7	0	7	0
8	0	8	0

Tests Nos. 2 & 3) - Coil-to-Coil Shorts

at 1500 volts, 60 Hz (Bendix HIPOT No. Y10)

Room Ambient		+70°C Ambient (2 Hr. Soak)	
Coil-to-Coil	Leakage ma	Coil-to-Coil	Leakage ma
1 - 2	0	1 - 2	0
1 - 8	0	1 - 8	0
2 - 3	0	2 - 3	0
3 - 4	0	3 - 4	0
4 - 5	0	4 - 5	0
5 - 6	0	5 - 6	0
6 - 7	0	6 - 7	0
7 - 8	0	7 - 8	0

(Test No. 4) - Coil Resistance

at Room Ambient Kelvin Bridge No. P111

Coil No.	Res. Ohms	Coil No.	Res. Ohms
1	5.015	5	4.915
2	4.987	6	4.900
3	4.955	7	4.895
4	4.930	8	4.993

(Test No. 5) - Coil Internal Shorts

Voltage drop across each coil at 1.0 Amp., 60 Hz.

Coil No.	No. F14 Amps.	No. R89 Volts	Coil No.	No. F14 Amps.	No. R89 Volts
1	1.0	25.23	5	1.0	25.24
2	1.0	25.20	6	1.0	25.24
3	1.0	25.25	7	1.0	25.20
4	1.0	25.22	8	1.0	25.21

- Test No. 4 - Coil Resistance

  Measure and record the resistance of each coil. The resistance shall not vary by more than 5 percent.

- Test No. 5 - Coil Internal Shorts

  Apply a 60 Hz voltage across each coil with a current meter in series. Adjust the voltage to give 1.0 amperes current. Record the voltage. The voltage shall not vary by more than 5 percent. This test should be of a momentary nature to avoid excessive power dissipation in the coil under test.

SECTION 7

RECOMMENDATIONS

The application of the integrated variable reluctance orbit motor-epicyclic transmission concept to the requirements of CMG torquers has been accomplished on this program. It is recommended that continued development be applied toward optimization of the drive concept in the areas of

(1) Alternate design arrangements

(2) Proximity sensor timing optimization

(3) Evaluate coil winding and energization options

(4) Evaluate hermetically sealed designs

(1) Alternate Design Arrangements

The internal ring gear-outer pole arrangement of the flight-weight actuators is equivalent to the design configuration shown in Section 3, Figure 3-4(d). This arrangement, defined as the high-ratio center output, provides the minimum inertia for any high ratio arrangement for a given torque size. However, a higher structural stiffness actuator could be accomplished by use of the high-ratio outer member output configuration shown as Figure 3-4(a). Here the gearing members are at a larger diameter and have higher stiffness characteristics but conversely, a high inertia value.

Depending on the specific application requirements, analytical and hardware tradeoffs should be conducted on all of the four arrangements shown in Figure 3-4 since each option has its own specific advantages.

(2) Proximity Sensor Timing Optimization

Both the breadboard and flightweight units used four sensors for generating self-commutation signals. Consequently, they necessarily had to be mechanically positioned in a symmetrical location relative to the stator coils (i.e., either centrally located between poles or on the pole centerline) to provide equivalent timing for both directions of motor rotation. A technique suggested for future tests would use eight sensors, four for CW rotation and four for CCW rotation. The location of the sensors could then be optimized for optimum motor performance.

(3) Coil Winding and Energization Options

There are two coil design areas where additional work to optimize the actuator design would be beneficial; (A) coil winding, series or parallel options and (B) evaluate two poles versus four pole powered performance.

(A) Coil Winding Configuration

Each stator pole of the breadboard actuator was wound with four coils. By connecting the coils various ways, different numbers of effective turns could be obtained. The required torque and speed was obtained with the first and second coil series connected and the third and fourth coil series connected. The two resulting sets of series coil pairs were then connected in parallel. Since one half of the current to a pole goes through each series coil pair, the total number of ampere turns per pole is

$$NI = 2\left(\frac{1}{2} I_t \times \frac{1}{2} N_t\right) = \frac{1}{2} I_t N_t$$

where

NI = effective number of ampere turns

I_t = total amperes to a pole

N_t = total number of turns on a pole

Thus the effective number of ampere turns is one-half the total current times the total number of turns. The back emf is proportional to the number of turns between the excitation lead and the common lead. The effective value is one-half the total number of turns. Thus the coil configuration should have been equivalent to a single coil with one-half the total number of turns, and a larger wire size to obtain the same equivalent resistance.

A problem was encountered with current circulating around the loop formed by the parallel coil sets. This loop current was eliminated by using diodes.

A single coil of larger wire size was used on each pole of the flightweight motor. The number of turns and wire size were selected to obtain the same back emf and resistance as the breadboard motor. However the predicted flightweight actuator performance was not equal to the breadboard performance and further investigations are necessary to determine the cause of the drop in performance.

(B) Two Pole Performance

Both the breadboard and flightweight units were operated with four poles energized at one time. The pole force analyses of Section 4 as shown on page 4-32 for example indicate that two of four poles (F_1 and F_2) are producing over 90 percent of the total force produced by energizing four coils. Although the torque level would be

degraded slightly by the use of two coils rather than four coils, it appears the overall actuator efficiency, coil duty cycle and controller duty cycle could all be improved. The capability to operate with only two coils energized was designed into the flightweight self-commutated controllers. However, time was not available on this program to allow testing of the flightweight actuators in this mode.

(4) Hermetically Sealed Designs

Bendix has built several versions of a fluid power low ratio Dynavector drive configuration shown in Figure 3-4(b) and (c). The unique feature of these two arrangements is that the reaction gear mesh formed by gears N_1 and N_2 were designed as a one-to-one mesh. Both gears had the same number of teeth and therefore the ring gear orbited but did not rotate. This arrangement would allow the use of a bellows or other form of flexible diaphragm between the rotor and stator thereby providing a hermetic seal of all electrical components and the reaction gear mesh. Only the output shaft bearings would be exposed to the vacuum operating conditions.